Geothermal Resources Council Transactions, Vol. 25, August 26-29, 2001

GL04385

Geologic and Geophysical Evidence for Intra-Basin and Footwall Faulting at Dixie Valley, Nevada

Richard P. Smith[1], Kenneth W. Wisian[2], and David D. Blackwell[2]

[1]Idaho National Engineering and Environmental Laboratory, Idaho Falls, ID 83415;
[2]Department of Geological Sciences, Southern Methodist University, Dallas, TX 75175

Keywords

Dixie Valley, structure, faults, dikes, gravity, seismic reflection, geologic mapping, earthquakes.

ABSTRACT

A "nested graben" structural model, in which multiple faults successively displace rocks downward to the deepest part of the basin, is supported by recent field geologic analysis and correlation of results to geophysical data for Dixie Valley. Aerial photographic analysis and detailed field mapping provide strong evidence for a deep graben separated from the ranges to the east and west by multiple normal faults that affect the Tertiary/Quaternary basin-fill sediments. Correlation with seismic reflection and gravity surveys shows that some faults recognized by minor displacements at the surface produce significant stratigraphic offsets at depth in basin-fill sediments and help to explain gravity gradients displaced basin-ward from the range-front. The concept of a complex series of faults (both synthetic and antithetic) separating the Stillwater Range from Dixie Valley allows for the possibility that the geothermal circulation encompasses multiple faults both inboard and outboard of the range-front fault. This geometry increases the exploration potential of the area by providing additional possibilities for fault-controlled permeability and larger volumes of permeable rocks.

Introduction and Methods

Geologic evidence for intra-basin and footwall faulting in Dixie Valley was examined by aerial photograph analysis and field mapping in 2000, following development of geophysical information suggesting that the "single range-front fault" model does not adequately describe the producing geothermal reservoir (Blackwell *et. al.*, 1999, 2000; also, see the summary of different models in Benoit, 1999). The purpose of this field re-examination was to develop a geologic map of recognized fault features in the region surrounding the geothermal reservoir (Figure 1, overleaf), and to merge the field observations with available geophysical data and borehole information.

The methods for this study consisted of the following steps:

1. Review of the published literature on the structural geology and tectonics of the Dixie Valley area. This review revealed that several investigators in the past have presented evidence for and interpretations of a stepwise downward displacement of the valley along multiple faults that underlie and affect the valley-fill sediments (Thompson *et. al.*, 1967; Whitney, 1980; Wallace and Whitney, 1984).
2. Standard field mapping techniques were used in the area surrounding the geothermal reservoir. In this area, a series of available seismic reflection lines and detailed gravity surveys provide an independent basis on which to evaluate field mapping results (Figure 1). A set of false-color, infrared aerial photographs, which provided stereoscopic coverage of the area of Figure 1 at a scale of 1:24,000, were examined for evidence of faulting. It was found that surface displacements of greater than about half a meter were recognizable, and that lineaments associated with faulting were easily recognized. Springs were readily identified by vegetation. All features indicative of faulting were transferred to 1:24,000 topographic maps of the area. These maps served as base maps for the field mapping effort in which recognized scarps and lineaments were examined. Initial aerial photographic interpretations were verified or modified by the field observations, and surface displacements measured where possible.
3. Examination of seismic reflection sections to identify offsets and folding of reflectors for correlation with structural features identified in the field mapping effort.
4. Acquisition of gravity data in the area and construction of a gravity contour map for correlation with structural features identified in the field mapping effort.

Intra-Basin Faults

Intra-basin faults are recognized by scarps with up to a meter of surface displacement, fissures, graben, linear arrangements of springs, and lineaments (both tonal and vegetation alignments) in basin-fill sediments. The Buckbrush fault, in the eastern side

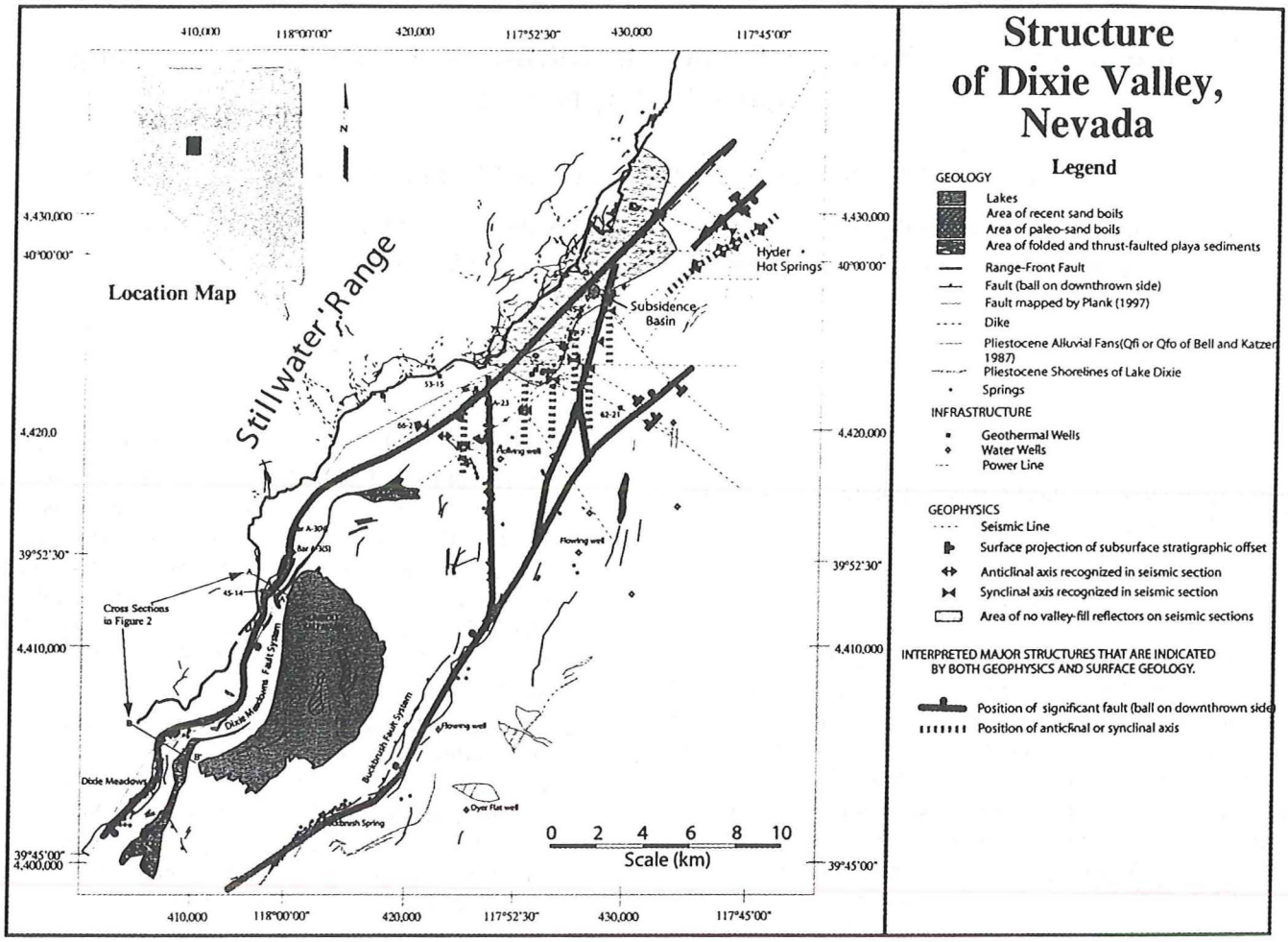

Figure 1. Map of Dixie Valley showing mapped features related to faulting and subsurface structures recognized from geophysical surveys

of the basin (Figure 1) exhibits down-to-the-west displacement and may have two branches that curve into the range-front fault in the vicinity of the geothermal power plant. Synthetic (down-to-the-east) faults occur in the Dixie Hot Springs area and affect both alluvial fans from the range front and playa sediments of the salt marsh. In some areas, alluvial fan deposits on the hanging wall of the faults have slid basin-ward on fine-grained water-saturated playa sediments, forming wide graben systems where they pull away from the fault scarp and belts of folded and thrust-faulted playa sediments ahead of the slide blocks (Figures 1 and 2). The numerous warm springs at the Dixie Hot Springs/Dixie Meadows area are localized by one of these pull-apart zones, and the playa sediments to the east are crumpled by the eastward movement of the toe of the alluvial fan.

Springs in Dixie Valley

Springs along the Buckbrush fault system bring cold, fresh water from artesian aquifers at depth to the surface. As indicated by driller's logs of wells in the map area and in the settlement of Dixie, just south of the map area, those artesian aquifers are layers of gravel and sand beneath clay-rich playa sediments (hardpan) at depths of 100 to 400 feet below the surface. The fault system cuts through these aquifers and provides permeable channels of disrupted materials along the fault surfaces for water to move to the surface. In several places along the Buckbrush system, inactive springs characterized by dead vegetation (grass, shrubs, saplings) occur. This suggests that plumbing systems for the springs are ephemeral and become sealed with time, and that repeated displacements on the fault system are required to maintain active springs. Some of the inactive springs may have been abandoned during the 1954 earthquakes, as new fault movements rearranged passageways. A likely mechanism for sealing of permeable passageways in these springs is plastic deformation of clay-rich playa and lake sediments.

Springs in the Dixie Meadows area, on the west side of the valley (Figure 1) are hot or warm springs, and probably tap geothermal waters moving up the Dixie Meadows fault system directly beneath. The maintenance of plumbing systems for these springs also require repeated fault movements, but in this case because of sealing of fractures by hydrothermal mineralization from the ascending hot waters. These springs may have been affected by 1954 ground motion and minor fault displacements, and were probably rejuvenated, or perhaps even initiated, by the pre-1954 earthquake event (the Bend Event). That event has been bracketed in age between 1.5 and 6.86ka by

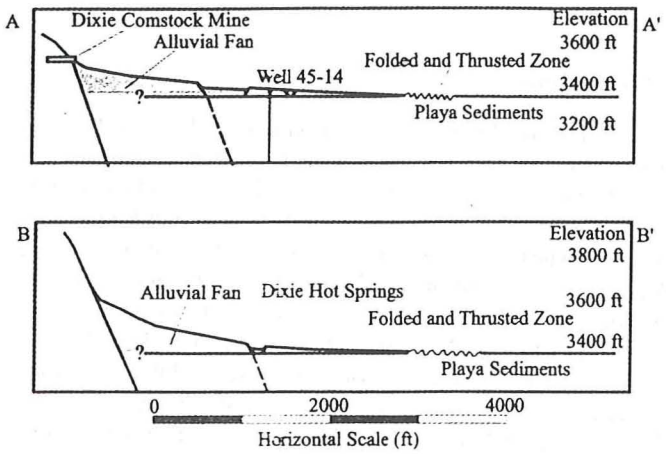

Figure 2. Cross sections of wide graben and folded playa sediments along the Dixie Meadows fault zone. See Figure 1 for locations of cross sections.

paleoseismic studies along the southern part of the Dixie Valley fault (Caskey *et. al.*, 2000). The mid- to late-Holocene age of this event is probably also responsible for rejuvenation of permeability and hydrothermal fluid transport in the producing geothermal reservoir and at several fumaroles along the range-front fault between Dixie Hot Springs and the north end of the Dixie Valley.

Footwall Faults and Mafic Dikes

Southeast-dipping faults with dip-slip slickensides occur in the bedrock of the Stillwater Range several kilometers behind the range-front. Some of these were mapped in the power plant area by Plank (1997). A large southeast-dipping fault south of the power plant area curves southwestward from drill hole 53-15, forming a large spoon-shaped sliver behind the range-front fault (Figure 1). It may represent an abandoned segment of the fault system as the range-front fault moved basin-ward in Late Tertiary or Quaternary time, or a relay ramp structure between two segments of the fault. This fault has not accumulated significant displacement because little or no offset of mafic dikes (Figure 1) is discernable where they are cut by the fault.

Mafic dikes were mapped in the footwall to provide displacement and age control for faults occurring there. We hoped to find a suite of late Tertiary dikes that may have served as feeders for the Miocene basalts that cap the Stillwater Range and floor the valley-fill sediments in the basin. Such a suite of dikes would have allowed easy distinction between late Tertiary extensional faults and older faults unrelated to Basin and Range extension. However, the only young dikes found were the two in Little Cottonwood Creek, just west of the power plant, that were mapped and dated by Plank (1997). All the others shown on Figure 1 are older dikes, emplaced in Mesozoic or early Tertiary time during or shortly after formation of the country rocks. They show, as indicated above, that the footwall fault south of the power plant has not accumulated significant displacement, but do not provide much age information for the faulting.

Seismic Reflection Lines

Seismic reflection lines (Figure 1) were examined to locate stratigraphic offsets (offsets of reflectors) in the valley-fill sediments. Faults were inferred in places where offsets were unambiguous, and projected to the surface. The surface projections of those faults are shown in Figure 1, and in several areas correspond to faults identified at the surface by surface mapping. The positions of anticlinal and synclinal axes recognized in the seismic sections are also indicated in Figure 1.

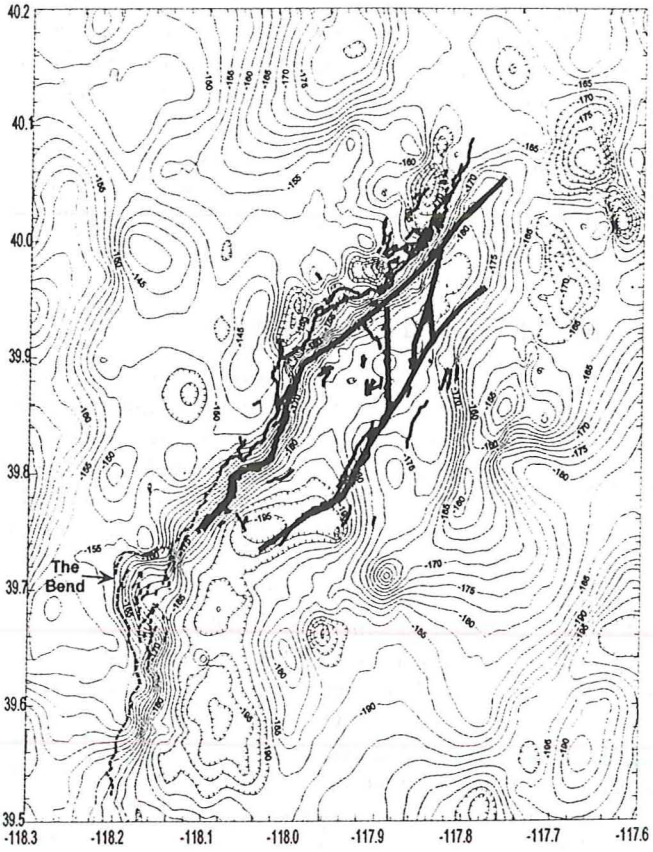

Figure 3. Gravity map of Dixie Valley with mapped faults in heavy solid lines, and inferred generalized fault systems in broad gray lines (from Figure 1). Ground ruptures of the 1954 earthquake (from Caskey *et. al.*, 1996) shown by dashed lines.

Gravity Surveys

Gravity data provides a useful constraint on the subsurface structure in Dixie Valley. A detailed gravity study of the valley was conducted in 1996 (Blackwell *et. al.*, 1999) and extended in 2000 to a total of nearly 1000 points. The resultant data were merged with regional gravity data to produce a Bouguer Gravity map for the Dixie Valley area (Figure 3); the surface faulting and generalized interpretations of major structures are also plotted. The regions of strong gradients on the west side of the valley define the structural offset between the basement and valley fill. 2-D modeling of the gravity data (Blackwell *et. al.*, 1999) shows that along much of the valley, piedmont faults accommodate most

of the displacement between the range-front and the valley bottom. These findings agree with those of Bell and Katzer (1987) for the southern section of the valley. In the area just northeast of "the Bend" the mapped trace of the fault diverges significantly from the position that would be interpreted from the gravity gradient – it is unclear weather this is due to structural complexity or to compositional (and density) variations in the footwall rocks. The gravity data suggests that along the whole of the western side of Dixie Valley, faults are steeply dipping.

Structure in the eastern side of Dixie Valley is less clearly related to the gravity data. The trends of surface faulting correlate weakly with areas of gravity gradient. The gradients themselves are not as strong on the eastern side as would be expected for this highly asymmetrical valley. In places where the surface faulting cuts across the valley, there is some correlation with north trending gradients, but it is not clear whether the north trending high gradient areas are structural or compositional in origin.

Interpretations and Conclusions

Our best interpretation of locations of significant intra-basin faults are shown as broad gray lines in Figure 1. The Buckbrush and the Dixie Meadows fault zones appear to be continuous from the southern margin of Humboldt Salt Marsh to the power plant area, and to form a deeper graben within the topographic expression of Dixie Valley. Within this graben, several anticlinal and synclinal axes recognized in seismic sections, appear to have northerly trends in the power plant area (Figure 1). The fault pattern suggests that several faults intersect or closely interact with each other in the area of the producing reservoir. The intersection of the Dixie Meadows fault system with two or more north-trending branches from the Buckbrush fault system occurs in the area of the geothermal reservoir and in the area in which reflectors are absent in seismic reflection sections. Large volumes of fractured rocks at these fault intersections may help to explain both the location of the reservoir and the absence of seismic reflectors in the area.

Surface geologic mapping and geophysics support the concept of a complex series of synthetic and antithetic faults separating the Stillwater Range from Dixie Valley and allows for the possibility that the geothermal circulation encompasses multiple faults both inboard and outboard of the range-front fault. This geometry increases the exploration potential of the area by providing additional possibilities for fault-controlled permeability and for larger volumes of permeable rocks.

Future Work

Correlation of fault data from geologic mapping and geophysics with well logs (both lithologic and geophysical) with be the next step in this project. We hope to be able to make a more definite assessment of the fault(s) hosting the reservoir and to provide criteria for selection of new drill targets.

Acknowledgements

Funding for this work was provided by the U.S. Department of Energy, Office of Geothermal and Wind Technologies, under Contracts DE-AC07-99ID13727 (INEEL) and DE-FG07-97IDI3504 (Southern Methodist University). Joel Renner and Suzette Payne reviewed the manuscript. Thanks are due to Steve Wesnousky, Director of the Center for Neotectonic Studies at the University of Nevada, Reno, and John Caskey of San Francisco State University for providing access to the UNR collection of low-sun-angle, 1:12,000 aerial photographs of the area. Mike Rohe, INEELGeosciences Department provided able field assistance, and Linda Tedrow, INEEL Spatial Analysis Laboratory, prepared the digital map.

References

Bell, J.W. and Katzer, T. (1987) Surficial Geology, Hydrology, and Late Quaternary Tectonics of the IXL Canyon Area, Nevada As Related to the 1954 Dixie Valley Earthquake; Nevada Bureau of Mines and Geology, Bulletin 102, p.2-52.

Benoit, Dick (1999) Conceptual models of the Dixie Valley, Nevada Geothermal Field; Geothermal Resources Council Transactions, v.23, p.505-511.

Blackwell, David D., Wisian, Kenneth W., Benoit, Dick., and Gollan, Bobby (1999) Structure of the Dixie Valley Geothermal System, a "Typical" Basin and Range Geothermal System, From Thermal and Gravity Data; Geothermal Resources Council Transactions, v.23, p.525-531.

Blackwell, David D., Golan, Bobbie, and Benoit, Dick (2000) Thermal regime in the Dixie Valley Geothermal System; Geothermal Resources Council Transactions, v.24, p.223-228.

Caskey, S.J., Wesnousky, S.G., Zhang, P., and Slemmons, D.B. (1996) Surface faulting on the 1954 Fairview Peak (Ms7.2) and Dixie Valley (Ms6.8) earthquakes, central Nevada; Bulletin of the Seismological Society of America, v.86, n.3, p.761-787.

Caskey, S.J., Bell, J.W., Slemmons, D.B, and Ramelli, A.R. (2000) Historical surface faulting and paleoseismology of the central Nevada seismic belt: *in* Lageson, D.R., Peters, S.G, and Lahren, M.M., editors, Great Basin and Sierra Nevada; Geological Society of America Field Guide 2, p.23-44.

Plank, Gabriel L. (1997) Structure, Stratigraphy, and Tectonics of a part of the Stillwater Escarpment and Implications for the Dixie Valley Geothermal System; University of Nevada, Reno, MS Thesis, 153p.

Thompson, G.A., Meister, L.J., Herring, A.T., Smith, T.E., Burke, D.B., Kovach, R.L., Burford, R.O., Salehi, I.A., and Wood, M.D. (1967) Geophysical study of Basin-Range structure, Dixie Valley region, Nevada: Air Force Cambridge Research Laboratory, Report No. 66-848.

Wallace, R.E. and Whitney, R.A. (1984) Late Quaternary history of the Stillwater seismic gap, Nevada; Bulletin of the Seismological Society of America, v.74, no.1, p.301-314.

Whitney, R.A. (1980) Structural-Tectonic analysis of northern Dixie Valley, Nevada; Masters Thesis, University of Nevada, Reno

Preliminary Results of a High-Resolution Aeromagnetic Survey to Identify Buried Faults at Dixie Valley, Nevada

R.P. Smith[1], V.J.S. Grauch[2], and D.D. Blackwell[3]

[1]Idaho National Engineering and Environmental Laboratory, Idaho Falls, ID 83401-2107
[2]U.S. Geological Survey, MS 964, Federal Center, Denver, CO 80225
[3]Department of Geological Sciences, Southern Methodist University, Dallas, TX 75175

Key Words
High-resolution aeromagnetic survey, Dixie Valley, faults, structure, mapping

Abstract
Preliminary results from a high-resolution aeromagnetic survey (200m line spacing) acquired in Dixie Valley early in 2002 provides confirmation of intra-basin faulting based on subtle surface indications. In addition the data allow identification of the locations and trends of many faults that have not been recognized at the surface, and provide a picture of intrabasin faulting patterns not possible by other means. The data reveal a suite of northeasterly-trending curving and branching faults that surround a relatively coherent block in the area of Humboldt Salt Marsh, the deepest part of the basin. The producing reservoir occurs at the north end of this coherent block, where rampart faults from the northwest side of the valley merge with anthithetic faults from the central and southeast parts of the valley.

Introduction and Methods

Recent geologic mapping focused on fault distribution near the producing geothermal reservoir in Dixie Valley relied on subtle surface features (small scarps, small graben, linear alignments of springs, vegetation and color lineaments) to define fault locations beneath and within the intrabasin sediments. (Smith et al, 2001) In order to increase confidence in the locations of buried faults a high-resolution aeromagnetic survey was conducted over a 940 km^2 area. The area extends from Dixie Meadows northeastward to the Sou Hills, and from the eastern front of the Stillwater Range to the west edge of the Clan Alpine Range (Figure 1) and includes almost all of the area in which the recent geologic mapping was done.

Parameters for the high-resolution aeromagnetic survey (Table 1) are similar to those for other surveys which have provided information on the distribution of buried faults in basin-fill sediments (Grauch, 2001; Grauch et al., 2001; Grauch and Millegan, 1998). The main distinguishing feature of this survey is the extreme topographic relief at the east front of the Stillwater Range, which dictated the use of a helicopter to acquire data near the range-front fault. Detailed descriptions of the procedures followed for data acquisition and processing are contained in U. S. Geological Survey and PRJ, Inc. (in press).

Table 1. Specifications of the Dixie Valley high-resolution aeromagnetic survey (2002)

Dates of Acquisition	January 20 – February 2, 2002
Line Spacing	200 m, lines trend NW – perpendicular to regional structures
Tie lines	1000 m, lines trend NE – parallel to regional structures
Observation height above ground (average)	120 m
Instrument/Aircraft	Cesium-vapor magnetometer with sampling rate of 0.1 seconds towed below a Bell Jet Ranger helicopter
Area Surveyed	~940 km^2
Total flight-line length	5740 line km

After data processing to remove diurnal effects, noise, and the Earth's magnetic field, the total-field aeromagnetic data were gridded at a 50-m interval (Figure 2). Preliminary analysis focused on enhancing the signature of shallow faults in the aeromagnetic data by using the gradient window method (Grauch and Johnston, in press), a modification of the horizontal-gradient method. The horizontal-gradient method (Cordell and Grauch, 1985; Blakely and Simpson, 1986) is based on a principle from gravity methods that steep gradients occur over near-vertical contacts between units with differing physical properties. For magnetic data, the same principle can be applied after transforming the data into a form that is mathematically similar to gravity data, called pseudogravity (Baranov, 1957). Local peaks (or ridges) in the magnitude of the horizontal gradient of pseudogravity give the locations of steepest gradients, intuitively similar to taking the first derivative of a curve. A modification of the method, which isolates the horizontal-gradient magnitudes associated with short-wavelength anomalies (Grauch and Johnston, in press), was applied to the Dixie Valley data after transforming to pseudogravity (Figure 3). Future study will include analyses to estimate the depths and refine map locations of faults with respect to anomalies visible on the map.

Fault Patterns Indicated by Aeromagnetic Anomalies and Geologic Mapping in Dixie Valley

The total-field aeromagnetic map (Figure 2) shows the same gross features as earlier, low-resolution aeromagnetic maps (Smith, 1968; Thompson et al., 1967). Notably, the patterns of major positive and negative aeromagnetic anomalies are similar; the large positive anomalies have been interpreted to represent large bodies of mafic rocks in the basement beneath the valley fill sediments or horst blocks of mafic basement rocks within the valley.

In addition to the large positive and negative anomalies, the map (Figure 2) shows a suite of northeast-trending, short wave-length, linear anomalies which have been emphasized by the narrow ridges in the horizontal gradient map (Figure 3). Many of the linear anomalies are continuous for 10 or more km, and commonly show branching and curving shapes. In addition, a group of short wavelength negative anomalies (dimples) present in the area of Hyder Hot Springs may represent altered areas where magnetic minerals have been destroyed along plumbing pathways that feed the hot springs. Alternatively, the negative anomalies may be due to buried, extinct vents related to Tertiary volcanic rocks that have reverse-polarity remanent magnetization (Hudson and Geissman, 1991). In areas where bedrock is exposed at the surface (along the northwestern edge and the central part of the southeastern edge of the surveyed area) the pattern of anomalies is much rougher than in areas covered with thick alluvial sediments.

Superposition of mapped faults (Smith et al., 2001; Whitney, 1980; Thompson et al., 1967) onto the horizontal gradient map shows that many of the short wavelength, linear magnetic anomalies have a close correspondence to the mapped fault traces (Figure 4). The correspondence is identical to that in the Albuquerque Basin where "the linear anomalies have become important geologic mapping tools that are used to connect and extend isolated exposures of faults, to confirm ambiguous surface evidence of faults, to infer buried faults, and to pinpoint areas to look for fault evidence on the ground" (Grauch 2001;Grauch et al., 2001). After extensive investigations of possible sources of the linear anomalies in the Albuquerque Basin, Grauch et al (2001) show that they are explained by fault offsets that juxtapose sediment layers of differing magnetic properties, and that they represent offsets that occur within the upper 500-600 meters of the valley-fill sediments.

The close correspondence of mapped faults in Dixie Valley to narrow ridges in the horizontal gradient map (Figure 4) suggests that the aeromagnetic data can be used to extend the knowledge of faulting within the basin-fill sediments. By using the horizontal-gradient map (Figure 3) to infer the traces of faults we develop a more complete map of fault distribution in the valley (Figure 5). Faults can be interpreted from the horizontal-gradient magnitude by following the ridges in the horizontal-gradient magnitude map (Figure 3). This interpretation can be somewhat subjective, because peak magnitudes can also follow lithologic contacts, abrupt variations in magnetic properties within one rock unit, and steep basement relief. In contrast, the absence of linear magnetic anomalies does not necessarily imply the absence of faults; a lack of contrast in magnetic properties of the materials juxtaposed at the fault or minor offset along the fault could could preclude aeromagnetic detection (Grauch et al., 2001).

The complete pattern of shallow faults (Figure 5) shows that faults that have a strong surface expression also have a strong aeromagnetic signal, that there are many faults in the valley that exhibit no surface expression, and that some of the faults that have surface expression are sections of longer faults.

Interpretation of Fault Patterns in Dixie Valley

Intrabasin faults in Dixie Valley trend generally northeast, subparallel to the range front fault (Figure 5), but they commonly exhibit curving and branching shapes. Notably, the Buckbrush fault system, a major intrabasin system with numerous springs localized along its trace, broadens and branches in a classic "horsetail" fashion just south of Humboldt Salt Marsh. This suggests that it terminates to the south of the mapped area and that displacement is transferred to nearby faults to the east or west. There is a tendency for all the faults, including the exposed range-front fault to turn to a more easterly direction at the north end of Dixie Valley, in the Sou Hills-Hyder Hot Springs area. The mapped range-front fault and several faults inferred from aeromagnetic anomalies in the northeastern part of the area turn quite abruptly eastward, indicating a significant change in fault geometry at the northern end of the valley.

The inferred presence of a buried synthetic rampart fault just outboard of the range-front fault is strengthened by the aeromagnetic anomalies present there. The aeromagnetic signature is especially convincing in the northern part of the area between the geothermal field and the Sou Hills (Figure 4). Along the western side of the valley near the geothermal field, faults inferred

from the aeromagnetic data (Figure 5) are supported by gravity and geologic mapping (Blackwell et al., 1999, 2000; Smith et al., 2001) and confirmed by recent drilling. At the southern end, near Dixie Meadows, the horizontal gradient anomaly and the steepest part of the gravity gradient (Blackwell et al. 1999; Smith et al., 2001) are coincident, and lie outboard of the Dixie Meadows graben system. This suggests a moderate eastward dip for the rampart fault, unlike the areas in the vicinity of the deep wells 36-14 and 45-14 where drilling shows that the fault is essentially vertical. It is clear that the extension that produced the Dixie Meadows graben system is thin-skinned basin-ward sliding of alluvial fan material on saturated fine-grained sediments of the salt marsh (Caskey et al., 2000; Smith et al, 2001), and therefore does not necessarily owe its existence to surface displacement along a deep rampart fault. However, the close spatial correlation of the gravity and magnetic gradients reflect the presence of a deeper structure whose surface expression could control the location of the graben system

The only part of the basin without surface or aeromagnetic evidence of intrabasin faulting is the area in and around the Humboldt Salt Marsh. This seems to be the deepest part of the basin, flanked on both sides by intrabasin fault systems that downdrop the central block. The geothermal field is located at the north end of this deep, coherent block, where its flanking fault systems merge. The area of merging is also marked by an abundance of springs and flowing wells, suggesting that a number open fault systems occur here, extending from the deep bedrock, where they provide space for the geothermal fluids, into near-surface sediments, where they allow rise of water from artesian aquifers near the surface.

Conclusions and Recommendations

This is a test of high-resolution aeromagnetic surveys in basins other than the Albuquerque Basin, where the technique was first demonstrated. There was some early concern that the deep, narrow basin geometry, the extremely steep front of the Stillwater Range, and the presence of very magnetic mafic rocks in the bedrock in Dixie Valley would limit the usefulness of the technique here. But the data have proven to reveal the intra-basin fault pattern with unexpected clarity. The data allow identification of the positions and attitudes of numerous faults that have no surface expression, and provide a geometric relationship of the geothermal field to the fault pattern that will aid further geothermal exploration in the area. As additional processing and filtering of the data are performed, the fault pattern will be refined, and the relationship of deep to shallow aeromagnetic signatures of faulting will be further clarified.

This effort has shown that topographic constraints on aeromagnetic data acquisition can be overcome by use of helicopter flight platforms, and that the method can provide useful data in basins where bedrock composition and basin geometry are not ideal. This is a technique that may prove useful for geothermal exploration, structural investigations, and groundwater problems in many sediment-filled basins of extensional environments.

References

Baranov, V. (1957) A new method for interpretation of aeromagnetic maps--pseudogravity anomalies; Geophysics, v. 22, p. 359-383.

Blackwell, D.D., Wisian, K.W., Benoit, D., and Gollan, B. (1999) Structure of the Dixie Valley Geothermal System, a "Typical" Basin and Range Geothermal System, From Thermal and Gravity Data; Geothermal Resources Council Transactions, v.23, p.525-531.

Blackwell, David D., Golan, Bobbie, and Benoit, Dick (2000) Thermal regime in the Dixie Valley Geothermal System; Geothermal Resources Council Transactions, v.24, p.223-228.

Blakely, R. J., and Simpson, R. W. (1986) Locating edges of source bodies from magnetic or gravity anomalies; Geophysics, v. 51, p. 1494-1498.

Caskey, S.J., Bell, J.W., Slemmons, D.B., and Rameli, A.R. (2000) Historical surface faulting and paleoseismology of the central Nevada seismic belt; in Lageson, D.R., Peters, S.G., and Lahren, M.M., editors, Great Basin and Sierra Nevada: Geological Society of America Field Guide 2, p23-44.

Cordell, Lindrith, and Grauch, V. J. S. (1985) Mapping basement magnetization zones from aeromagnetic data in the San Juan Basin, New Mexico; in Hinze, W. J., editor, The utility of regional gravity and magnetic maps: Society of Exploration Geophysicists, p. 181-197.

Grauch, V J S (2001)High-resolution aeromagnetic data, a new tool for mapping intrabasinal faults; example from the Albuquerque Basin, New Mexico: Geology, vol.29, pp.367-370.

Grauch, V.J.S., and Millegan, P. S., 1998, Mapping intrabasinal faults from high-resolution aeromagnetic data: The Leading Edge, 17, p.53-55.

Grauch, V.J.S.; Hudson, M.R., Minor, S.A. (2001) Aeromagnetic expression of faults that offset basin fill, Albuquerque Basin, New Mexico; Geophysics, vol.66, p.707-720.

Grauch, V.J.S., and Johnston, C.S. (in press) Gradient window method: A simple way to isolate regional from local horizontal gradients in potential-field gridded data: 72nd Annual International Meeting, Society of Exploration Geophysicists, Expanded Abstracts, in press.

Hudson, M. R., and Geissman, J.W. (1991) Paleomagnetic evidence for the age and extent of middle Tetiary counterclockwise rotation, Dixie Valley region, west central Nevada: Journal of Geophysical Research, v. 96, no. B3, p. 3979-4006.

Smith, R.P., Wisian, K.W., and Blackwell, D.D. (2001) Geologic and Geophysical Evidence for Intra-basin and Footwall Faulting at Dixie Valley, Nevada; Geothermal Resources Council Transactions, v. 25, p. 323-326.

Smith, T.E. (1968) Aeromagnetic measurements in Dixie Valley, Nevada; Implications on Basin-Range structure; Journal of Geophysical Research, v.73, p.1321-1331.

Thompson, G.A., Meister, L.J., Herring, A.T., Smith, T.E., Burke, D.B., Kovach, R.L., Burford, R.O., Salehi, I.A., and Wood, M.D. (1967) Geophysical study of Basin-Range structure, Dixie Valley region, Nevada; Air Force Cambridge Research Laboratory, Report No. 66-848.

U. S. Geological Survey and PRJ, Inc. (in press) Description of digital aeromagnetic data collected over Dixie Valley, Churchill and Pershing Counties, Nevada: U. S. Geological Survey Open-File Report 02-.

Whitney, R.A. (1980) Structural-Tectonic analysis of northern Dixie Valley, Nevada; Masters Thesis, University of Nevada, Reno.

Figures

Figure 1. Location and Index map

Figure 2. Shaded-relief image of total-field aeromagnetic data, illuminated from the northwest.

Figure 3. Shaded-relief image of the horizontal-gradient magnitude of gradients associated with local (shallow) features, computed after transformation of the aeromagnetic data to

pseudogravity and application of the gradient window method (Grauch and Johnston, in press) using the residual in a 1 X 1 km moving window. Illumination from the northwest.

Figure 4. Horizontal Gradient Magnitude (HGM) map (Figure 3) with mapped faults superimposed.

Figure 5. The complete distribution of shallow faults as indicated by surface mapping and high-resolution aeromagnetic anomalies. Selected deeper faults are also inferred from aeromagnetic anomalies along the western range front and from seismic profiles.

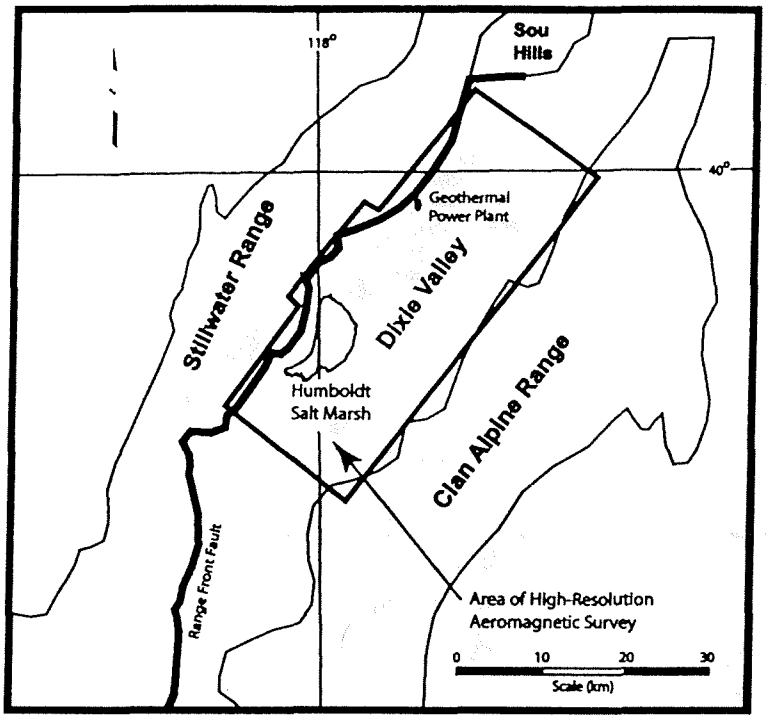

Figure 1. Index map showing the area of the high-resolution aeromagnetic survey.

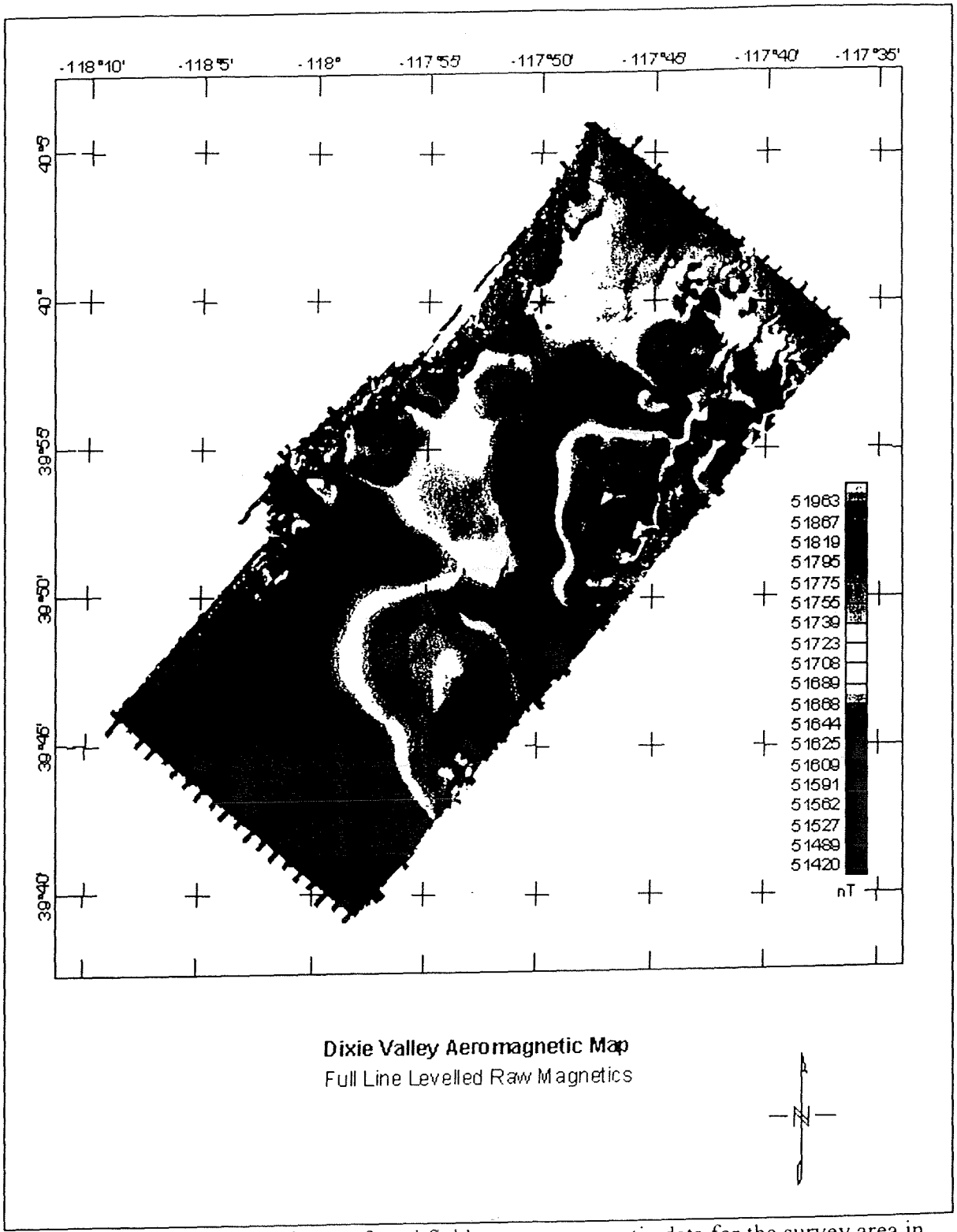

Figure 2. Color shaded relief map of total field raw aeromagnetic data for the survey area in Dixie Valley.

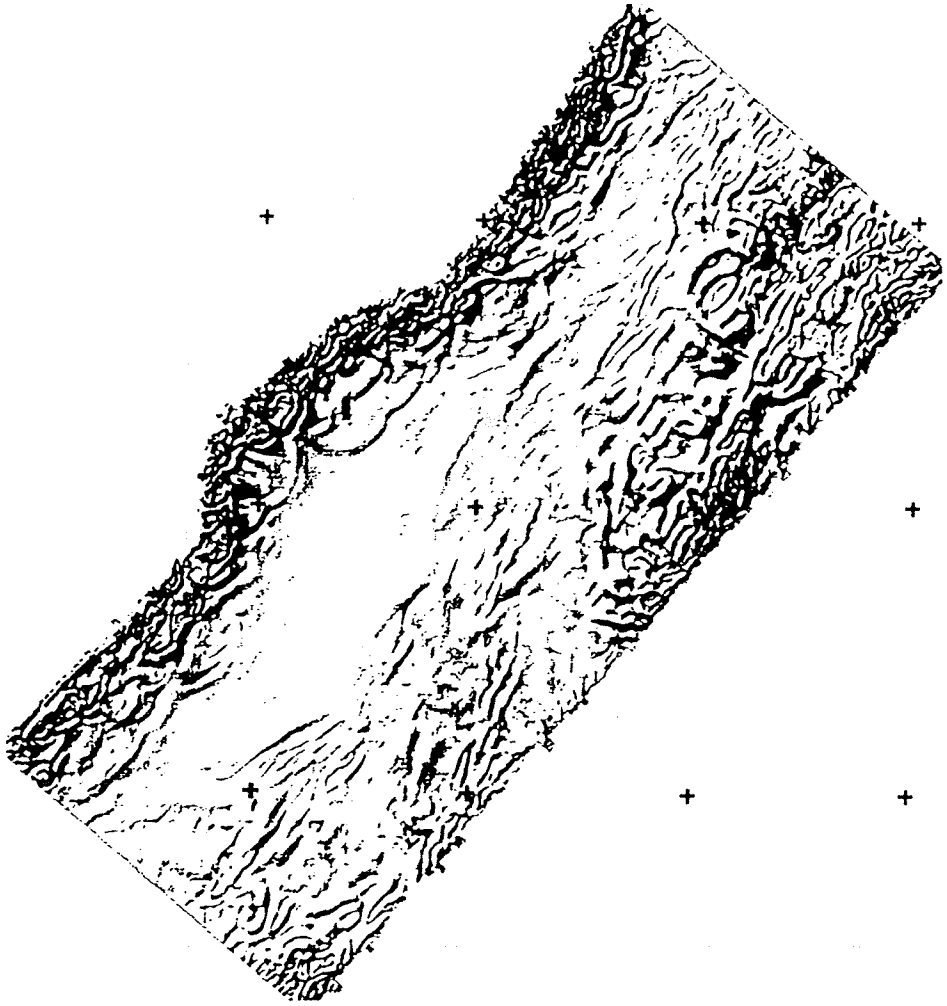

Figure 3. Shaded-relief image of the horizontal-gradient magnitude of gradients associated with local (shallow) features, computed after transformation of the aeromagnetic data to pseudogravity and application of the gradient window method (Grauch and Johnston, in press) using the residual in a 1 X 1 km moving window. Illumination from the northwest.

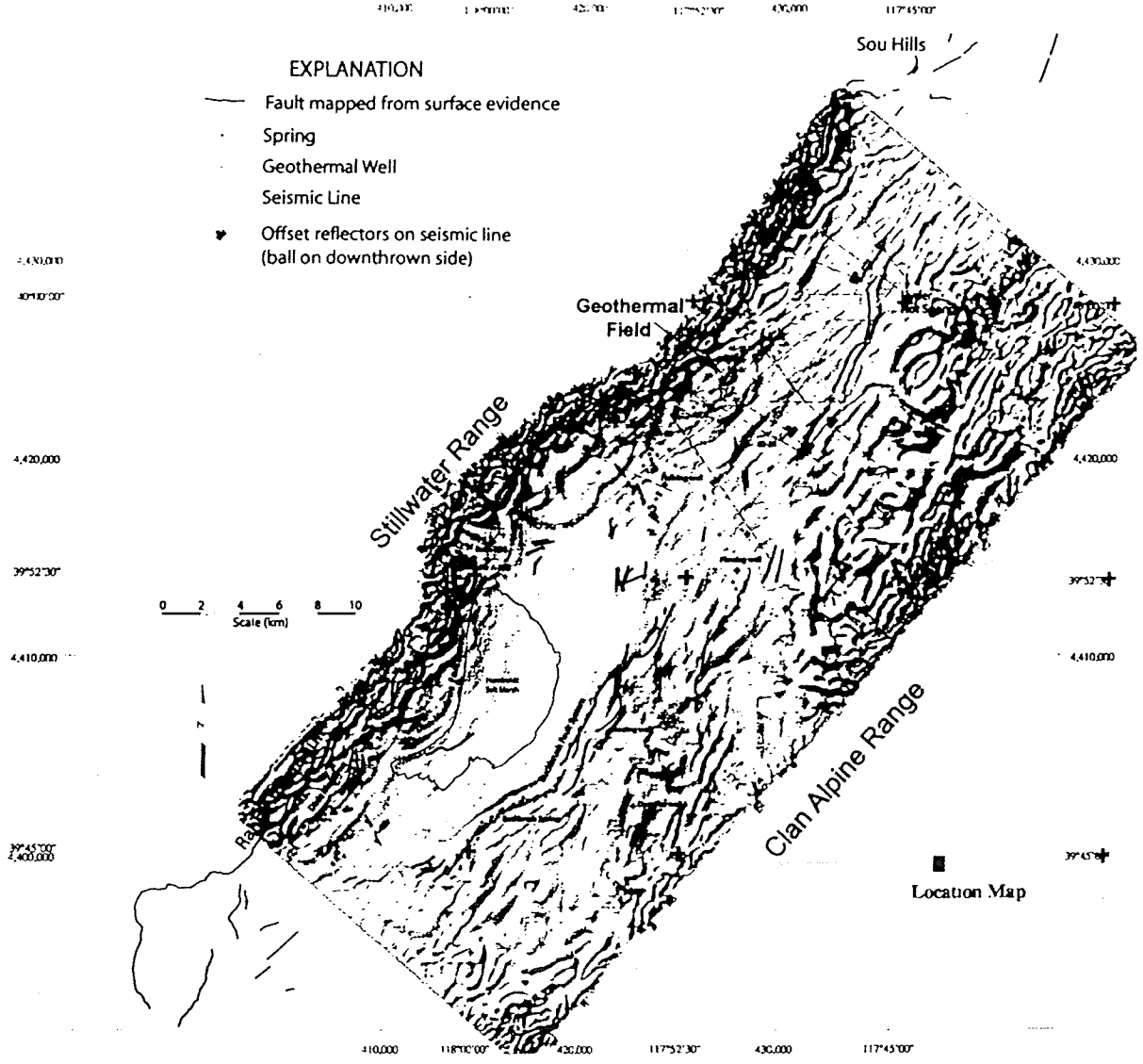

Figure 4. Horizontal Gradient Magnitude (HGM) map (Figure 3) with mapped faults superimposed..

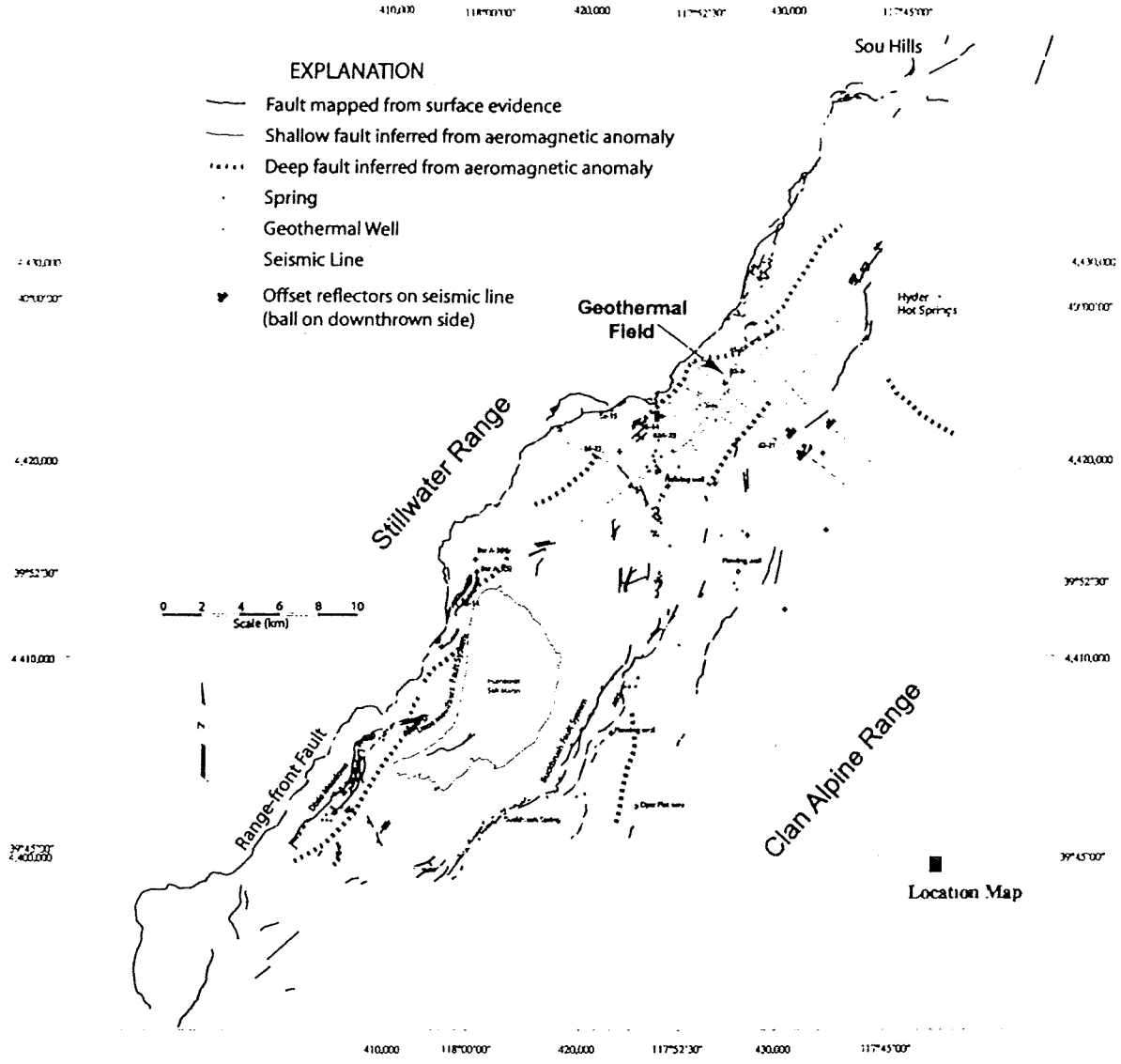

Figure 5. The complete distribution of shallow faults as indicated by surface mapping and high-resolution aeromagnetic anomalies. Selected deeper faults are also inferred from aeromagnetic anomalies along the western range front and from seismic profiles.

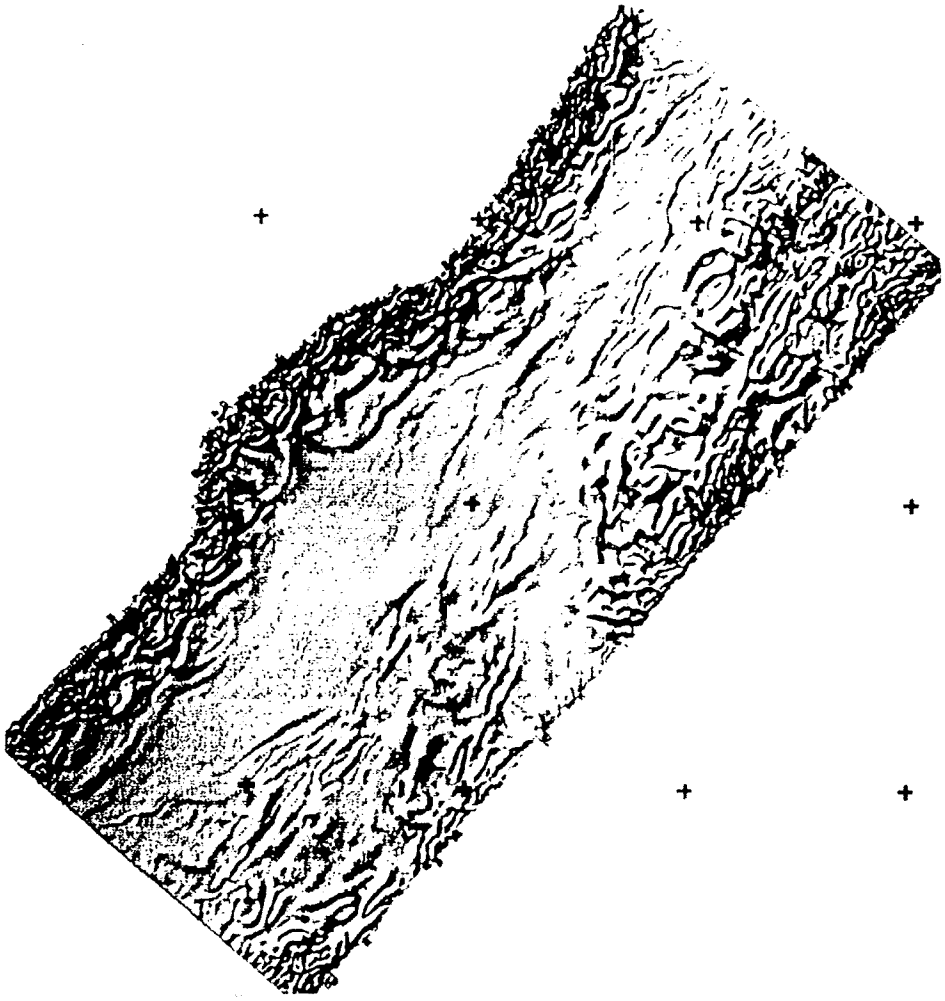

Figure 3. Shaded-relief image of the horizontal-gradient magnitude of gradients associated with local (shallow) features, computed after transformation of the aeromagnetic data to pseudogravity and application of the gradient window method (Grauch and Johnston, in press) using the residual in a 1 X 1 km moving window. Illumination from the northwest.

TECTONICS, VOL. 4, NO. 6, PAGES 547-564, OCTOBER 1985

EAST-TRENDING DEXTRAL FAULTS IN THE WESTERN GREAT BASIN: AN EXPLANATION FOR ANOMALOUS TRENDS OF PRE-CENOZOIC STRATA AND CENOZOIC FAULTS

John H. Stewart

U.S. Geological Survey,
Menlo Park, California

Abstract. Two postulated major east trending strike-slip fault zones, here named the Coaldale and Excelsior fault zones, are delineated mainly on the basis of faults in Cenozoic rocks in eastern California and western Nevada and coincide with apparent major right-lateral offsets in the distribution and facies of pre-Cenozoic rocks. Apparent right-lateral offset of pre-Cenozoic rocks on the Coaldale fault zone is 60 to 80 km and on the Excelsior fault zone is 45 to 55 km. This offset accounts for major disruption in trends of pre-Cenozoic rocks in eastern California and western Nevada, a disruption previously interpreted as the result of either an originally curving continental margin or tectonic distortion of originally linear trends by large-scale bending (oroflexural folding) or by crustal-scale folding related to north-east-southwest compression. Main offset on the Coaldale and Excelsior fault zones appears to be late Mesozoic in age. A pre-mid-Cretaceous age is indicated because mid-Cretaceous and younger plutonic rocks are not cut by major strike-slip faults on line with the fault zones. Major movement is probably younger than the Dunlap Formation, which is dated paleontologically as Early Jurassic but which may also contain rocks as young as Cretaceous. Local reactivation of the faults in the Cenozoic, perhaps under a different stress regime, accounts for offset of Cenozoic rocks. The Coaldale and Excelsior fault zones terminate major northwest trending late Cenozoic and possibly older faults. The Owens Valley-White Mountain fault system in eastern California and the Furnace Creek fault zone in southeastern California and westernmost Nevada terminate northward at the Coaldale fault zone. A system of south-east trending right-lateral and high-angle faults in western Nevada, including the Bettles Well fault, terminate southward at the Excelsior fault zone. Major movement on northwest trending faults such as the Furnace Creek and Bettles Well fault may be mostly late Cenozoic in age, but present information does not preclude the possibility that these fault zones initiated prior to, and are offset by, the Coaldale and Excelsior fault system. The unusual trends of pre-Tertiary rocks and of the Coaldale and Excelsior fault zones in eastern California and western Nevada appear to be restricted to the Walker Lane belt, a broad northwest trending structural zone characterized by right-lateral shear in western Nevada and eastern California. Possibly initial shear produced the northwest trending faults, and a later "kink" in this system produced oroflexural folding and the east-trending right-lateral Coal-

Paper number 5T0448.

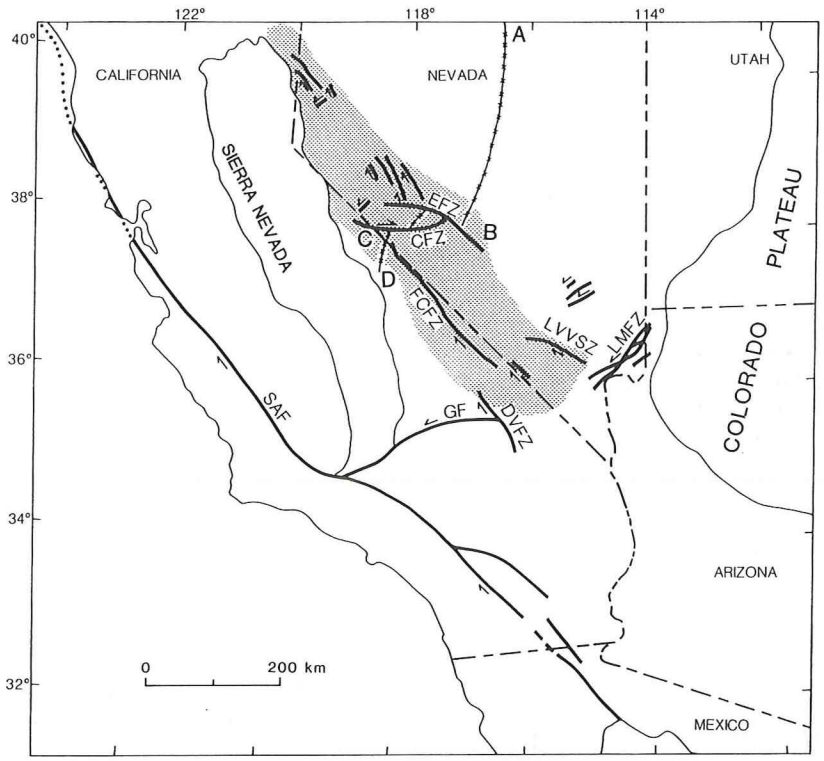

Fig. 1. Index map of California and Nevada showing major strike-slip faults, generalized distribution and facies trends of Paleozoic rocks, and the Walker Lane belt. Stippled area is Walker Lane belt. Heavy lines are major strike-slip faults, arrows indicate relative movement. Line with crosses is generalized trend of Paleozoic rocks. Symbols: CFZ, Coaldale fault zone; DVFZ, Death Valley fault zone; EFZ, Excelsior fault zone; FCFZ, Furnace Creek fault zone: GF, Garlock fault; LMFZ, Lake Mead fault zone; LVVSZ, Las Vagas Valley shear zone; SAF, San Andreas fault.

dale and Excelsior fault zones. This "kink" may have resulted from a change in the stress regime and structural complexities where the shear zone obliquely crossed the Paleozoic continental margin.

INTRODUCTION

The distribution trends of Proterozoic to Mesozoic rocks are generally south-southwest in central Nevada (AB, Figure 1), east-west or highly disrupted in western Nevada and eastern California (BC, Figure 1), and again south southwest in eastern California (CD, Figure 1). Two competing ideas have developed to explain this Z-shaped pattern (ABCD, Figure 1). According to the first, the pattern simply reflects the original shape of the continental margin. Ferguson and Muller [1949] applied the name Luning Embayment to the southeast indentation (ABC, Figure 1) in this supposedly irregular margin. In more modern terms, this interpretation relates the irregularly shaped continental margin to a complex pattern of late Proterozoic rifting [Oldow, 1982, 1983, 1984a, b; Oldow and Geissman, 1982; Geissman et al., 1984]. The second idea attributes the Z-shaped distribution pattern of the Proterozoic to Mesozoic rocks to tectonic distortion that has disrupted originally more linear trends. Albers [1967] proposed that the pattern was produced by large-scale bending or drag (oroflexural folding) in an area of dextral shear (the Walker Lane or belt, Figure 1), whereas Wetterauer [1977] related the tectonic distortion (which he referred to as the "Mina deflection") to a crustal-scale fold produced by northeast-southwest compression. In this article I suggest a third explanation of tectonic distortion, namely, that much of the offset is related to

right-lateral movement on two major east trending fault zones (the Coaldale and Excelsior faults). These fault zones appear also to have been important in controlling the pattern of late Cenozoic faults in the western Great Basin.

STRUCTURE

The fault zones described here are recognized mainly on the basis of the anomalous trends of faults that cut strata as young as late Cenozoic. In the surrounding region, most young high-angle faults strike northerly but near the postulated fault zones many young, steep faults strike more nearly east-west. In places the zones are characterized by locally broad linear belts of late Cenozoic silicic or basaltic igneous rocks that were apparently erupted along the fault, though perhaps under a different stress regime from that which originally produced the faults. The main time of movement, as described below, was in the late Mesozoic, but in many places the faults were reactivated in the late Tertiary and even the Quaternary. Locally, fault patterns in young basaltic units may mimic old fault patterns in underlying rocks. Although locally obscured by late Cenozoic volcanic and alluvial cover the fault zones are well defined for much of their length.

Coaldale Fault Zone

The Coaldale fault zone, which was recognized in part by Albers and Stewart [1972] and corresponds to the western part of the Warm Springs lineament of Ekren et al. [1976], forms a conspicuous zone of east to east-northeast trending faults east of Coaldale (Plate 1, location 1) [Moiola, 1969; Albers and Stewart, 1972; Robinson et al., 1976; Moore, 1981]. These faults may belong to a system of northeast trending faults along the southern margin of the Monte Cristo Range. Alternately, the main fault zone may continue eastward below Quaternary alluvium east of the Coaldale area (east of location 1). In either case, the Coaldale fault zone must curve to the northeast between the southeastern Monte Cristo Range and the Lone Mountain area, because the fault zone does not extend through the Mesozoic and older rocks of the Lone Mountain area.

West of the Coaldale area, the Coaldale fault zone is clearly recognized as a system of east trending faults along the south and southeast sides of Miller Mountain (Plate 1, location 2; Albers and Stewart [1972] and Stewart [1979]), and also north of Montgomery Pass (Plate 1, locations 3 to 4; Stewart [1982a, b], Stewart et al. [1982], and Dohrenwend [1982a, b]).

In the Adobe Hills area west of Montgomery Pass, east trending faults are not recognized, but the fault pattern is complex and fault trends change from generally northwest on the south to northeast on the northside of a westward projection of the Coaldale fault zone [Gilbert et al., 1968]. This change in trend is here considered to reflect near-surface faulting above the buried Coaldale fault zone. Faults in the Montgomery Pass and Adobe Hills areas cut a young basalt flow (2 to 5 Ma; Gilbert et al. [1968] and Crowder et al. [1972]) that is considered to be younger than the main movement on the Coaldale fault. The elongate east-west outcrop of the basalt (Plate 1, locations 3 to 5) is compatible with the idea of eruption along a continuation of the Coal-dale fault zone. The inferred follows a conspicuous east trending aeromagnetic anomaly in the Montgomery Pass-Adobe Hills area [Ekren et al., 1976], and this may in part indicate buried feeder systems for the basalt.

West of the Adobe Hills area, the Coaldale fault zone, if it exists, lies below Quaternary alluvial deposits. The fault zone may extend as far west as the Sierra Nevada, judging by the distribution of Paleozoic rocks discussed below, but such a continuation is not evident in surface geology. It may curve slightly to the north and join a system of northwest trending faults farther west (westernmost part of the area shown in Plate 1). The trends of surface faults and the distribution of pre-Tertiary rocks indicate that the Coaldale fault zone does not join with the east-northeast lineament in the Sierra Nevada described by Albers [1981].

Excelsior Fault Zone

A system of east trending faults along the south side of the Excelsior Mountains is here named the Excelsior fault zone. The fault zone extends along the base of the steep southern face of the Excelsior Mountains (Plate 1, location 6), where, in some places, it forms the boundary between Paleozoic to Cenozoic rocks on the north

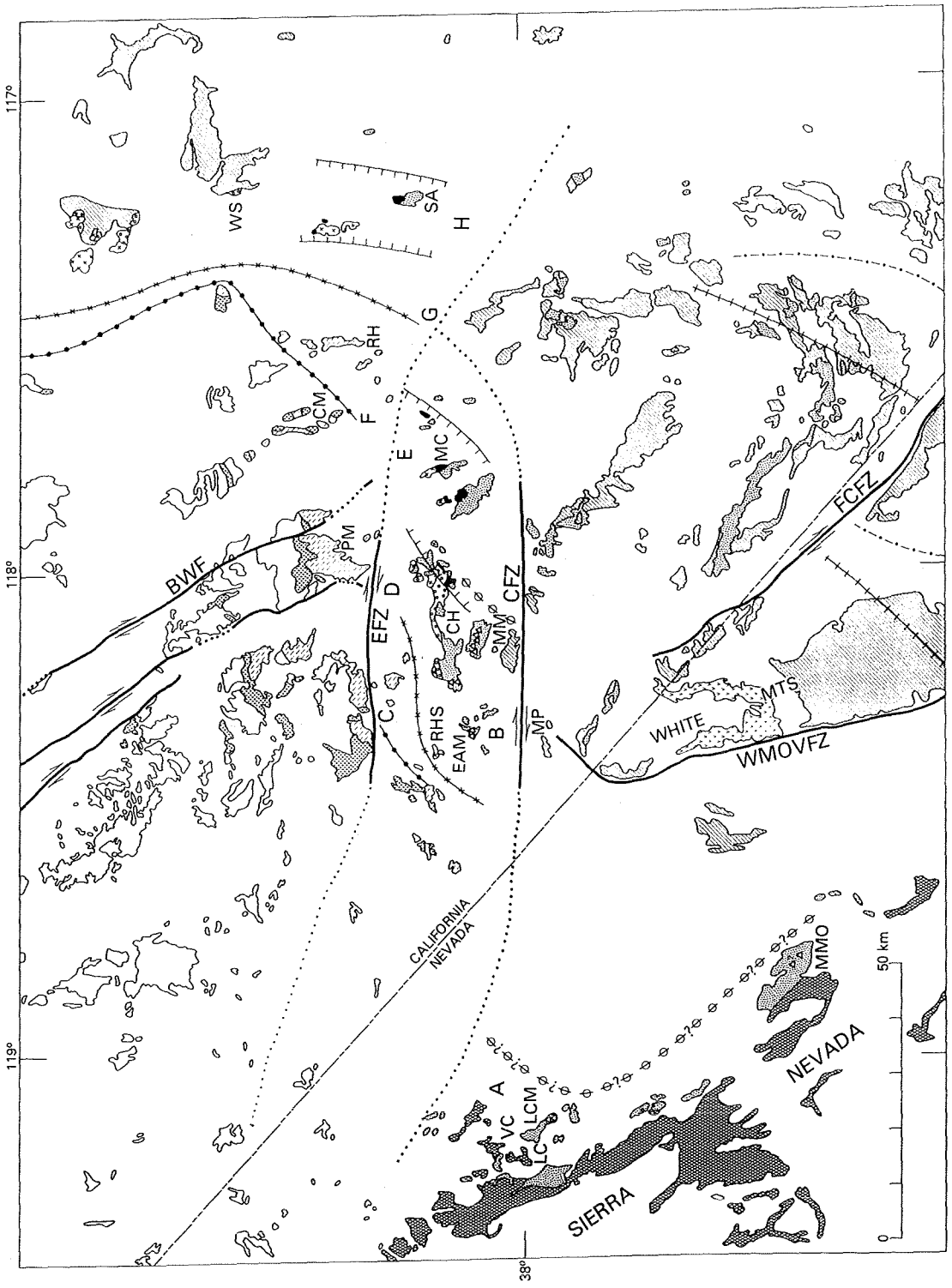
117°
118°
119°
39°
WS
SA
H
G
RH
CM
F
E
MC
PM
BWF
D
EFZ
CH
MM
CFZ
C
RHS
EAM
B
MP
FCFZ
WHITE
MTS
WMOVFZ
CALIFORNIA
NEVADA
A
VC
LCM
LC
SIERRA
MMO
NEVADA
50 km
0

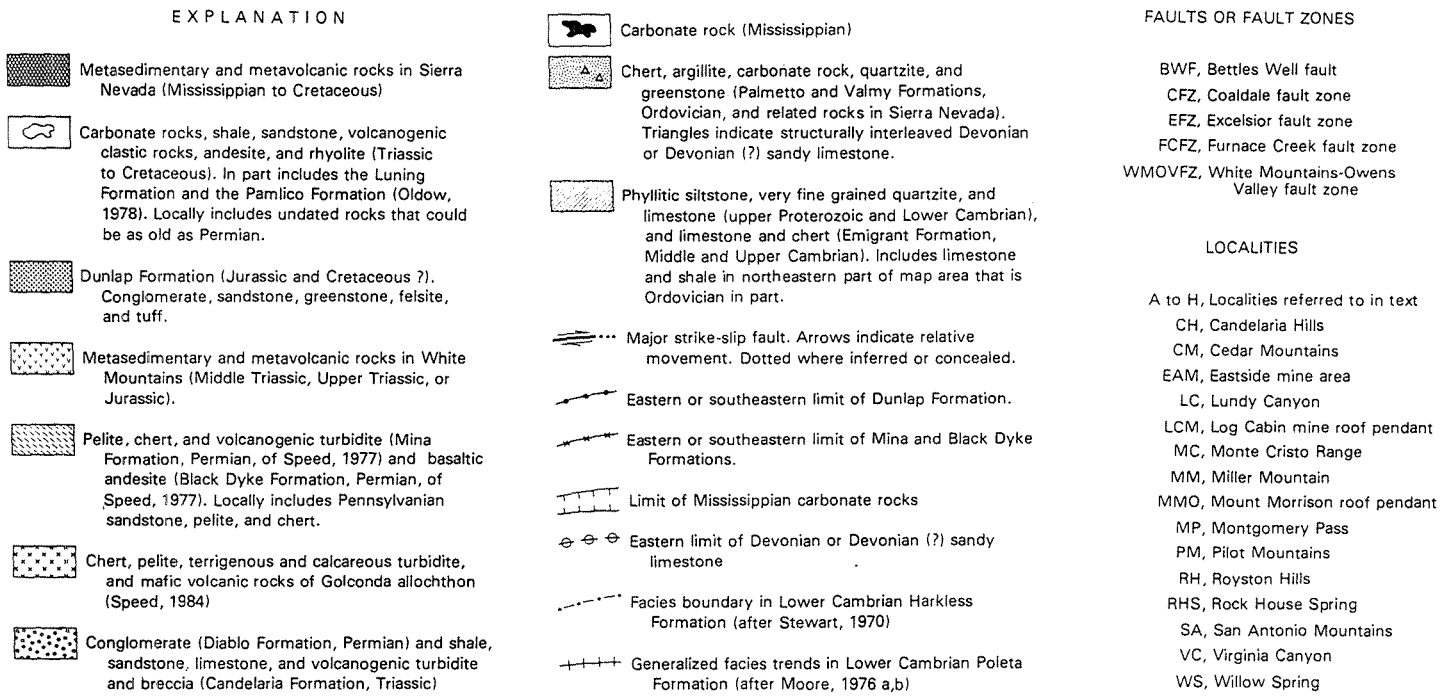

Fig. 2. Map showing distribution of pre-Tertiary rocks in eastern California and western Nevada. Compiled mainly from same sources listed in Plate 1 with additions from Speed [1984] and R. A. Schweickert (written communication, 1984).

and Quaternary alluvium on the south [Garside, 1982a, b; Stewart et al., 1982; Dohrenwend, 1982a, b] and, in other places, cuts Quaternary alluvium. East of the Excelsior Mountains, it forms the northern boundary (Plate 1, location 7) of outcrops of Cenozoic volcanic rocks and Quaternary and (or) Tertiary gravel deposits [Garside, 1982a; Dohrenwend, 1982a, b]. Farther east (Plate 1, location 8) it cuts Cenozoic sedimentary deposits and Quaternary or Tertiary gravels south of the Pilot Mountains (J. H. Stewart, unpublished field mapping, 1983). In the northwest part of the Monte Cristo Range a few faults are included in the Excelsior fault zone (Plate 1, location 9), but elsewhere in the range the zone cannot be traced on the basis of surface faults.

Within the Monte Cristo Range, however, a diffuse band of Late Cenozoic silicic extrusive and shallow intrusive rocks and a conspicuous outcrop of basalt and basaltic andesite (Plate 1, location 10) both are elongate east-southeast and are on line with the Excelsior fault zone. These are here considered to be intrusions and flows that were erupted along the fault zone. Many individual intrusive masses (not separated on Plate 1) within the silicic igneous band are also elongated east-southeast, further suggesting that intrusion was along a zone having that trend.

The distribution of several other Cenozoic units in the Monte Cristo Range is also in accord with an inferred major structural zone that crosses the northern part of the range. For example, andesitic rocks are widespread in the southern part of the range but generally terminate along the inferred Excelsior fault zone. Sedimentary rocks, on the other hand, are thin in the southern part of the range and thicken abruptly across the inferred fault zone. Finally, sedimentary rocks in the basalt and basaltic andesite unit are cut in at least one place by syndepositional faults that appear to be on line with the Excelsior fault zone.

Continuation of the Excelsior fault zone east of the Monte Cristo Range is uncertain. I propose here that it extends southeastward through the northernmost part of the Lone Mountain area and into the San Antonio Mountains. Such a continuation is compatable with the distribution of Paleozoic rocks discussed below, and it is also suggested by continuation of the band of silicic extrusive and shallow intrusive rocks from the Monte Cristo Range to the northernmost part of the Lone Mountain area (Plate 1, locations 11 and 12) and to the San Antonio Mountains (Plate 1, location 13) [Bonham and Garside, 1979]. Dikes of silicic rocks in the Lone Mountain area trend east-southeast near locality 11 and south-southeast near locality 12. These trends suggest that a diffuse band of intrusive rocks is continuous in the subsurface from the Monte Cristo Range southeastward to the San Antonio Mountains, although this zone widens and is poorly defined in the San Antonio Mountains.

If the Excelsior fault zone trends southeastward in the San Antonio Mountains, it may continue along this trend and join a conspicuous zone of southeast trending faults and abundant silicic intrusive and extrusive rocks in the Cactus Range [Ekren et al., 1971], 40 km farther southeast. If, on the other hand, the trend of the Excelsior fault zone in the San Antonio Range is more nearly east trending, the fault zone could join with the Warm Springs lineament [Ekren et al., 1976], an east trending feature marked by topographic, structural, and stratigraphic discontinuities in central Nevada.

The western extent of the Excelsior fault zone is also uncertain. The fault zone does not appear to cut Cretaceous granitic rocks in the western part of the Excelsior Mountains [Stewart et al., 1982; John, 1983], but as described below (see "Age of offset"), the granitic rocks may post date the main movement on the fault zone. If so, the Excelsior fault zone may have originally extended farther west and may be part of a zone of west to west northwest faults, linear features, and hydrothermally altered rocks extending west from the Excelsior Mountains into easternmost California (the Sweetwater Mountains–Garfield Flat lineament of Rowan and Purdy [1984]).

OFFSETS ON FAULT ZONES BASED ON DISTRIBUTION OF PROTEROZOIC, PALEOZOIC, AND MESOZOIC ROCKS

The seemingly abrupt change in character of pre-Tertiary rocks across both the Coaldale and Excelsior fault zones is suggestive of major strike-slip movement that has juxtaposed rocks once more widely separated. The distribution of upper Proterozoic, Paleozoic, and Mesozoic rocks suggests from 60 to 80 km of right-lateral

offset on the Coaldale fault zone and from 45 to 55 km of right-lateral offset on the Excelsior fault zone (Figure 2).

Estimates of offset on the Coaldale fault zone are based on the distribution of Ordovician, Devonian, upper Paleozoic, and Triassic rocks. A distinctive sequence of quartzofeldspathic hornfels, calc-silicate hornfels, sandy limestone, and quartzite in the Log Cabin mine roof pendant in the Sierra Nevada region [Kistler, 1966] may be offset from lithologically similar rocks on the north side of the Coaldale fault zone in Nevada. A graptolite in the sequence in the Log Cabin mine roof pendant (collected at NW 1/4, NW 1/4, SE 1/4 section 17, T. 1 N., R. 26 E.) was examined by R. J. Ross, Jr., (written communication, 1979) who states that the specimen is definitely a graptolite but that it cannot be precisely identified because of poor preservation. He indicates that it is Early Ordovician to Early Devonian in age, but favors a Middle to Late Ordovician age. Lithologically similar and paleontologically dated Ordovician and possibly Silurian rocks also occur in the Mountain Morrison roof pendant in the Sierra Nevada [Rinehart and Ross, 1964; Figure 2]. Rocks associated with the possible Ordovician rocks in the Log Cabin mine roof pendant are undated, but include distinctive sandy limestone beds, consisting of fine to coarse sand grains in a calcareous matrix. The sandy limestone occurs in massive layers from 1 m to 10 m thick interstratified with fine crystalline laminated and cross-stratified limestone locally containing slump structures. Cross-stratified calcareous sandstone [Rinehart and Ross, 1964] in the Mount Morrison roof pendant is somewhat similar to the sandy limestone in the Log Cabin mine roof pendant and may be correlative. The sequence in the Log Cabin mine roof pendant is remarkably similar to paleontologically dated Ordovician gratolite-bearing phyllitic shales and Devonian cross-stratified sandy limestone in the Eastside mine [Stewart, 1981b] and Miller Mountain area [Stanley et al., 1977; Stewart, 1979], suggesting 70 km of offset (A to B, Figure 2) on the Coaldale fault zone.

In the Sierra Nevada, regional correlation of rocks younger than Ordovician to Devonian(?) sequences described above is uncertain. These younger strata consist of a thick succession of Mississippian(?) to Cretaceous metasedimentary and metavolcanic rocks (Figure 2). Nokleberg [1983] has suggested that a major fault near the Log Cabin mine roof pendant separates these younger rocks from the Ordovician and, as here recognized, possible Devonian rocks. R. A. Schweickert (written communication, 1984), on the other hand, suggests that the younger rocks unconformably overlie the Ordovician and Devonian(?) rocks. If they do indeed occur in the same succession as the older rocks, they may correlate with or be a lateral facies of rocks in Nevada. A unit 1 km to 2 km thick of quartzofeldspathic siltstone and fine sandstone in Lundy and Virginia Canyons, 5 to 15 km west to northwest of the Log Cabin mine area, may correlate [Schweickert and Lahren, 1984] with the Lower Triassic Candelaria Formation of Candelaria Hills area of western Nevada. The Candelaria Formation is also recognized near Willow Springs (Figure 2), but rocks originally mapped as Candelaria Formation near Rock House Spring (Figure 2) [Ferguson and Muller, 1949; Stewart, 1984; Stewart et al., 1984] are now thought be Mississippian to Lower Triassic rocks of the Golconda allochthon [Speed, 1984b, Figure 1b]. Offset of the Candelaria Formation in the Candelaria Hills from possibly related rocks at Virginia and Lundy Canyons is 60 to 80 km.

Although exact correlations await more detailed work, other units in the Mississippian(?) to Cretaceous sequence in the Sierra Nevada may correlate with units in western Nevada. Schweichert and Lahren [1984] suggest a close tie of the rocks in the Log Cabin mine-Virginia Canyon-Lundy Canyon region with rocks in Nevada north of the Coaldale fault zone, a suggestion that fits closely with the ideas presented here.

An upper Proterozoic and Cambrian sequence [Stewart, 1979; Moore, 1976a, b] on Miller Mountain north of the Coaldale fault zone appearas to be displaced relative to sections south of the fault zone, although an estimate of the amount cannot be made. The sequence consists of three formations (Campito, Poleta, and Harkless Formations) that are widely exposed south of the fault. The internal stratigraphy of the Poleta Formation [Moore, 1976a] and the faunal succession in the Harkless Formation (C. A. Nelson, in Stewart [1979]) in the Miller Mountain area are not the same as in areas to the south of the fault zone, where the Campito, Poleta, and Harkless are fairly uniform faunally and stra-

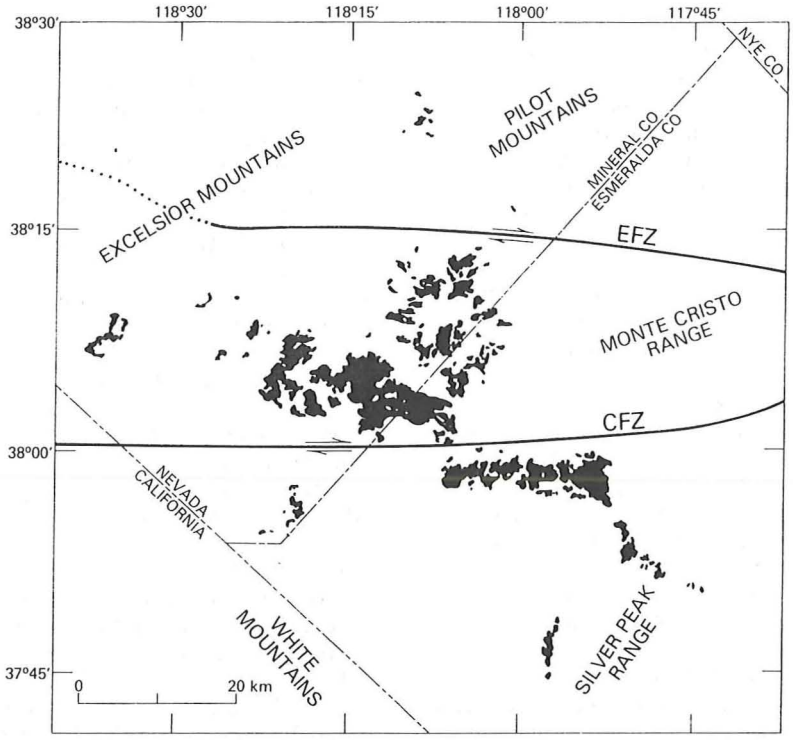

Fig. 3. Distribution of Upper Oligocene and Lower Miocene ash flow tuffs of the Candelaria Hills sequence. After Robinson and Stewart [1984]. Symbols: CFZ, Coaldale fault zone; EFC, Excelsior fault zone.

tigraphically. This change in lithic and faunal character may mean that the Miller Mountain area is offset relative to rocks to the south. An original position farther west is inferred, because sequences across the fault zone both to the south and southeast are in detail unlike those at Miller Mountain.

Similar to the Coaldale fault zone, the Excelsior fault zone also marks a seemingly abrupt change in the distribution of pre-Tertiary rocks. Such change is most evident in the region from the Pilot Mountains eastward to the southern Cedar Mountains and Royston Hills. Here the Permian Mina Formation of Speed [1977] occurs north of the fault zone whereas the main units south of the fault zone are Ordovician chert, argillite, and greenstone, and Mississippian carbonate rocks. Apparent offset of the Late Mississippian carbonate rock is about 45 km (E to H), of the Permian Mina and Black Dyke Formations of Speed [1977] about 50 km (D to G), and of the Jurassic and Cretaceous(?) Dunlap Formation about 55 km (C to F) (Figure 2).

AGE OF OFFSET

Most of the offset on the Coaldale and Excelsior fault zones is clearly older than late Oligocene because a sequence of upper Oligocene and lower Miocene ash flow tuffs [Robinson and Stewart, 1984] occurs on both sides of each fault zone (Figure 3). This sequence contains 17 ash flow units, several of which are recognized in all the major areas of outcrop of the sequence and on both sides of both fault zones. Some post-Oligocene and Miocene lateral offset of the units is possible, perhaps even in a left lateral sense, but right lateral offset on the order of that suggested by pre-Tertiary rocks (60 to 80 km on the Coaldale fault zone and 45 to 55 km on the Excelsior fault zone) is not indicated.

Wetterauer [1977], on the basis of a minimum age for folds that he related to the deflection of pre-Tertiary trends, suggested that the disruption of pre-Tertiary rocks in western Nevada was older than 69 Ma. This disruption is here con-

sidered to be mostly due to right-lateral strike-slip faulting along the Coaldale and Excelsior faults, but whether the folds that Wetterauer [1977] relates to the disruption are synchronous with the formation of these faults is uncertain. Geissman et al. [1984], based on paleomagnetic data from Cretaceous plutons and strata, concluded that little, if any, clockwise rotation (oroflexural folding) of rocks in the Mina region had occurred since mid-Cretaceous time, and thus that any such rotation must be older than mid-Cretaceous. The model presented here does not require oroflexural folding, although some is likely. If it did occur, and if it is related to the same stresses that produced the Coaldale and Excelsior faults, a pre-mid-Cretaceous age is established for these two faults.

Movement of the faults before mid-Cretaceous is also suggested by the continuity of plutons across the proposed westward continuations of the Excelsior and Coaldale fault zones. The 104-Ma granodiorite of Huntoon Valley [John, 1983, pluton 120] occurs both north and south of the proposed westward continuation of the Excelsior fault zone, and major Cretaceous plutons (mostly 80 to 95 Ma, John [1983]) in the Sierra Nevada do not appear to be disrupted by east-west strike-slip faults on line with the Coaldale fault zone.

Permian rocks of markedly different facies are juxtaposed along the Excelsior fault zone, indicating that most movement on that fault zone, and presumably also on the related Coaldale fault zone, is younger than Permian. The Upper Triassic Luning Formation and Pamlico Formation of Oldow [1978] and the Dunlap Formation, which is dated paleontologically as Early Jurassic but which may also contain rocks as young as Cretaceous [Speed, 1981], also appear to be disrupted by the fault zones. Thus faulting may be mainly younger than these formations as well. Alternatively, but probably less likely, these units, particularly the orogenic sediments [Ferguson and Muller, 1949] of the Dunlap Formation, could be syn- or post faulting and represent a product of the tectonic activity that produced the faults. If the major offset along the Coaldale and Excelsior fault zones was pre-Late Triassic (pre-Luning), then the Late Triassic and younger rocks in western Nevada and eastern California could have been deposited in an eastward embayment (the Luning Embayment of Ferguson and Muller [1949]). However, the apparent disruption of the Jurassic and Cretaceous (?) Dunlap Formation by the fault zones is more easily interpreted to mean that faulting was younger than the Dunlap Formation, rather than the Dunlap being syn- or post faulting.

In summary, major movement on the Coaldale and Excelsior fault zones appears to be pre-mid-Cretaceous in age because plutonic rocks of mid-Cretaceous or younger age are not cut by major strike-slip faults on line with the fault zones. Major movement is probably younger than the Early Jurassic to Cretaceous(?) Dunlap Formation. Thus major movement most likely occurred between Early Jurassic and mid-Cretaceous. Possibly the fault zones had an older history, and the Jurassic or Cretaceous offset followed older flaws in the Proterozoic basement rocks, but the sedimentary patterns of Proterozoic and Paleozoic rocks do not indicate the presence of such older tectonic features. Faults related to the Coaldale and Excelsior fault zones locally cut Cenozoic rocks, indicating a Cenozoic reactivation of the older fault systems.

REGIONAL PATTERN OF CENOZOIC FAULTS

The Coaldale and Excelsior fault zones, despite their presumed Mesozoic age, appear to disrupt the late Cenozoic fault pattern in eastern California and western Nevada (Figure 4). The White Mountain fault, the northern continuation of the Owens Valley fault, curves eastward and joins the Coaldale fault zone. It clearly does not extend across that fault zone. Farther east, the Furnace Creek fault zone which appears to have had about 80 km of right-lateral offset in the Death Valley region during the Cenozoic [Stewart, 1983], may have had only 30 to 40 km of offset in its northern part [Stewart, 1970]. Details of faulting near the northern end of the Furnace Creek fault zone are not clear, but young faults there [Albers and Stewart, 1972; Robinson and Crowder, 1973] appear to cover a broader area, fan out to the east, and die out before they reach the Coaldale fault zone.

Between the Coaldale and Excelsior fault zones, middle and late Cenozoic faults are oriented predominantly northeast to almost east. One of these faults, the Candelaria fault, has been studied in detail by Speed and Cogbill [1979] who indicate left-oblique motion on that fault. Such offset is not consistent with

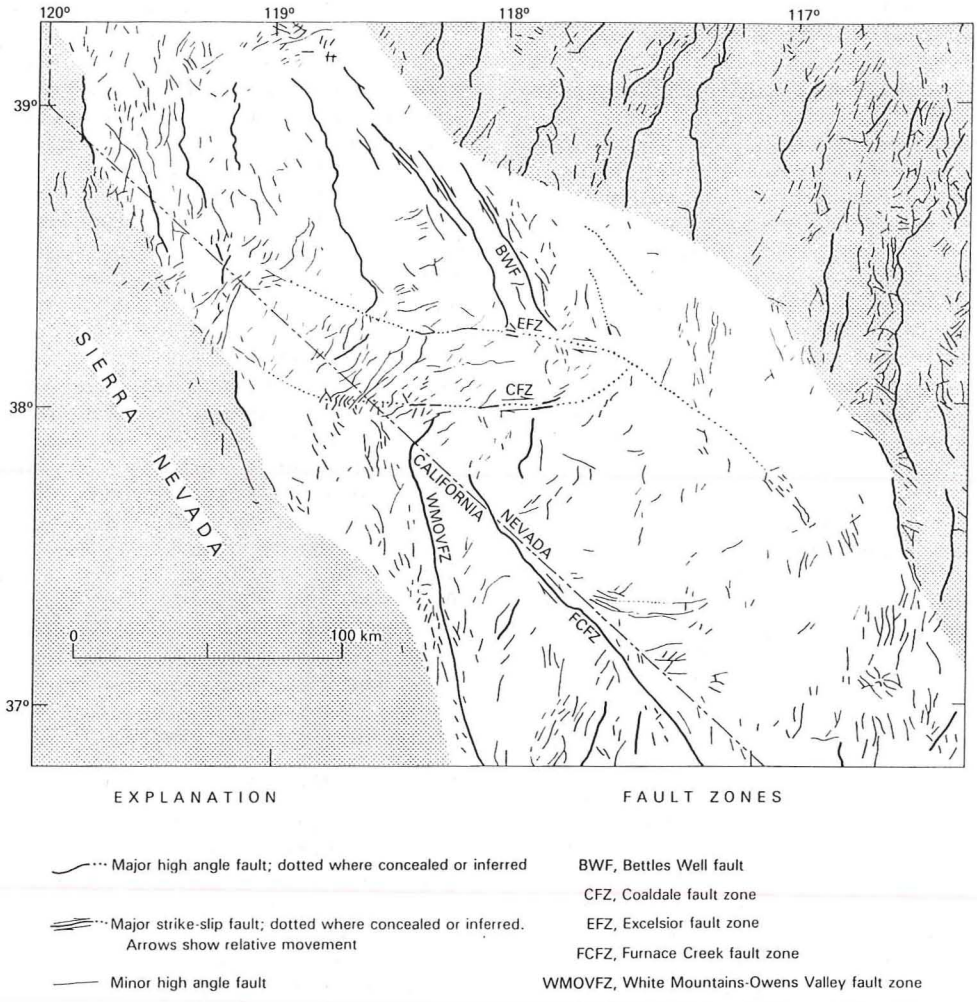

Fig. 4. Map showing major high angle faults in eastern California and western Nevada. Shaded patterns show, in west, stable block of Sierra Nevada and, in east, area of typical north northeast basin-range faults. Unshaded area is Walker Lane belt of diverse fault trends. Compiled mainly from same sources listed in Figure 2.

the right-lateral offset proposed here for the similarly oriented Coaldale and Excelsior faults. A possible explanation for this apparent inconsistency, is that the original movement on these faults was right-lateral, but that late Cenozoic movement following the same fault breaks was left-lateral in response to a different stress orientation. The possible left-lateral offset of upper Oligocene and lower Miocene tuffs (Figure 3) may have a similar explanation.

To the north of the Excelsior fault zone a system of north-northwest faults, the Bettles Well and related faults, has a combined right-lateral offset during the late Cenozoic of possibly 32 km [Hardyman et al., 1975; Ekren et al., 1980]. These faults die out southward near the Excelsior fault zone. Several faults (Plate 1 and Figure 4) curve westward as they approach the Excelsior fault zone from the north.

Major movement on northwest trending faults such as the Furnace Creek fault zone and Bettles Wells fault may have occured in the late Cenozoic [Hardyman et al., 1975; Ekren et al., 1980; Stewart, 1983], but present information does not preclude the possibility of initial movement on these faults during the Mesozoic [Albers, 1967; Buckley, 1974]. Thus the

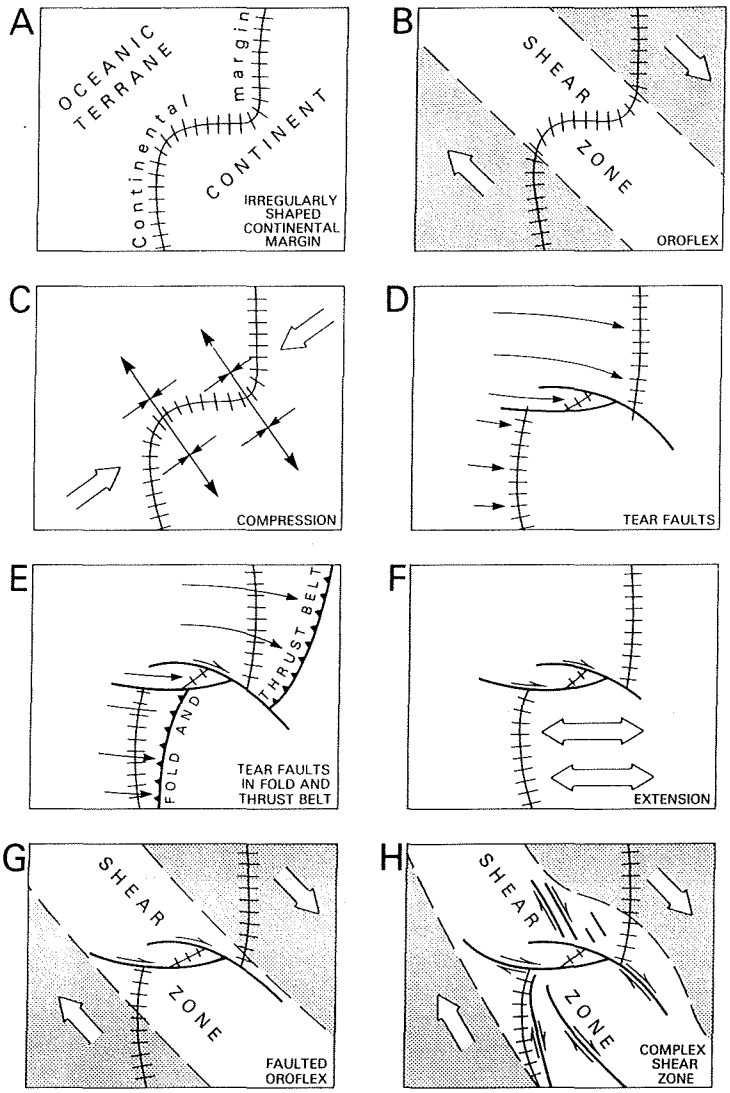

Fig. 5. Models of the paleogeographic and tectonic setting of eastern California and western Nevada. Line with cross-hatch pattern shows trend of sedimentary facies. Heavy lines are faults; arrows show relative movement. Large arrows show relative movement of large blocks. Stippled pattern indicates relatively unsheared blocks.

northwest trending faults (or their ancestors) may be older than, and offset by, the Coaldale and Excelsior right-lateral faults zones. This interpretation is supported by the apparent right-lateral displacement of the zone of northwest trending faults across the Coaldale and Excelsior fault zones, from the system containing the Furnace Creek fault on the south to the system containing the Bettles Well fault on the north. In addition, the eastward curve of northwest trending faults as they approach the Coaldale fault zone from the south and westward curve of faults as they approach the Excelsior fault zone from the north, can be related to drag of the older faults system along the right-lateral Coaldale and Excelsior fault zones. The apparent right-lateral offset of the northwest-trending right-lateral system (Furnace Creek and related faults) south of the Coaldale fault zone to the system (Bettles Well and related faults) north of the Excelsior fault zone is about 60 km, if supposed drag at the northern end of the Furnace Creek fault

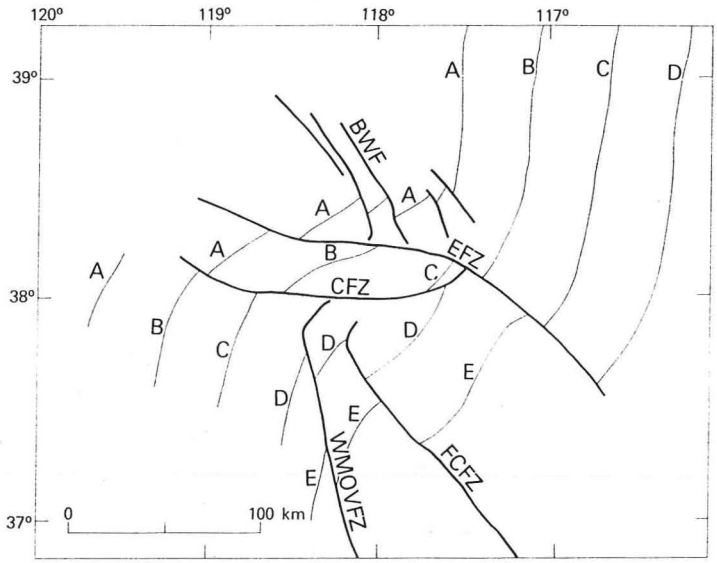

Fig. 6. Interpretive map showing style of deformation related to Coaldale and Excelsior fault zones. Letters indicate lines that were originally linear.

zone is removed, whereas right-lateral offset on the Coaldale and Excelsior fault zones based on the distribution of pre-Cenozoic rocks is 105 to 135 km (60 to 80 km on the Coaldale fault zone and 45 to 55 on the Excelsior fault zone). Thus if the Coaldale and Excelsior fault zones do indeed offset older northwest-trending faults, then either (1) the northwest trending faults south of the Coaldale fault zone were not originally continuous with those north of the Excelsior fault zone, (2) the estimates of right-lateral offset based on the distribution of pre-Tertiary rocks are too high, or (3) the Furnace Creek fault zone, as well as the White Mountain-Owens Valley fault zone, must correlate with hidden northwest trending faults east of the Bettles Well fault, or the Bettles Well and related faults must correlate with hidden faults west of the White Mountain-Owens Valley fault zone.

If the northwest trending faults are Mesozoic, they must have been reactivated in late Cenozoic time to account for the observed right-lateral displacements of Late Cenozoic rocks along these faults. Such late Cenozoic right-lateral movement may have distorted the presumably originally linear Excelsior fault zone into it present curving trace.

DISCUSSION

Several significantly different paleogeographic and tectonic models have been proposed to explain the change in distribution patterns and facies trends of Proterozoic, Paleozoic, and Mesozoic rocks in eastern California and western Nevada. Perhaps the simplest model, as noted above, is that the continental margin originally was irregular (Figure 5a) as a result of a complex pattern of Late Proterozoic rifting [Oldow, 1982, 1983, 1984a, b; Oldow and Geissman, 1982; Geissman et al., 1984]. Other models depend on tectonic distortion of originally nearly straight facies or distribution trends. Albers [1967] proposed that the trends were disrupted by large scale folding or drag (oroflexural folding) in an area of dextral shear (Figure 5b), whereas Wetterauer [1977] proposed that the distortion is due to crustal-scale folding produced by compression (Figure 5c). Other possibilities are that

Pass

in

r fault
[1982],

the distortion is due to tear faults in the continental margin (Figure 5d), tear faults in a fold and thrust belt (Figure 5e), or faults resulting from greater extension on the south sides of the faults than on the north sides (Figure 5f). Finally, the distortion may be due to oroflexural folding in combination with east-west right-lateral faulting (Figure 5g) or to a complex shear system with oroflexural folding and right-lateral faulting along east-west as well as north to northwest trends (Figure 5, 6).

By themselves, the facies patterns of pre-Cenozoic rocks in eastern California and western Nevada could be interpreted as reflecting deposition along an irregularly shaped continental margin, but the coincidence of the apparent disruption in trends of pre-Cenozoic rocks with the mapped Coaldale and Excelsior fault zones is highly suggestive that these facies trends were disrupted by faulting and do not reflect original depositional patterns. Oldow [1984b], however, has argued that the anomalous facies patterns developed along a promontory in the continental margin and are not due to oroflexural folding. He sites as evidence that fold orientations related to the mid-Paleozoic Antler orogeny in areas of supposed oroflexural folding have the same orientation as Antler folds outside areas of postulated oroflexural folding. Oldow's interpretation, however, does not argue against the idea presented here because much of the proposed distortion may be due to dextral faulting rather than to oroflexural folding.

The unusual trends of Proterozoic, Paleozoic, and Mesozoic rocks, deviating significantly from the dominant region north-south grain, are restricted to the Walker Lane belt (Figure 1) which is characterized by right lateral faults and oroflexural folding extending from southern Nevada to northeastern California [Albers, 1967; Stewart et al., 1968]. This spatial association suggests that the unusual trends described here are the result of some kind of tectonic distortion in the Walker Lane belt as indicated by models b, g, and h (Figure 5). Only models g and h show the east trending faults recognized here. In model g, northwest trending faults (not shown on Figure 5g) can be considered to develop subsequent to the east trending faults and to abut against, and terminate at, the east trending faults. In model h, the northwest trending faults are considered older than, and are truncated by, the east trending faults. Possibly, initial shear in the Walker Lane belt developed northwest trending right-lateral faults and a later "kink" in this system produced oroflexural folding and east trending right-lateral faults. This "kink" may have resulted from a change in the stress regime and structural complexities where the shear zone obliquely crossed the Paleozoic continental margin.

Acknowledgments. I wish to thank J. P. Albers, P. C. Bateman, L. J. Geissman, J. S. Oldow, J. M. Profett, Jr., R. A. Schweickert, D. B. Snyder, W. S. Snyder, R. C. Speed, and M. L. Zoback for helpful discussions and comments on the manuscript.

REFERENCES

Albers, J. P., Belt of sigmoidal bending and right-lateral faulting in the western Great Basin, Geol. Soc. Am. Bull., 78(2), 143-155, 1967.

Albers, J. P., A lithologic-tectonic framework for the metallogenic provinces of California, Econ. Geol., 76(4), 765-790, 1981.

Albers, J. P., and J. H. Stewart, Geology and mineral deposits of Esmeralda County, Nevada, Nev. Bur. Mines Geol. Bull., 78, 80 pp., 1972.

Bonham, H. F., Jr., and L. J. Garside, Geology of the Tonopah, Lone Mountain, Klondike, and northern Mud Lake quadrangles, Nevada, Nev. Bur. Mines Geol. Bull., 92, 142 pp., 1979.

Buckley, C. P., Interpretation of Mesozoic displacement along the Furnace Creek fault, Fish Lake Valley, Nevada, Geol. Soc. Am. Abstr. Programs, 6(3), 149-150, 1974.

Crowder, D. F., P. T. Robinson, and D. L. Harris, Geologic map of the Benton Quadrangle, Mono County, California, and Esmeralda and Mineral Counties, Nevada, scale 1:62,500, Geol. Quad. Map GQ-1013, U.S. Geol. Surv., Reston, Virginia, 1972

Dohrenwend, J. C., Surficial geologic map of the Walker Lake 1° by 2° quad-rangle, Nevada-California, scale 1:250,000, Map MF-1382-C, U.S. Geol. Surv., Reston, Virginia, 1982a.

Dohrenwend, J. C., Map showing late Cenozoic faults in the Walker Lake 1° by 2° quadrangle, Nevada-California, scale 1:250,000, Map MF-1382-D, U.S. Geol. Surv., Reston, Virginia, 1982b.

Ekren, E. B., R. E. Anderson, C. L. Rogers, and D. C. Noble, Geology of northern Nellis Air Force Base Bombing and Gunnery Range, Nye County, Nevada, U.S. Geol. Surv. Prof. Pap., 651, 91 pp., 1971.

Ekren, E. B., R. C. Bucknam, W. J. Carr, G. L. Dixon, and W. D. Quinlivan, East-trending structural lineaments in central Nevada, U.S. Geol. Surv. Prof. Pap., 986, 16 pp., 1976.

Ekren, E. B., F. M. Byers, Jr., R. F. Hardyman, R. F. Marvin, and M. L. Silberman, Stratigraphy, preliminary petrology, and some structural features of Tertiary volcanic rocks in the Gabbs Valley and Gillis Ranges, Mineral County, Nevada, U.S. Geol. Surv. Bull., 1464, 54 pp., 1980.

Ferguson, H. G., and S. W. Muller, Structural geology of the Hawthorne and Tonopah quadrangles, Nevada, U.S. Geol. Surv. Prof. Pap., 216, 55 pp., 1949.

Garside, L. J., Geologic map of the Camp Douglas quadrangle, Nevada, scale 1:24,000, Map 63, Nev. Bur. of Mines and Geol., Reno, Nev., 1982a.

Garside, L. J., Geologic map of the Moho Mountain quadrangle, Nevada, scale 1:24,000, Map 74, Nev. Bur. of Mines and Geol., Reno, Nev., 1982b.

Geissman, J. W., J. T. Callian, J. S. Oldow, and S. E. Humprhries, Paleomagnetic assessment of oroflexural deformation in west-central Nevada and significance for emplacement of allochthomous assemblages, Tectonics, 3(2), 179-200, 1984.

Gilbert, C. M., M. N. Christensen, Y. Al-Rawi, and K. R. Lajoie, Structure and volcanic history of Mono Basin, California-Nevada, Studies in Volcanology--A Memoir in Honor of Howel Williams, Mem. Geol. Soc. Am., 116, 275-329, 1968.

Hardyman, R. F., E. B. Ekren, and F. M. Byers, Jr., Cenozoic strike-slip, normal, and detachment faults in northern part of Walker Lane, west-central Nevada, Geol. Soc. Am. Abstr. Programs 7(7), 1100, 1975.

Jennings, C. W., Geologic map of California, scale 1:750,000, Calif. Geol. Data Map Ser., Calif. Div. of Mines and Geol., Sacramento, Calif., 1977.

John, D. A., Map showing distribution, ages, and petrographic characteristics of Mesozoic plutonic rocks in the Walker Lake 1^{o} x 2^{o} quadrangle, California and Nevada, scale 1:250,000, Map MF-1382-B, U.S. Geol. Surv., Reston, Virginia, 1983.

Kistler, R. W., Geologic map of the Mono Craters quadrangle, Mono and Tuolumne Counties, California, scale 1:62,500, Geol. Quad. Map GQ-462, U.S. Geol. Surv., Reston, Virginia, 1966.

Krauskopf, K. B., and P. C. Bateman, Geologic map of the Glass Mountain quadrangle, Mono County, California, and Mineral County, Nevada, scale 1:62,500, Geol. Quad. Map GQ-1099, U.S. Geol. Surv., Reston, Virginia, 1977.

Moiola, R. J., Late Cenozoic geology of the northern Silver Peak region, Ph.D. thesis, 139 pp., Univ. of Calif., Berkeley, 1969.

Moore, J. N., The Lower Cambrian Poleta Formation: A tidally dominated, open coastal and carbonate bank depositional complex, western Great Basin, Ph.D. thesis, 284 pp., Univ. of Calif., Los Angeles, 1976a.

Moore, J. N., Depositional environments of the Lower Cambrian Poleta Formation and its stratigraphic equivalents, California and Nevada, Brigham Young Univ. Geol. Stud., 23, part 2, 23-38, 1976b.

Moore, S. W., Geology of a part of the southern Monte Cristo Range, Esmeralda County Nevada, M.S. thesis, 157 pp., San Jose State Univ., Calif., 1981.

Nokleberg, W. J., Wallrocks of the central Sierra Nevada batholith, California: A collage of accreted tectono-stratigraphic terranes, U.S. Geol. Surv. Prof. Pap., 1255, 28 pp., 1983.

Oldow, J. S., Triassic Pamlico Formation--An allochthonous sequence of volcanogenic-carbonate rocks in west-central Nevada, Mesozoic Paleogeography of the Western United States, edited by D. G. Howell and K. A. McDougall, Soc. Econ. Paleontol. Mineral. Pac. Sect., Pac. Coast Paleogeogr. Symp. 2, 223-235, 1978.

Oldow, J. S., Spatial variability in the structure of the Roberts Mountains allochthon, western Nevada (abstract), Geol. Soc. Am. Abstr. Program, 14, 579 pp., 1982.

Oldow, J. S., Tectonic implications of a late Mesozoic fold and thrust belt in northwestern Nevada, Geology, 11, 542-546, 1983.

Oldow, J. S., Evolution of a late Mesozoic back-arc fold and thrust belt, northwestern Great Basin, USA, Tectonophysics, 102, 245-274, 1984a.

Oldow, J. S., Spatial variability in the structure of the Roberts Mountains allochthon, western Nevada, Geol. Soc. Am. Bull., 95(2), 174-185, 1984b.

Oldow, J. S., and J. W. Geissman, Oroflexural deformation in west-central Nevada reassessed: Evidence from paleomagnetic data (abstract), Eos Trans. AGU, 63, 309 pp., 1982.

Rinehart, C. D., and D. C. Ross, Geology and mineral deposits of the Mount Morrison quadrangle, Sierra Nevada, California, A Gravity Study of Long Valley by L. C. Pakiser, U.S. Geol. Surv. Prof. Pap., 385, 106 pp., 1964.

Robinson, P. T., and D. F. Crowder, Geologic map of the Davis Mountain quadrangle, Esmeralda and Mineral Counties, Nevada, and Mono County, California, scale 1:62,500, Geol. Quad. Map GQ-1078, U.S. Geol. Surv., Reston, Virginia, 1973.

Robinson, P. T., and J. H. Stewart, Uppermost Oligocene and lowermost Miocene ash flow tuffs of western Nevada, U.S. Geol. Surv. Bull., 1557, 53 pp., 1984.

Robinson, P. T., J. H. Stewart, R. J. Moiola, and J. P. Albers, Geologic map of the Rhyolite Ridge quadrangle, Esmeralda County, Nevada, scale 1:62,500, Geol. Quad. Map GQ-1325, U.S. Geol. Surv., Reston, Virginia, 1976.

Rowan, L. C., and T. L. Purdy, Map of the Walker Lake 1^{o} by 2^{o} quadrangle, California and Nevada showing the regional distribution of linear features, scale 1:250,000, Map MF-1382-P, U.S. Geol. Surv., Reston, Virginia, 1984.

Schweickert, R. A., and M. M. Lahren, Extent of Antler and Sonoma belts, sutures, and transcurrent faults in eastern Sierra Nevada, California, Geol. Soc. Am. Abstr. Programs, 16(6), 648 pp., 1984.

Speed, R. C., Excelsior Formation, west central Nevada: Stratigraphic appraisal, new divisions, and paleogeographic interpretations, Paleozoic Paleogeography of the Western United States, edited by J. H. Stewart, C. H. Stevens, and A. E. Fritsche, Soc. Econ Paleontol. Mineral. Pac. Sec., Pac. Coast Paleogeogr. Symp. 1, 325-336, 1977.

Speed, R. C., Preliminary geologic map of the Sodaville quadrangle, Mineral County, Nevada, scale 1:24,000, Map MF 1300, U.S. Geol. Surv., Reston, Virginia, 1984a.

Speed, R. C., Paleozoic and Mesozoic continental margin collision zone features: Mina to Candelaria, Nevada, traverse, in Western Geological Excursions, Geological Society of America, 1984, Annual Meetings, Reno, Nevada, vol. 4, edited by Joseph Lintz, Jr., 66-80, Geological Society of America, Boulder, Colo., 1984b.

Speed, R. C., and A. H. Cogbill, Candelaria and other left-oblique slip faults of the Candelaria region, Nevada, Geol. Soc. Am. Bull., 90, part 1, 149-163, 1979.

Stanley, K. O., C. K. Chamberlain, and J. H. Stewart, Depositional setting of some eugeosynclinal Ordovician rocks and structurally interleaved Devonian rocks in the Cordilleran mobile belt, Nevada, Paleogeography of the Western United States, edited by J. H. Stewart, C. H. Stevens, and A. E. Fritsche, Soc. Econ. Paleontol. Mineral. Pac. Sect., Pac. Coast Paleogeogr. Symp. 1, 259-274, 1977.

Stewart, J. H., Upper Precambrian and Lower Cambrian strata in the southern Great Basin, California and Nevada, U.S. Geol. Surv. Prof. Pap., 620 206 pp., 1970.

Stewart, J. H., Geologic map of Miller Mountain and Columbus quadrangles, Nevada, scale 1:24,000, OF Rep. 79-1145, U.S. Geol. Surv., Reston, Virginia, 1979.

Stewart, J. H., Geologic map of the Jacks Spring quadrangle, Mineral County, Nevada, scale 1:24,000, OF Rep. 81-368, U.S. Geol. Surv., Reston, Virginia, 1981a.

Stewart, J. H., Geologic map of the Basalt quadrangle, Mineral County, Nevada, scale 1:24,000, OF Rep. 81-369, U.S. Geol. Surv., Reston, Virginia, 1981b.

Stewart, J. H., Extension tectonics in the Death Valley area, California: Transport of the Panamint Range structural block 80 km northwestward, Geology, 11, 153-157, 1983.

Stewart, J. H., Geologic map of the Teels Marsh quadrangle, Mineral County, Nevada, scale 1:24,000, OF Rep. 84-504, U.S. Geol. Surv., Reston, Virginia, 1984.

Stewart, J. H., and J. E. Carlson, Geologic map of Nevada, scale 1:500,000, U.S. Geol. Surv., Reston, Virginia, 1978.

Stewart, J. H., J. P. Albers, and F. G. Poole, Summary of regional evidence for right-lateral displacement in the western Great Basin, Geol. Soc. Am. Bull., 79, 1407-1414, 1968.

Stewart, J. H., J. E. Carlson, and D. C. Johannesen, Geologic map of the Walker

Lake 1° by 2° quadrangle, California and Nevada, scale 1:250,000, Map MF-1382-A, U.S. Geol. Surv., Reston, Virginia, 1982.

Stewart, J. H., F. J. Kleinhampl, R. C. Speed, and D. C. Johannesen, Geologic map of the Little Huntoon Valley quadrangle, Mineral County, Nevada, scale 1:24,000, OF Rep. 84-503, U.S. Geol. Surv., Reston, Virginia, 1984.

Wetterauer, R. H., The Mina deflection--A new interpretation based on the history of the Lower Jurassic Dunlap Formation, western Nevada, Ph.D. thesis, 155 pp., Northwestern Univ., Evanston, Ill., 1977.

J. H. Stewart, U.S. Geological Survey, Menlo Park, CA 94025

(Received February 8, 1985;
revised May 10, 1985;
accepted May 13, 1985)

ECONOMIC GEOLOGY

AND THE

BULLETIN OF THE SOCIETY OF ECONOMIC GEOLOGISTS

VOL. 89 JUNE–JULY, 1994 NO. 4

Gold Mineralization and Fault Evolution at the Dixie Comstock Mine, Churchill County, Nevada

PETER G. VIKRE

ASARCO Incorporated, 510 East Plumb Lane, Reno, Nevada 89502

Abstract

Gold ore at the Dixie Comstock mine, Churchill County, Nevada, is composed of quartz breccia, quartz stockwork, incipiently crushed gabbro, and minor fault gouge. The ore zone forms a mullion within a range-bounding normal fault, the Dixie Comstock mine fault, which originated in the middle Miocene and separates Jurassic gabbro and Tertiary volcanic rocks of the Stillwater Range to the west from Quaternary colluvium of Dixie Valley to the east. Within the mullion, a potentially bulk mineable resource of several million tons grading ~0.06 oz of gold per ton has been defined by drilling.

Within the fault zone, clasts of gabbro in quartz breccia, quartz stockwork gabbro, and incipiently crushed gabbro are altered to quartz, sericite, chlorite, montmorillonite, and sulfides. Gold occurs as electrum in quartz that cements quartz breccia, in quartz stockwork veins with quartz, pyrite, chalcopyrite, and montmorillonite in breccia clasts, and in veins in incipiently crushed gabbro. Fluid inclusion microthermometry and stable isotope analyses of mineralized quartz matrix and two later stages of quartz and calcite show that ore fluid was 180°C, near-boiling meteoric water.

An inverse stratigraphy of thermal spring silica detritus in hanging-wall colluvium, microthermometry and isotopic compositions of fluid inclusion water from quartz breccia, a subjacent geothermal reservoir, and radiometric ages of hydrothermal minerals in the fault cumulatively support a mid-Pleistocene age for gold mineralization. The lower average displacement rate on the Dixie Comstock mine fault that is required by the age and thickness of eroded thermal spring sinter and underlying quartz breccia and stockwork, compared to higher recent displacement rates along range-bounding faults on the western side of Dixie Valley, suggests that the current pattern of temporal clustering of fault displacements began by the mid-Pleistocene.

Introduction

THE Dixie Comstock gold mine is situated on the eastern margin of the Stillwater Range, Churchill County, Nevada, about 110 mi east of Reno (Fig. 1). The range margin, which separates the Stillwater Range to the west from Dixie Valley to the east, is sharply curvilinear, locally very steep, and the site of several thermal springs and sinters associated with Pleistocene to historic Basin and Range faulting and geothermal resources (Wallace and Whitney, 1984; Hudson and Geissman, 1987, 1991; Slemmons and Bell, 1987; Waibel, 1987; Wallace, 1987; Bell and Katzer, 1990; Parry et al., 1991). The Basin and Range province of the western United States covers Nevada and parts of adjacent states and is characterized by thin crust, elevated heat flow, and active seismic belts in addition to the pattern of north-south-aligned, alternating mountain ranges and valleys (Wallace, 1984; Oldow, 1992).

The mine was discovered in 1934 by panning drainages along the Stillwater Range margin. It produced an estimated 4,600 oz of gold from 10,000 tons of ore during intermittent operation from 1938 to 1970. Ore grades reportedly ranged from 0.5 to 3.0 oz Au/ton and small pockets of >15 oz Au/ton ore were mined; all production took place within 100 ft of the present surface (Vanderburg, 1940; W. Wilson, pers. commun., 1985; D. Hargrove, pers. commun., 1986). Mined ore consists of fault breccia of the Dixie Comstock mine fault that has been filled in and replaced to varying degrees by quartz, hereafter referred to as quartz breccia. Recent exploration has shown that most gold is confined to a mullion within

0361-0128/94/1574/707-13$4.00

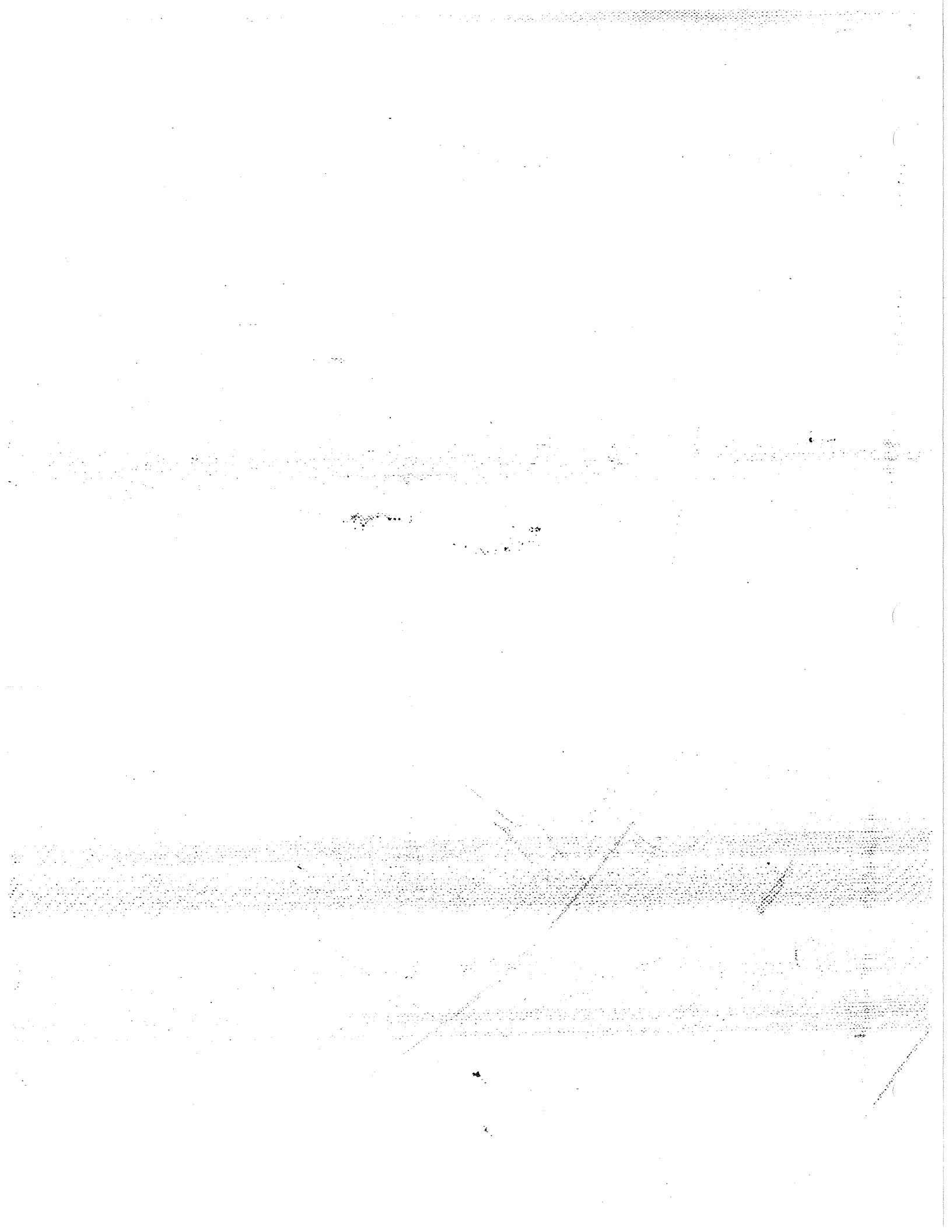

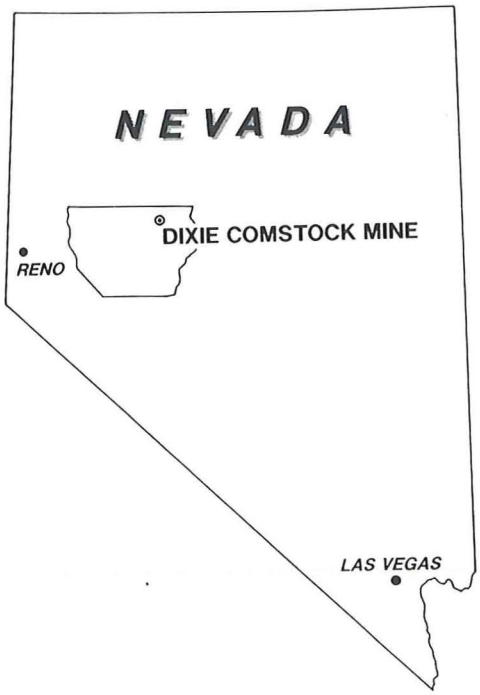

FIG. 1. Location map of the Dixie Comstock mine, Churchill County, Nevada.

the Dixie Comstock mine fault. Drilling by ASARCO Inc. in 1982 through 1984 defined an inventory of 1.8 million tons grading 0.058 oz Au/ton in the vicinity of old workings. Subsequent drilling of the same area by three other exploration companies resulted in similar resources.

This deposit is of geologic interest because of its close association with Basin and Range tectonism and geothermal activity, and proposed young age. The gold resource may be sufficiently voluminous to constitute a bulk deposit mineable by open pit.

Geology of the Mine Area

The Dixie Comstock mine fault separates footwall Jurassic and Tertiary rocks of the Stillwater Range from colluvium of Dixie Valley (Fig. 2). Jurassic rocks include coarse-grained hornblende gabbro and subordinate basalt, anorthosite, and albitite that compose the Humboldt lopolith (Page, 1965; Willden and Speed, 1974; Speed, 1976; Bell and Katzer, 1987). Along the steep scarp south from the mine is an alignment of small, irregular apophyses of an altered, granitic Cretaceous(?) intrusion (Table 1, sample DC89–5A) that contains quartz and pyrite stockwork veins in albitized carapaces (Fig. 2). Veins and lenses of calcite, barite, iron oxides, and copper sulfides in gabbro generally parallel the range margin and are associated with a colorful, sublinear array of light brown to white alteration zones that consist of quartz, albite, sericite, kaolinite, and iron oxide. Several of these alteration zones partially surround the granitic intrusion apophyses (Fig. 2) and all are probably related to them. The Late Cretaceous whole-rock

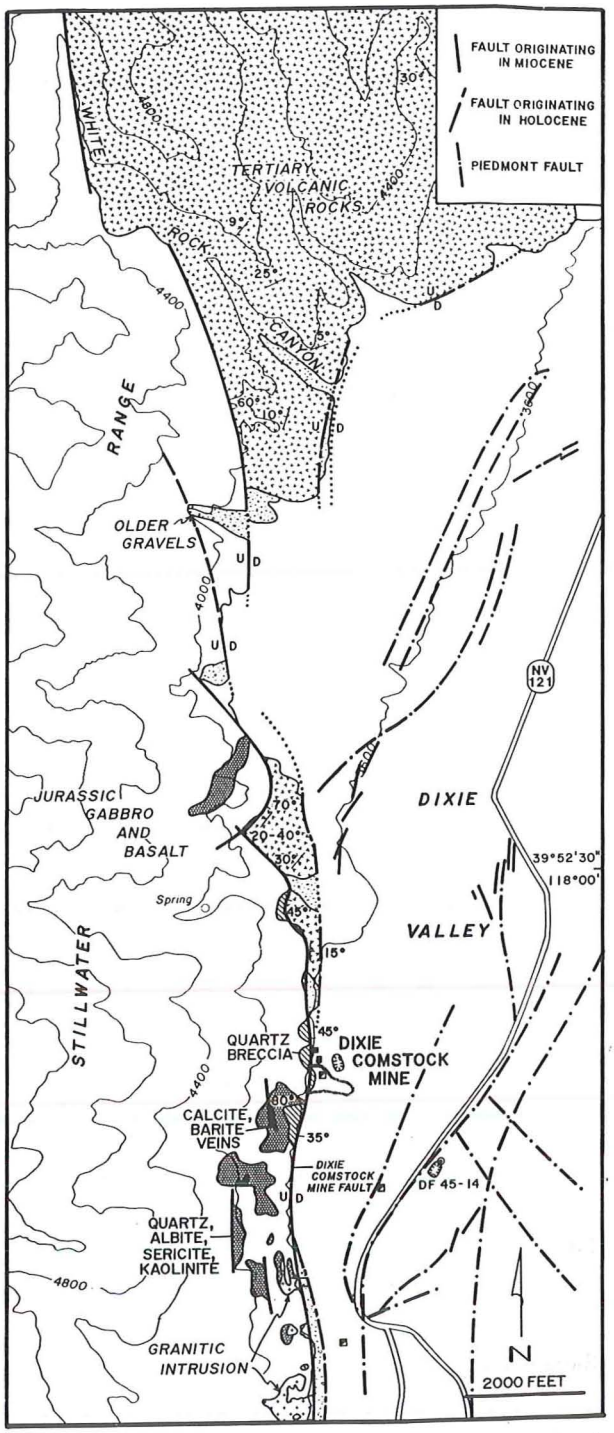

FIG. 2. Geologic map of the eastern Stillwater Range margin from the Dixie Comstock mine to White Rock Canyon. Dense dot patterns mark areas of quartz, albite, sericite, and kaolinite alteration of gabbro. Light dot pattern denotes terrace gravel deposits. Piedmont faults are interpreted from geophysical data and low-sun-angle photography (Bell et al., 1980). D = down, U = up.

TABLE 1. Radiometric Ages of Altered Rocks, Albite, and Calcite in the Vicinity of the Dixie Comstock Mine

Sample no.	Location	Mineral or rock dated	% $\overline{K_2O}$	$^{40}\overline{Ar}$ moles/g	$^{40}Ar/\Sigma^{40}Ar$%	Age (Ma)	Source
DC89-5A	1 mi S from Dixie Comstock mine portal	Albite from carapace of granitic intrusion	0.19	2.64495×10^{-11}	4.66	93.2 ± 7.8	1a
DC29-193	DDH, −193 ft, Dixie Comstock mine	Whole rock (altered gabbro)	1.08	1.1885×10^{-10}	62.6	74.9 ± 2.2	2
DC29-208.5	DDH, −208.5 ft, Dixie Comstock mine	Whole rock (sericitized gabbro)	6.24	1.354426×10^{-10}	65.2	15.0 ± 0.5	1a
DC29-210	DDH, −210 ft, Dixie Comstock mine	Whole rock (sericitized gabbro)	6.43	1.026935×10^{-10}	63.0	11.1 ± 0.3	1a
DC31-100.5	DDH, −100.5 ft, Dixie Comstock mine	Whole rock (sericitized gabbro)	2.11	4.1378×10^{-11}	60.0	13.6 ± 0.4	2
DC28-285	DDH, −285 ft, Dixie Comstock mine	Calcite (stage 3)	$^{234}U/^{238}U = 2.31 \pm 1.024$ $^{230}Th/^{234}U = 1.744 \pm 0.724$ $^{230}Th/^{232}Th = 12.2 \pm 4.5$			>0.35	1b

Sources: 1a, this paper, E.H. McKee, analyst, U.S. Geological Survey, Menlo Park, CA; 1b, this paper, H.P. Schwarcz, analyst, McMaster University, Hamilton, Ontario; 2, Russell et al. (1989)
DDH = diamond drill hole

age for altered gabbro near the Dixie Comstock mine (Table 1, sample DC29–193) indicates either several intrusive events or resetting by hydrothermal fluids.

Tertiary rocks, exposed south and north of the mine (Fig. 2; Hudson and Geissman, 1987; VanLandingham, 1988), consist mainly of ash-flow tuffs interbedded with lacustrine sedimentary rocks. These rocks occur in downfaulted blocks within and adjacent to the Humboldt lopolith and are probably late Oligocene to early Miocene (Speed, 1976; Hudson and Geissman, 1987). Paleomagnetic data and geologic mapping around White Rock Canyon (Fig. 2) indicate that the Tertiary rocks and underlying gabbro were rotated 25° counterclockwise during deposition of the ash-flow tuffs (Hudson and Geissman, 1987, 1991). Rotation was largely accomplished by right-lateral strike-slip movement on northwest-trending faults, although high-angle faulting also took place (Hudson and Geissman, 1987, 1991). The rotation did not affect basalts in the Stillwater Range that date at 17 to 13 Ma (Nosker, 1981), thus limiting the onset of high-angle, normal faulting that controls present topography to post-middle Miocene.

As exposed in mine workings and drill holes, colluvium of Dixie Valley consists of several tens of feet of weakly consolidated fan deposits and lacustrine sediments overlying poorly indurated, tuffaceous sediments (Fig. 3). Fan deposits consist of irregular lenses of quartz and feldspar sand, and irregularly oriented and sized cobbles of gabbro and subordinate Tertiary volcanic rocks. Adjacent to the Dixie Comstock mine, multisized, partially aligned clasts of mineralized quartz breccia occur within fan deposits and lacustrine and tuffaceous sediments exposed in the mine trench (Fig. 3), locally imparting ore grades to the sediments. Lacustrine sediments apparently correlate with beach gravels recognized in trenches near IXL Canyon, 15 mi southwest from the Dixie Comstock mine. These shoreline sediments were deposited by 12-ka pluvial lakes (Mifflin and Wheat, 1979; Bell and Katzer, 1990). One mile east of the mine colluvium is overlain by an ephemeral playa lake.

Quartz breccia and silica-rich clasts in trench colluvium are vertically zoned. Quartz breccia clasts are largely confined to fan deposits, lacustrine sediments, and green colluvium (Fig. 3C and D), and their abundance decreases downsection. Sparse, irregular blocks of chalcedonic silica with pockets of clay occur in the underlying green and white tuffs. Root and grass casts are present in green tuff and in chalcedonic silica clasts in white tuff, both in place and on the mine trench dump. This zonation is the inverse of silica stratigraphy that would be expected in a near-surface hydrothermal system where fossil-bearing sinter consisting of less dense and porous, unordered silica overlies compact quartz veins and replacement.

Alternatively, plant cast-sinter may have been derived from a younger, cospatial hydrothermal event because mine trench sediments below fan deposits are hydrothermally altered. Iron and manganese oxides encrust pebble and sand grains of lacustrine sediments, and the fine-grained matrix components of green tuff and white tuff (Fig. 3C and D) consist of poorly crystalline silica and phases amorphous to X-rays. Alteration of hanging-wall surface deposits sug-

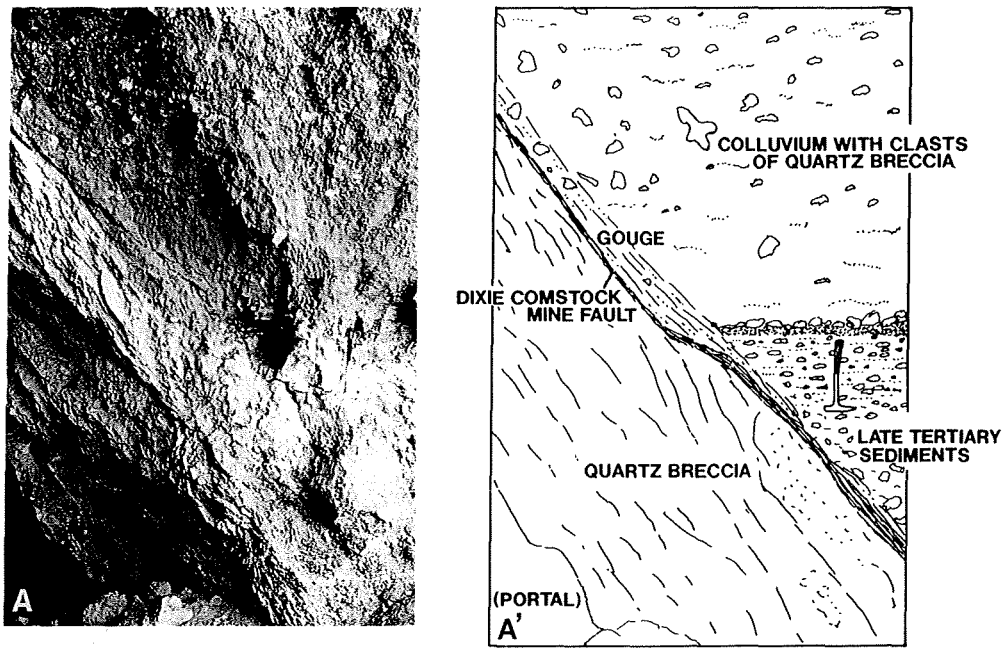

FIG. 3. A. Photograph and line drawing of the Dixie Comstock mine fault zone exposed in mine workings, with hammer for scale. Top edge of photograph is about 30 ft below the premine surface. B. Dixie Comstock mine trench created by excavation of approximately 15,000 yd^3 of postmineralization, hanging-wall colluvial deposits in the 1970s. View is toward the west. Portal (right center) is the 45-ft level of the mine. White claim post (arrow, top right center) is on the apex of the quartz breccia. C. North wall of the trench showing hanging-wall stratigraphy, with knife for scale. Stratigraphy from top to bottom is (1) fan deposits, (2) lacustrine sediments, (3) green colluvium, (4) green tuff, and (5) white tuff.

gests that hydrothermal circulation in the Dixie Comstock mine fault zone resumed after partial erosion of quartz breccia, approximately coinciding with deposition of lacustrine sediments. A geothermal exploration well (DF 45–14), collared 2,500 ft southeast from the Dixie Comstock mine (Fig. 2), encountered up to 270°F water 5,400 ft below the surface (Bell et al., 1980). In 1983, effluent from a pressure drain was depositing sulfide-rich precipitate that contained 27 ppb Au, 1.2 ppm Ag, 126 ppm As, and 58 ppm Hg. Cuttings of colluvium and volcanic rocks from the hole also contain anomalous concentrations of

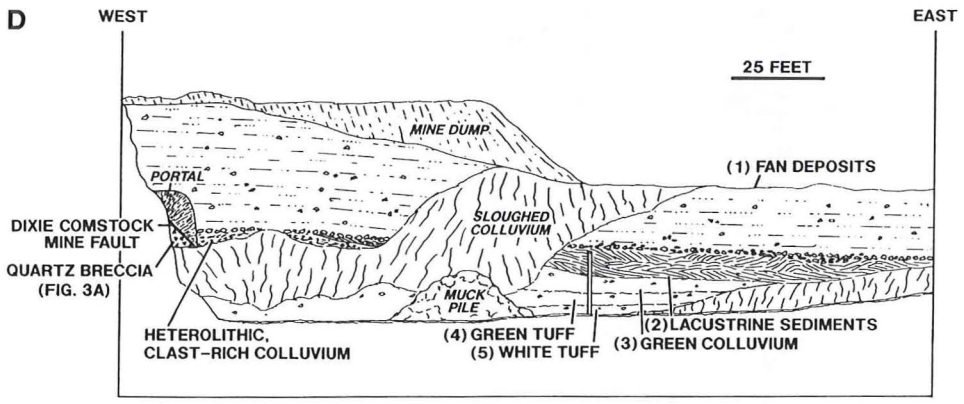

FIG. 3. D. Sketch of the north wall of the mine trench. All colluvial deposits contain angular clasts of quartz breccia or chalcedonic silica. A 0.5- to 1-ft-thick layer of quartz breccia cobbles lies on the lacustrine sediments. (1) Fan deposits—weakly indurated, partly sorted and bedded, heterolithic cobbles, sand and silt, dipping several degrees east. (2) Lacustrine sediments—weakly indurated pebbles, coarse sand and silt; heterolithic but largely gabbro clasts; finely laminated beds, abundant crossbedding; 1 to 5 percent FeO_x + MnO_x encrust clasts and grains. (3) Green colluvium—infrequent, unsorted, angular cobbles of quartz breccia in an olive-green to brown silty matrix, composed mainly of comminuted gabbro detritus. (4) Green tuff—infrequent, unsorted angular cobbles of quartz breccia and chalcedonic silica in a light green silt and clay matrix with local zones of plant fragments and roots replaced by friable microcrystalline silica. (5) White tuff—rare unsorted angular and irregularly shaped blocks of chalcedonic silica containing plant fragment casts in a light green to white clay matrix.

these elements. Well temperatures, precipitate, cuttings, and altered colluvium provide evidence that metal-bearing hydrothermal fluids have been intermittently present in the Dixie Comstock mine fault zone during the Quaternary.

The age of tuffaceous sediments in the mine trench, although greater than 12 ka (Chadwick et al., 1984; Bell and Katzer, 1990), is problematic. Conformable deposition of all prefan trench sediments suggests that the tuffs are late Holocene, but no Quaternary volcanic deposits are known in the area. Exotic tephras, reworked and thickened in the late Holocene pluvial climate (Mifflin and Wheat, 1979), are a possible source.

Dixie Comstock Mine Fault Zone

The portion of the Dixie Comstock mine fault zone which contains gold is up to 250 (76 m) ft thick, strikes north-south to N 10° E, and dips 40° to 45° east. It is exposed in mine workings and drainages north and south of the mine. Contiguous ore-grade gold within the fault zone forms a mullion that measures approximately 900 ft long (down-rake) by 300 ft wide by 20 to 90 ft thick and plunges 20° to 40° northeast. The apex of the mullion occurs in the mine workings where upper parts of it were locally stoped (Fig. 3B). The fault zone is composed of subparallel zones of gouge, matrix-supported quartz breccia and quartz stockwork, and along the footwall contact, incipiently crushed gabbro (Fig. 4). It may be slightly offset by steeper piedmont faults that parallel the Stillwater Range margin (Fig. 2).

In diamond drill core, unoxidized gouge is gray to green in color, foliated parallel to contacts and composed of silt to clay-sized montmorillonite, sericite, kaolinite, feldspar, and minor pyrite. It occurs mainly along or near the hanging-wall contact and is essentially pulverized, altered gabbro. Gouge and crushed hanging-wall gabbro are included together in Figure 4.

Based on examination of drill core and mine workings, fragments in matrix-supported quartz breccia vary from angular to rounded gabbro with preserved texture to gabbro replaced by up to 100 percent quartz, minor pyrite, and other sulfides. The clasts are as much as several ft in maximum dimension but average several inches. Matrix makes up 50 to 75 percent of the breccia and consists of several generations of fine-grained to microcrystalline quartz, <1 percent pyrite, minor silicates, and vug-filling calcite. Much of the gold, especially that grading >0.2 oz Au/ton, occurs in quartz breccia. With increasing depth into the footwall, the matrix to clast ratio decreases and quartz breccia grades into stockwork.

Examination of quartz breccia in an ore stock pile and on the trench dump reveals several other textures. Some matrix consists of massive to finely banded white or mottled white-gray (from fine-grained pyrite) microcrystalline quartz that may be silicified sediment. Thin (≤1 mm) concentric layers of semiclear to dark gray quartz enclose clasts in

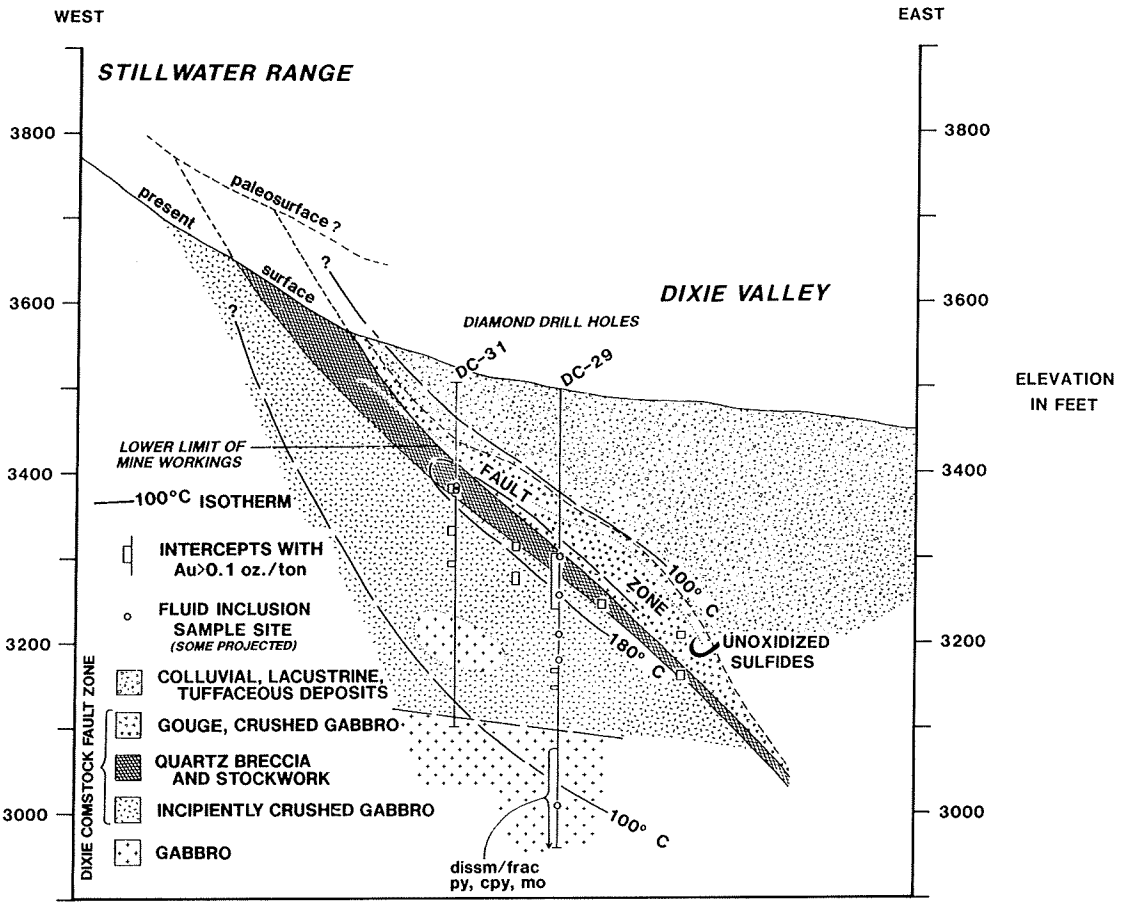

FIG. 4. West-east section through the Dixie Comstock mine and fault zone showing hanging-wall colluvium, gouge, quartz breccia and stockwork, incipiently crushed gabbro, gabbro, and higher grade gold intercepts in drill holes. Isotherms and proposed paleosurface are based on fluid inclusion microthermometry of diamond drill core and underground samples. Abbreviations: cpy = chalcopyrite, dissm = disseminated, frac = fracture, mo = molybdenite, py = pyrite.

some samples. Small clasts in other samples are well rounded and moderately well sorted. Irregular, thin crusts of opaline silica cover some quartz breccia surfaces.

Most quartz breccia is dense, extremely hard, and only occasionally vuggy. Triangular spurs along the Stillwater scarp north and south of the mine are covered by several tens of feet of quartz breccia and owe their preservation to the resistant quartz-rich matrix (Fig. 2).

Light green, soft, incipiently crushed gabbro lies along the footwall contact. It is up to 225 ft thick and in cored drill holes is in sharp contact with uncrushed footwall gabbro to the west and at depth. Incipiently crushed gabbro locally attains ore grade and makes up over 50 percent of the gold inventory. It consists of disaggregated anorthite and pyroxene grains loosely lithified by irregular (<1/8 in; <0.32 cm) seams of chlorite, minor montmorillonite, and sericite, essentially forming a weakly compacted breccia, with a low matrix to clast ratio. The seams are randomly oriented and their abundance varies with no discernible pattern. Other minerals present are calcite, quartz in thin (<0.5 in) veins, titanium oxides, magnetite, coarse-grained pyrite, and molybdenite. Vuggy calcite veins up to 5 in wide cut crushed gabbro.

Gabbro beneath incipiently crushed gabbro consists of several igneous phases: (a) coarse-grained hypidiomorphic-granular anorthite and pyroxene, (b) holocrystalline, intergranular basalt intrusive into (a), and (c) segregations of zoned, automorphic feldspar crystals. Pyroxene is partially altered to chlorite, and 0.5 to 1.0 percent coarse-grained, disseminated pyrite is invariably present.

Gold (in electrum) occurs as discrete grains in quartz that cements matrix-supported breccia, and with quartz, pyrite, and chalcopyrite in breccia frag-

ments (Fig. 5). Lesser amounts of gold occur intermittently in incipiently crushed gabbro and locally attain grades exceeding 0.1 oz/ton, even where no silica is present. Assays suggest that minor amounts of electrum are also entrained in gouge. Late vuggy and vein calcite contains no electrum or sulfides.

Heavy mineral concentrates from two 5-ft drill intervals in incipiently crushed gabbro that grade >0.05 oz/ton gold consist predominantly of disseminated and narrow-vein pyrite that is unassociated with silica. These intervals are 90 to 125 ft below the quartz breccia that constitutes the higher grade portion of the gold inventory. Gold in the concentrates occurs as discrete grains of electrum and in electrum-chalcopyrite intergrowths, similar to the gold occurrences within the overlying quartz breccia (Fig. 5).

Several other sulfides occur sparingly in the deposit. Molybdenite coats fractures and is disseminated in gabbro in deeper parts of core holes. Disseminated molybdenite and pyrite in gabbro may be considerably older than other hydrothermal phases. Cinnabar thinly encrusts fracture surfaces of some underground quartz breccia samples and occurs as local concentrations in clasts within tuffaceous sediments on the trench dump. Sulfides in all three components of the fault zone are largely unoxidized, and iron oxides occur only within several tens of feet of the surface.

Within quartz breccia and stockwork in drill core are local zones of sericitized gabbro that have not been completely brecciated and replaced by quartz. Sericite from several of these zones has K-Ar ages of 15.0, 11.1, and 13.6 Ma (Table 1, samples DC-29–208.5, DC-29–210, and DC-31–100.5). Fluid inclusion homogenization temperatures and fault displacement rate data presented later indicate that sericite predates quartz breccia and gold mineralization. Sericite ages apparently record early hydrothermal fluid circulation in the Dixie Comstock mine fault and support a post-middle Miocene age for initial Basin and Range faulting in this area. The age of gold mineralization is interpreted to be Pleistocene based on thickness of cover and erosion rates that are discussed in following sections.

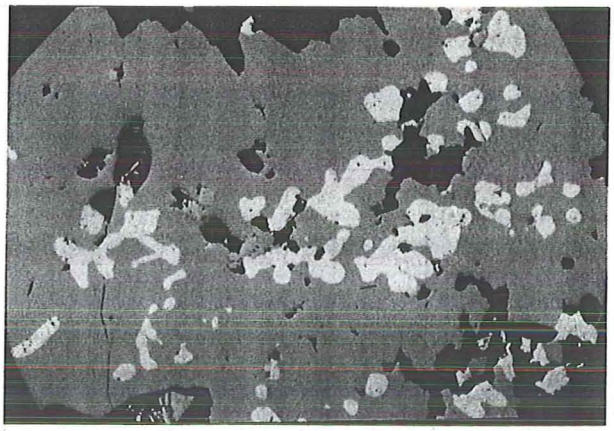

FIG. 5. Microphotograph of electrum (light, reflective inclusions) in chalcopyrite in an underground sample from the Dixie Comstock mine. Electrum in this sample consists of ~53 wt percent Au and 47 wt percent Ag. Width of frame is approximately 0.6 mm.

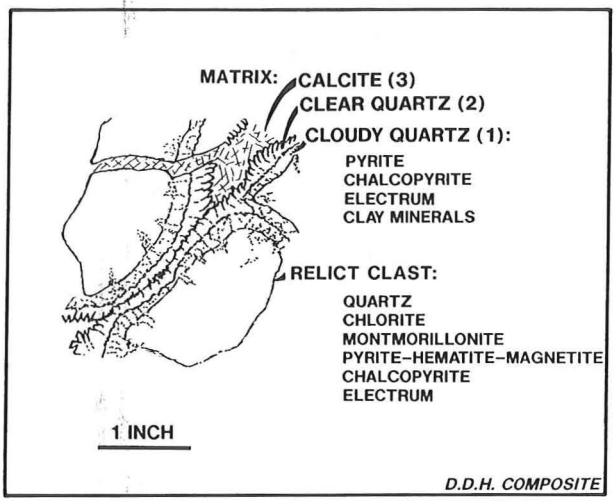

FIG. 6. Schematic depiction of the three stages of matrix hydrothermal minerals and relict gabbro clasts, compiled from examination of diamond drill core.

Paragenesis

Three stages of hydrothermal mineralization are recognized in quartz breccia from drill core (Fig. 6). Quartz that replaced gabbro clasts contains electrum, pyrite, and minor chalcopyrite, all of which coexist with chlorite, montmorillonite, and iron oxides. Based on common minerals, this relict clast assemblage is apparently coeval with the earliest matrix, stage 1, which consists of cloudy quartz, electrum, pyrite, rare chalcopyrite, and clay minerals. Total sulfide in clasts approaches 5 vol percent whereas early matrix sulfide rarely exceeds 1 vol percent. Correspondingly, electrum is several times more abundant in replaced clasts, suggesting that alteration of pyroxene and feldspar locally controlled gold deposition. Electrum in cloudy quartz of the matrix is also appreciably more abundant in clay aggregates. Stage 1 electrum contains 55 to 61 mole percent silver (Table 2, samples DC-83-1 and DC-29–214.4). Electrum from narrow sulfide veins in incipiently crusted gabbro contains 52 to 56 mole percent silver (Table 2, samples DC-29–348–353 and DC-28-345–350) and probably correlates with the stage 1 assemblage in quartz breccia.

The second stage of mineralization consists of clear, euhedral, locally vuggy quartz, that was depos-

TABLE 2. Compositions (wt %) of Electrum in Ore-Grade Samples from the Dixie Comstock Mine

Sample no.	No. of analyses	Au	Ag	S	Sum	N_{Ag}^{el}
DC83-1a	3	54.45	46.79	0.21	101.45	61.1
DC83-1b	2	52.20	47.50	0.25	99.95	62.4
DC29-214.4a	2	58.82	39.22	0.18	98.22	54.9
DC29-214.4b	2	58.50	39.14	0.05	99.27	55.0
DC29-348-353	1	56.58	39.86	0.22	96.66	56.3
DC28-345-350	2	62.93	37.26	0.20	100.39	51.9

Determined by electron microprobe; N_{Ag}^{el} is mole percent silver in electrum.

ited over electrum + sulfide matrix, cloudy quartz (stage 1). The contact between early matrix cloudy quartz (stage 1) and later matrix clear quartz (stage 2) is sharp. The youngest matrix mineral and third stage of mineralization is coarse-grained calcite that fills vugs in clear quartz (stage 2) or occurs as veins cutting all earlier assemblages.

Fluid Inclusion Homogenization Temperature Data

Coarse-grained hydrothermal minerals in the Dixie Comstock mine fault zone are uncommon. Only limited microthermometric measurements were made on fluid inclusions in quartz and calcite from nine drill core, drill cuttings, and underground samples. Some fluid inclusion data were also collected from barite and calcite veins up to 0.25 mi southwest of the mine.

Fluid inclusions from which data were collected are thought to be primary because they mostly occur isolated in crystal growth zones. Inclusions in all samples are liquid rich and contain no daughter minerals. Inclusions in clear quartz overgrowths (the second stage of mineralization) in several mine samples contain no vapor phase and are assumed to be entirely liquid. Inclusion size never exceeds 10 μm, and collection of accurate salinity data by freezing inclusions proved infeasible. Low homogenization temperatures and predominance of meteoric water (see later section) in inclusions suggest low fluid salinities. An average of 30 determinations was used to define each of the temperature modes cited below, which differ by no more than several degrees from median T_h. Examples of fluid inclusion microthermometric data are shown in Figure 7.

Inclusions in stage 1 cloudy quartz intergrown with pyrite, chalcopyrite, and electrum gave T_h modes of 175° to 185°C. Inclusions in several stage 1 quartz samples homogenized over a wide temperature range, displaying no clear mode (Fig. 7). Inclusions in stage 2 clear quartz homogenized at modal temperatures ranging from 170° to 210°C, although single-phase (liquid) inclusions observed in quartz of this stage undoubtedly formed at lower temperatures. Inclusions in stage 2 clear quartz usually displayed a much larger T_h range than mineralized stage 1 cloudy quartz, and some inclusions homogenized at temperatures greater than 250°C. Inclusions in three stage 3 calcite samples homogenized to liquid, giving modes of 165°, 172°, and 176°C.

A sample of vein calcite 0.25 mi southwest of the mine gave a fluid inclusion homogenization temperature mode of 158°C. A sample of vein barite from the same location gave no clear temperature mode, having a T_h range of 140° to 200°C.

Quartz that replaced gabbro clasts cannot be clearly related in time to electrum precipitation, although quartz, electrum, sulfides, and clay minerals appear to be texturally coeval. Electrum in early matrix cloudy quartz (stage 1) is unequivocally a coprecipitant, and isotherms in Figure 4 record temperature distribution of this paragenetic stage. However, temperatures at which stage 2 clear quartz and stage 3 calcite were deposited are nearly indistinguishable from those of electrum-bearing, stage 1 quartz.

Therefore, most, if not all, electrum in quartz breccia was deposited at 175° to 180°C. Electrum in incipiently crushed gabbro may have precipitated at different temperatures, but those electrum composi-

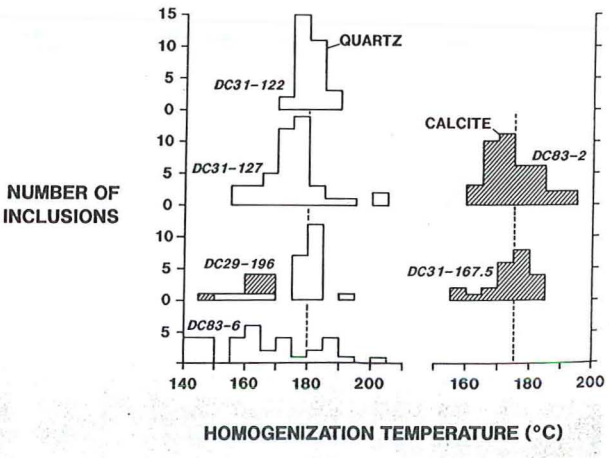

FIG. 7. Examples of fluid inclusion homogenization temperature histograms for the Dixie Comstock mine stage 1 quartz and stage 3 calcite (see Fig. 6). Data were derived from diamond drill core and underground samples. Several other samples displayed homogenization temperature variability similar to that of sample DC83-6.

tions (Table 2) and mineral associations are very similar to quartz breccia electrum. The position of the 100°C isotherm in Figure 4 is consistent with the preponderance of single-phase inclusions in deeper samples and presumed temperature buffering by water-saturated colluvium above the quartz breccia. It appears that higher fluid temperatures were largely confined to quartz breccia and stockwork and that heat was convected by fluid toward the surface, primarily in the Dixie Comstock mine fault zone.

Although little evidence for boiling was observed in drill hole samples, inclusions in quartz from surface mine workings trapped boiling fluids, as evidenced by a few coeval vapor- and liquid-rich inclusions, at slightly lower temperatures (160°–170+°C). Large homogenization temperature variability in several stage 1 samples also supports vapor-liquid separation during entrapment (Fig. 7). It is assumed that the drill hole inclusions were formed within a few degrees of boiling at 180°C and no pressure corrections have been applied to homogenization temperatures. According to pure water phase separation curves (Haas, 1971), fluids in quartz breccia in drill holes DC-31 and DC-29 circulated about 330 ft (100 m) below the surface (Fig. 4). If eroded sinter clasts are coeval with quartz breccia, then the paleosurface and water table were essentially coplanar and the thickness of eroded sinter, quartz breccia, and quartz stockwork is ≤330 ft (Fig. 4).

The fine grain size and fluid inclusion homogenization temperatures of ~180°C suggest that hydrothermal quartz of the quartz breccia may have originally been deposited as chalcedony or amorphous silica. The solubility of silica in geothermal systems below 180° is usually controlled by chalcedony (Fournier, 1985). Subsequent recrystallization of chalcedony or coalescing grain growth may have produced the observed quartz breccia matrix textures and may have modified primary fluid inclusions. Recognition of a chalcedonic precursor according to the criteria of Sander and Black (1988) is not clear in the fluid inclusion samples examined, but it remains possible that homogenization temperature modes are recording the chalcedony-quartz transition and that higher silica depositional temperatures have been overlooked.

Light Stable Isotope Data

Deuterium and oxygen isotope abundances in fluid inclusions were obtained from four stage 1 cloudy quartz and two stage 3 calcite drill core samples (Table 3) for which homogenization temperatures had been determined or could be closely estimated. The δD_{H_2O} values range from −106 to −123 per mil, and calculated $\delta^{18}O_{H_2O}$ values range from −6.7 to −14.3 per mil. Water in calcite is most depleted in deuterium and, in one sample, most enriched in ^{18}O. Analytic precision for hydrogen is ±5 per mil and for oxygen, ±0.5 per mil.

Isotopic compositions of deep geothermal well waters in Dixie Valley, $\delta D = \sim -101$ to −126 per mil and $\delta^{18}O = \sim -10.6$ to −14.8 per mil (Ingraham, 1982, appendix A), encompass Dixie Comstock mine quartz fluid δD and $\delta^{18}O$ values, although Dixie Comstock mine quartz fluid δD values are generally 5 to

TABLE 3. Light Stable Isotope Data for Fluid Inclusion Water in Quartz and Calcite, and for Pyrite Sulfur from Drill Holes at the Dixie Comstock Mine

Sample no.	Depth below the surface (ft)	Mineral	T[1] (°C)	δD_{H_2O} (‰)	$\delta^{18}O_{quartz,calcite}$ (‰)	$\delta^{18}O^2$ (‰)
DC29-214.4	−214.4 ft	Quartz	e180	−106	+0.8	−12.1
DC31-122	−122 ft	Quartz	179	−112	−1.6	−14.5
DC31-127A	−127 ft	Quartz	175	−108	−0.4	−13.6
DC31-127B	−127 ft	Quartz	175	−108	+0.1	−13.1
DC28-273	−273 ft	Calcite	e176	−116	+4.2	−6.7
DC31-167.5	−167.5 ft	Calcite	176	−123	−3.4	−14.3

Sample no.	Depth below the surface (ft)	Mineral	$\delta^{34}S$ (‰)
DC28-228.5-231.5	−228.5 to −231.5	Pyrite	−7.5
DC28-253-258	−253 to 258 ft	Pyrite	−6.7
DC28-458-463	−458 to 463 ft	Pyrite	−3.5
DC29-188-193.5	−188 to 193.5 ft	Pyrite	−7.2
DC29-524-529	−524 to 529 ft	Pyrite	−3.0
DC31-201.5-204	−201.5 to 204 ft	Pyrite	+3.9

Analyses done by Geochron Laboratories (Cambridge, MA); e = estimated from fluid inclusion homogenization temperatures where no clear mode is present

[1] Determined from fluid inclusion homogenization

[2] Calculated using the equation: $10^3 \ln\alpha = 3.34\ (10^{-6}\ T^{-2}) - 3.31$ for quartz-water (Matsuhisa et al., 1979) and $10^3 \ln\alpha = 2.78\ (10^{-6}\ T^{-2}) - 2.89$ for calcite-water (Friedman and O'Neil, 1977), extrapolated to lower temperatures indicated by fluid inclusion homogenization

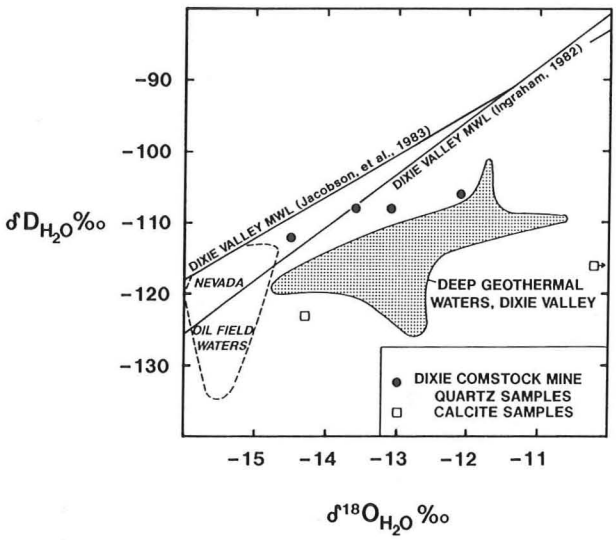

FIG. 8. Isotopic composition of stage 1 cloudy quartz fluid from diamond drill hole samples at the Dixie Comstock mine and deep geothermal waters in Dixie Valley. Nevada oil field water analyses provided by R.L. Jacobson (University of Nevada, Desert Research Institute) on water samples collected by the author and field operators.

10 per mil higher (Fig. 8). Quartz fluids and one calcite fluid composition are displaced up to several per mil from a local meteoric water line (determined by Ingraham, 1982) by water-rock oxygen exchange. Much greater exchange is indicated by a second calcite fluid isotopic composition (Fig. 8). Isotope compositional similarities show that quartz breccia meteoric water and, in part, late calcite meteoric water resemble modern deep geothermal water in Dixie Valley and that Dixie Comstock mine hydrothermal phases were deposited from nearly unexchanged meteoric water (Fig. 8).

The $\delta^{34}S$ values determined for six pyrite drill core samples range from -7.5 to +3.9 per mil (Table 3). Analyzed pyrites were derived from stage 1 quartz breccia matrix and from incipiently crushed gabbro. Five values are between -3.0 and -7.5 per mil, possibly reflecting igneous sulfur that has been isotopically depleted under low pH and/or high f_{O_2} fluid conditions that favor dissolved sulfate. It is also possible that several generations of pyrite were analyzed. The variations in sulfur isotope compositions of pyrite bear no discernable spatial relation to the Dixie Comstock mine fault nor to quartz breccia paragenesis.

The isotopic compositions of water and sulfur in the Dixie Comstock mine yield no definitive genetic information. Meteoric waters are known to circulate to many thousands of feet below the surface in Great Basin geothermal fields (Ingraham, 1982; Jacobson et al., 1983) and oil fields (Fig. 8). Furthermore, hundreds of feet of water-saturated colluvium in Dixie Valley provide an immense fluid reservoir and nearly unlimited access to hydrothermal components for shallow mineralization.

Faulting History

Three epochs of faulting are recognized along the eastern margin of the Stillwater Range from White Rock Canyon to south of the Dixie Comstock mine: Oligocene-Miocene, middle Miocene, and Quaternary.

Late Oligocene-early Miocene rotational faulting, identified from paleomagnetic and fault-slip data on ash-flow tuffs and lacustrine rocks dated at 32 to 22 Ma, was concurrent with deposition of the ash-flow tuffs (Hudson and Geissman, 1987). Rotational faults are thought to predate 17 to 13 Ma basalts in the Stillwater Range that are relatively undeformed and flat lying.

Oligocene-Miocene volcanic rocks are also displaced by normal faults that dip 35° to 60° east. These faults were active during the second epoch, which includes the Dixie Comstock mine fault. They were active by the middle Miocene (Fig. 2), since sericitized gabbro samples in the Dixie Comstock mine fault have K-Ar ages that range from 15.0 to 11.1 Ma (Table 1). In the area of Figure 2, the Dixie Comstock mine fault consists of several curvilinear segments, 0.5 to 2 mi long, which separate Mesozoic from Tertiary rocks, Mesozoic and Tertiary rocks from colluvium of Dixie Valley, and older terrace gravel deposits from colluvium. Based on geothermal well logs (Bell et al., 1980), middle Miocene-initiated faults cumulatively displaced Mesozoic and Tertiary rocks of the Stillwater Range for thousands of feet (Fig. 9) and created an ancestral Dixie Valley.

Pleistocene-Holocene normal faults, the third epoch, are largely parallel to or coplanar with middle Miocene faults along the present range margin. In the Dixie Comstock mine, they manifest as hanging-wall gouge and crushed gabbro above quartz breccia and may include the quartz breccia also. North and south of the mine Quaternary faults displace fan deposits as well as Tertiary volcanic rocks from colluvium of Dixie Valley (Fig. 2) and are thought to be as young as 10,000 yr (Wallace and Whitney, 1984). At the Dixie Comstock mine, clasts of quartz breccia and chalcedonic silica occur in hanging-wall Holocene colluvial deposits (Fig. 3), providing evidence that the quartz breccia was exposed by Quaternary fault displacements.

Piedmont faults, recognized from geophysical data and low-sun-angle photography, are also considered to have originated in the Quaternary, based on scarp examination near IXL Canyon, 15 mi southwest of the Dixie Comstock mine (Bell and Katzer, 1987, 1990). Movement on piedmont faults there has both

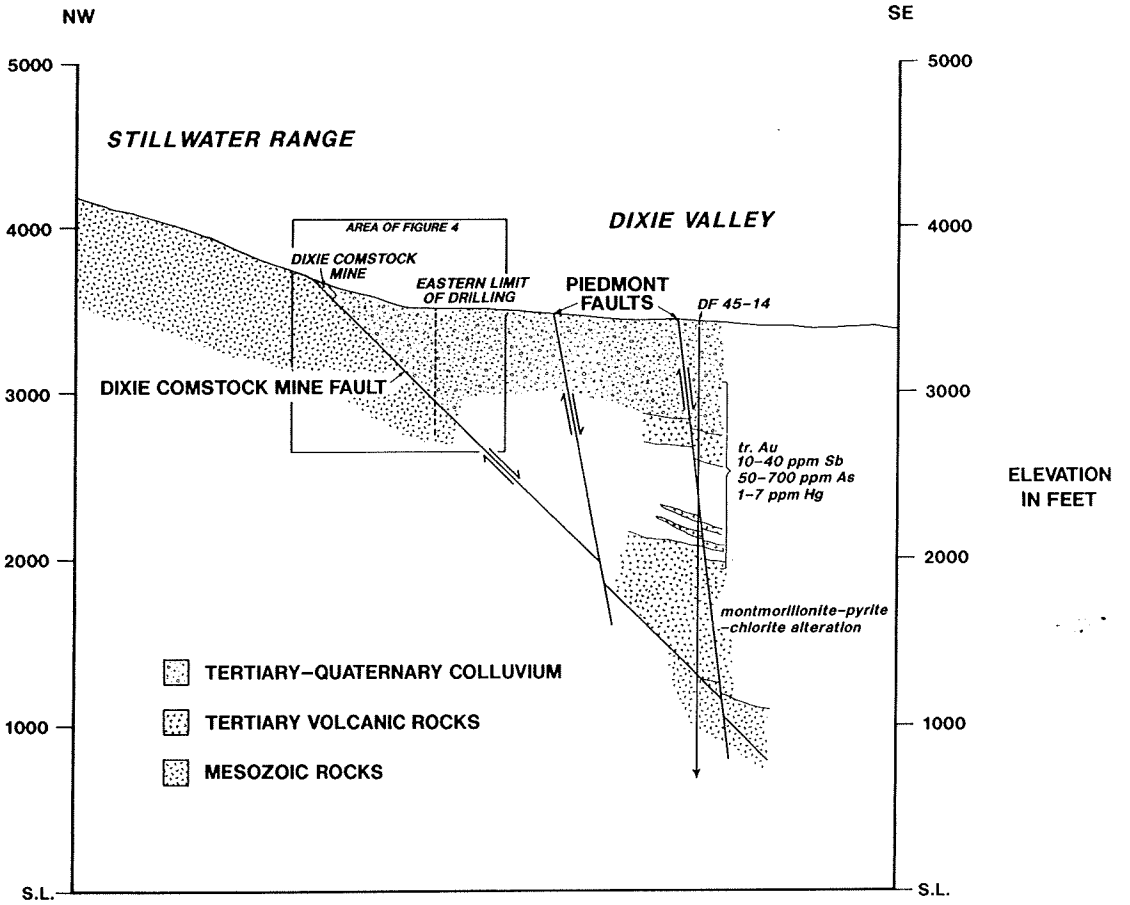

FIG. 9. Northwest-southeast section through the Dixie Comstock mine and geothermal well DF 45–14 showing projected structure and stratigraphy. Anomalous Au, Sb, As, and Hg in intercalated colluvium and volcanic rocks suggests intermittent Quaternary hydrothermal activity.

alternated and coincided with range-bounding fault displacement during the Holocene. In the vicinity of the Dixie Comstock mine, piedmont faults are hundreds to thousands of feet east of the range margin (Fig. 2) and may downdrop quartz breccia and Tertiary volcanic rocks to the east (Figs. 2 and 9). Their dip would, therefore, exceed 45°.

Some constraints on the age of quartz breccia gold mineralization can be derived from extrapolation of current fault displacement rates and from the amount of eroded premineralization cover. Two assumptions must be made:

1. Quartz breccia is not displaced relative to footwall gabbro, thus providing a footwall datum. Because Holocene postmineralization gouge and crushed gabbro within the fault zone are along the hanging-wall contact above the quartz breccia, this requirement is apparently satisfied, although cumulative postmineralization movement within incipiently crushed gabbro in the footwall beneath quartz breccia could be appreciable. If quartz breccia did not remain fused to footwall gabbro, the estimated age is minimum.

2. The thickness of cover at the time of mineralization can be accurately determined from quartz breccia fluid inclusion data. The depositional temperature of Dixie Comstock mine quartz breccia is approximately 180°C, giving a minimum thickness of premineralization cover of about 330 ft (100 m). Relatively shallow cover during and limited erosion after mineralization are supported by sinter clasts in hanging-wall colluvium.

Quaternary fault displacement timing and rates in Dixie Valley of ~0.3 to 0.5 mm/yr (Wallace and Whitney, 1984; Okaya and Thompson, 1985; Bell and Katzer, 1990) correlate with accelerated extension (Thompson and Burke, 1973) and suggest that most displacement along the eastern Stillwater Range margin has taken place during the last few million years. At an average Holocene displacement rate of 0.4 mm/yr, approximately 0.25 Ma of uplift (and erosion) are required for the present level of quartz

breccia exposure. This relatively young age for quartz breccia gold mineralization is supported by the similarity in isotopic compositions of Dixie Comstock mine quartz fluid and modern deep geothermal waters from Dixie Valley (Fig. 8) as well as by colluvial stratigraphy.

A uranium-thorium age of >0.35 Ma, determined for stage 3 calcite from drill core (Table 1), suggests a mineralization age somewhat older than that estimated from present fault displacement rates. Thus, erosion of estimated postmineralization cover (~330 ft; 100 m) may have begun by the middle Pleistocene. Although one calcite radiometric age is not necessarily definitive and fluid inclusion temperatures are somewhat imprecise, both data imply intermittently lower average fault displacement rates in the Pleistocene. If gold mineralization is as old as 0.5 Ma, approximately 660 ft of postmineralization cover would have been removed at present fault displacement rates, requiring significantly higher depositional temperatures (up to 210°C) than measured. Therefore, "seismic gaps," "displacement grouping" (Wallace and Whitney, 1984; Wallace, 1987), or temporal clustering of displacement along Dixie Valley range margin faults may be as old as middle Pleistocene.

Conclusions

Age, temperature, and stratigraphic data obtained from hydrothermal minerals deposited in the Dixie Comstock mine fault, which separates the Stillwater Range from Dixie Valley, indicate that: (1) displacement along this range-bounding fault began at least by the middle Miocene, (2) of the several hydrothermal events which utilized the fault, a mid-Pleistocene event deposited potentially bulk mineable gold in a mullion, (3) gold mineralization took place at ~180°C beneath ~330 ft (~100 m) of cover, (4) gold and associated quartz, sulfides, silicates, and calcite were precipitated from heated ground water, and (5) the present pattern of spatial and temporal clustering of fault displacements in Dixie Valley is apparently mid-Pleistocene or older.

Acknowledgments

Appreciation is extended to ASARCO Incorporated for sponsoring this research and its publication. Ted McKee graciously provided three K-Ar ages which helped to order igneous and hydrothermal events. The comments of two *Economic Geology* reviewers significantly improved clarity of the paper.

June 2, November 18, 1993

REFERENCES

Bell, E.J., Campana, M.E., Jacobsen, R.L., Larson, L.T., Slemmons, D.B., Bard, T.R., Bohm, B.W., Ingraham, N.L., Jucal, R.W., and Whitney, R.A., 1980, Geothermal reservoir case study, northern Basin and Range province, northern Dixie Valley, Report: Reno, University of Nevada, Mackay Mineralogical Research Institute, 233 p.

Bell, J.W., and Katzer, T., 1987, Surficial geology, hydrology, and late Quaternary tectonics of the IXL Canyon area, Nevada, as related to the 1954 Dixie Valley earthquake: Nevada Bureau of Mines and Geology Bulletin 102, 52 p.

—— 1990, Timing of late Quaternary faulting in the 1954 Dixie Valley earthquake area, central Nevada: Geology, v. 18, p. 622–625.

Chadwick, O.A., Hecker, S., and Fonseca, J., 1984, A soils chronosequence at Terrace Creek: Studies of late Quaternary tectonism in Dixie Valley, Nevada: U.S. Geological Survey Open-File Report 84–90, 29 p.

Fournier, R.O., 1985, The behavior of silica in hydrothermal solutions: Reviews in Economic Geology, v. 2, p. 45–59.

Friedman, I., and O'Neil, J.R., 1977, Compilation of stable isotope fractionation factors of geochemical interest: U.S. Geological Survey Professional Paper 440 KK, 12 p.

Haas, J.L., 1971, The effect of salinity on the maximum thermal gradient of a hydrothermal system at hydrostatic pressure: ECONOMIC GEOLOGY, v. 66, p. 940–946.

Hudson, M.R., and Geissman, J.W., 1987, Paleomagnetic and structural evidence for middle Tertiary counterclockwise block rotation in the Dixie Valley region, west central Nevada: Geology, v. 15, p. 638–642.

—— 1991, Paleomagnetic evidence for the age and extent of middle Tertiary counterclockwise rotation, Dixie Valley region, west-central Nevada: Journal of Geophysical Research, v. 96, p. 3979–4006.

Ingraham, N.L., 1982, Environmental isotope hydrology of the Dixie Valley geothermal system, Dixie Valley, Nevada: Unpublished M.S. thesis, Reno, University of Nevada,96 p.

Jacobson, R.L., Ingraham, N.L., and Campana, M.E., 1983, Isotope hydrology of a Basin and Range geothermal system: University of Nevada, Reno, Desert Research Institute, Publication 41087, 18 p.

Matsuhisa, Y., Goldsmith, J.R., and Clayton, R.N., 1979, Oxygen isotopic fractionation in the system quartz-albite-anorthite-water: Geochimica et Cosmochimica Acta, v. 43, p. 1131–1140.

Mifflin, M.D., and Wheat, M.M., 1979, Pluvial lakes and estimated pluvial climates of Nevada: Nevada Bureau of Mines and Geology Bulletin 94, 57 p.

Nosker, S.A., 1981, Stratigraphy and structure of the Sou Hills, Pershing County, Nevada: Unpublished M.S. thesis, Reno, University of Nevada, 60 p.

Okaya, D.A., and Thompson, G.A., 1985, Geometry of Cenozoic extensional faulting: Dixie Valley, Nevada: Tectonics, v. 4, p. 107–125.

Oldow, J.S., 1992, Late Cenozoic displacement partitioning in the northwestern Great Basin: Walker Lane Symposium, Geological Society of Nevada, Reno, NV, 1992, Proceedings, p. 17–52.

Page, B.M., 1965, Preliminary geologic map of a part of the Stillwater Range, Churchill County, Nevada: Nevada Bureau of Mines and Geology, Map 28, scale 1:250,000.

Parry, W.T., Hedderly-Smith, D., and Bruhn, R.L., 1991, Fluid inclusions and hydrothermal alteration on the Dixie Valley fault, Nevada: Journal of Geophysical Research, v. 96, p. 19,733–19,748.

Sander, M.V., and Black, J.E., 1988, Crystallization and recrystallization of growth-zoned vein quartz crystals from epithermal systems—implications for fluid inclusion studies: ECONOMIC GEOLOGY, v. 83, p. 1052–1060.

Slemmons, D.B., and Bell, J.W., 1987, 1954 Fairview Peak earthquake area, Nevada: Boulder, Colorado, Geological Society of America, Centennial Field Guide, v. 1, p. 73–76.

Speed, R.C., 1976, Geologic map of the Humboldt lopolith and surrounding terrain, Nevada: Geological Society of America Map MC-14, scale ~1:80,000.

Thompson, G.A., and Burke, D.B., 1973, Rate and direction of spreading in Dixie Valley, Basin and Range province, Nevada: Geological Society of America Bulletin, v. 84, p. 627–632.

Vanderburg, W.O., 1940, Reconnaissance of mining districts in Churchill County, Nevada: U.S. Bureau of Mines Information Circular 7093, p. 48.

VanLandingham, S.L., 1988, Comment and reply on "Paleomagnetic and structural evidence for middle Tertiary counterclockwise block rotation in the Dixie Valley region, west-central Nevada": Geology, v. 16, p. 756–757.

Waibel, A.F., 1987, An overview of the geology and secondary mineralogy of the high temperature geothermal system in Dixie Valley, Nevada: Geothermal Resources Council Bulletin, Sept/Oct., v. 16, p. 5–11.

Wallace, R.E., 1984, Patterns and timing of late Quaternary faulting in the Great Basin province and relation to some regional tectonic features: Journal of Geophysical Research, v. 89, p. 5763–5769.

—— 1987, Grouping and migration of surface faulting and variations in slip rates on faults in the Great Basin province: Seismological Society of America Bulletin, v. 77, p. 868–876.

Wallace, R.E. and Whitney, R.A., 1984, Late Quaternary history of the Stillwater seismic gap, Nevada: Seismological Society of America Bulletin, v. 79, p. 301–314.

Willden, R., and Speed, R.C., 1974, Geology and mineral deposits of Churchill County, Nevada: Nevada Bureau of Mines and Geology Bulletin 83, 95 p.

ZONING AND CHRONOLOGY OF HYDROTHERMAL EVENTS IN THE HUMBOLDT RANGE, PERSHING COUNTY, NEVADA

PETER G. VIKRE — *ASARCO Inc., Reno, NV 89502*
EDWIN H. McKEE — *U.S. Geological Survey, Menlo Park, CA 94025*

The Humboldt Range, an elongate north-south horst in the west-central Great Basin of Nevada (fig. 1), abounds in a variety of hydrothermal mineral deposits (Johnson, 1977). The distribution of metal mines and prospects displays a spatial relation to both intrusive rocks and older stratigraphy. K-Ar dates for hydrothermal phases reported here indicate that most if not all deposits were formed during several Cretaceous intrusive events.

The Humboldt Range consists mainly of Triassic rocks (fig. 2). Lower Triassic volcanic rocks of the Koipato Group are overlain by limestones of the Star Peak Group which in turn are overlain by phyllite, partly Jurassic in age, of the Auld Lang Syne Group (Silberling and Wallace, 1967; Wallace and others, 1969a, 1969b). These lower Mesozoic strata are intruded by granitic rocks. The largest intrusion, the Rocky Canyon stock, has been dated by K-Ar methods at 71.4 ± 3.0 m.y. by Silberman and others (1973). Numerous other dikes and apophyses of coarse-grained granitic rocks, along with magnetic data, suggest that granitic intrusions underlie the entire central part of the range. The suspected position of buried Cretaceous intrusions is outlined on figure 3.

The distribution of ore deposits shows that tungsten, gold, silver, antimony, and mercury are concentrically concentrated around the Rocky Canyon stock and intrusive subcrop (fig. 3). Tungsten occurrences are somewhat scattered relative to coarse-grained intrusions, but the largest deposit borders the Rocky Canyon stock. With local exceptions, gold, silver, antimony, and mercury deposits are annularly distributed around the subsurface intrusive center with mercury occurrences distal. Gold and silver deposits occur in overlapping zones while antimony and mercury display a more regular circumferential relationship.

Stratigraphic control on both the type and size of metal deposit is evident when metal production is ranked against stratigraphy (fig. 4). The bulk of gold mineralization occurs in rhyolite and greenstone of the Lower Triassic Koipato Group. The large silver deposits are in rhyolites of the Koipato Group as well as in overlying limestones of the Star Peak Group. Antimony and mercury mines are found in rocks of various age, but are most abundant in carbonate and clastic rocks that are younger than the Star Peak Group. The relationship of metals to stratigraphy is reflected in the antiformal structure of the Humboldt Range. The uplifted core of the range, thought to consist largely of Cretaceous intrusions, is generally surrounded by strata that are progressively younger to the north, east, and south. Superpositioning stratigraphy (fig. 2) with metal distribution (fig. 3) largely explains the association of deposit type, size, and stratigraphy as seen on figure 4.

The timing of metal zonation has been established by radiometric dating of hydrothermal phases. The location of samples dated by K-Ar methods and the analytical data are listed in the Sample Descriptions section.

Age determination was done in the laboratories of the U.S. Geological Survey, Menlo Park, Calif., using standard isotope-dilution procedures as described by Dalrymple and Lanphere (1969). The analyses were performed on pure mineral concentrates (98% purity by grain count) prepared by heavy liquid, magnetic, electrostatic, and hand-picking procedures. Potassium analyses were performed by lithium metaborate flux fusion-flame photometry techniques, the lithium serving as an internal standard (Ingamells, 1970). Argon analyses were performed using a 60-sector, 15.2 cm-radius, Nier-type mass spectrometer or on a five-collector mass spectrometer (Stacey and others, 1981).

The precision of the data, shown as the ± value, is the estimated analytical uncertainty at one standard deviation (σ). It represents uncertainty in the measurement of radiogenic ^{40}Ar and K_2O in the sample and is based on experience with replicated analyses in the Menlo Park laboratories. The decay constants used for ^{40}K are those adopted by the International Union of Geological Sciences Subcommission on Geochronology (Steiger and Jager, 1977).

The K-Ar ages range from 42.9 ± 1.2 m.y. to 103.4 ± 10 m.y. The four youngest dates, 42.9, 55.7, 57.9, and 63.4 m.y. are from microcline separates which have probably sustained significant argon loss and are consequently younger than the depositional age of the veins. The ages for white mica and biotite span 36 m.y. (fig. 5), suggesting that several intrusive events have altered rocks and produced mineral deposits in the Humboldt Range. The Cretaceous intrusive body apparently consists of nested or juxtaposed stocks, approximately 70 to 100 m.y. in age, ranging in composition from quartz monzonite to granodiorite.

K-Ar ages for coarse-grained, equigranular intrusive rocks in northern Nevada define two Cretaceous epochs (Smith and others, 1971; Silberman and McKee, 1971; Carlson and others, 1975). One epoch lasted from about 105 to 85 m.y. before present. The other event took place about 80 to 70 m.y. ago and includes intrusion of the Rocky Canyon stock (fig. 5). Ages of metal deposits in the Humboldt Range suggest that older intrusive rocks corresponding in age to the earlier epoch exist at depth.

The ages of vein and wall rock white mica clearly indicate that tungsten, gold, and silver deposits are related in time to these intrusive events. Although data are sparse, tungsten deposits formed 90 to 85 m.y. ago and gold deposits formed 75 to 70 m.y. ago. Silver mineralization may have taken place twice; once 100 to 85 m.y. ago and also 80 to 70 m.y. ago. The one mercury and one antimony deposit dated suggest that hydrothermal concentrations of these elements are coeval with older silver deposits. Irregularities in metal zonation (fig. 3) can be attributed to shifts in intrusion centers with time. The overall consistency of metal deposit distribution indicates that intrusions of individual granitic melt were restricted to a relatively confined pathway during the Late Cretaceous.

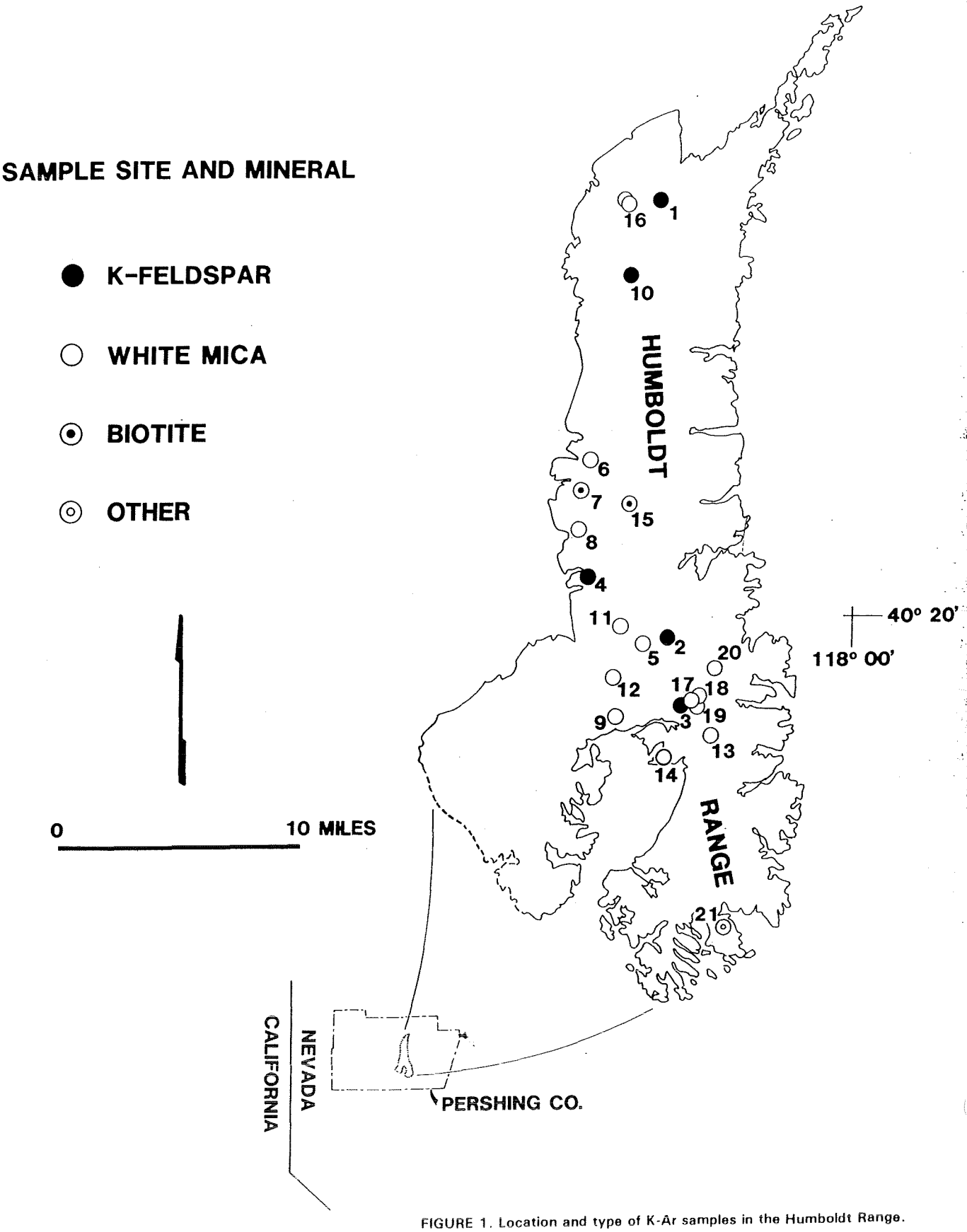

FIGURE 1. Location and type of K-Ar samples in the Humboldt Range.

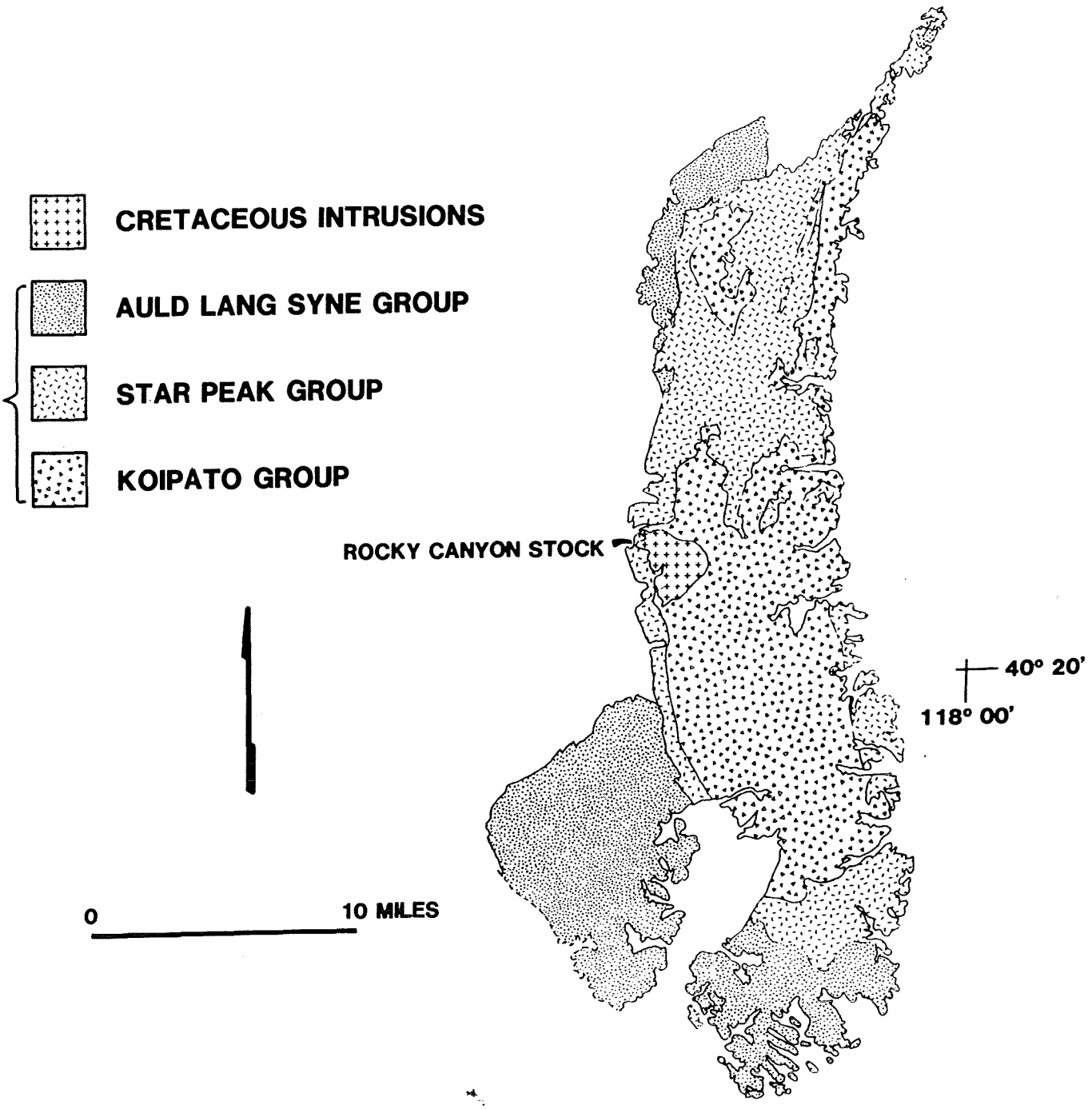

FIGURE 2. Geologic map of the Humboldt Range.

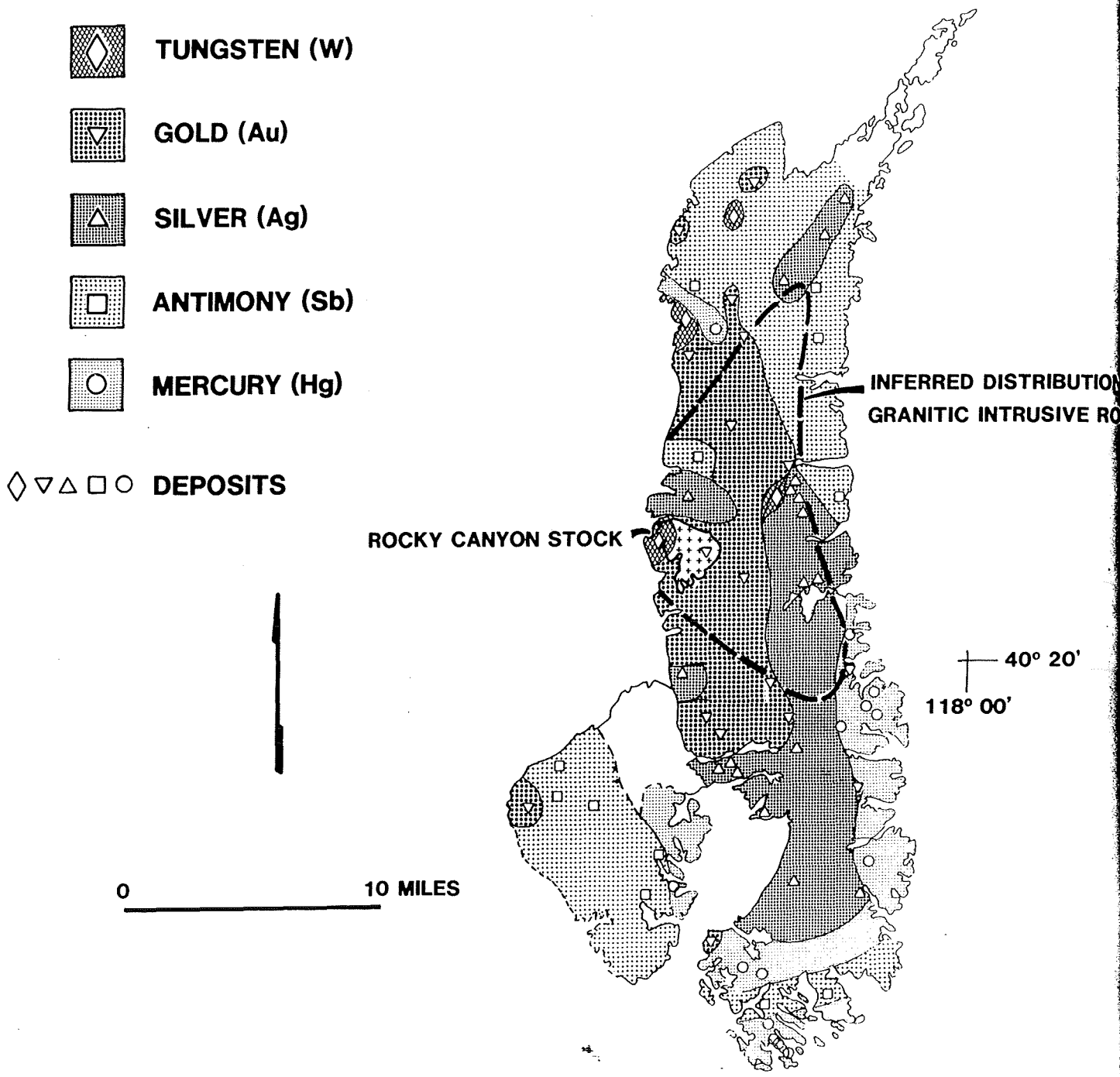

FIGURE 3. Distribution of metal deposits and granitic intrusive rocks.

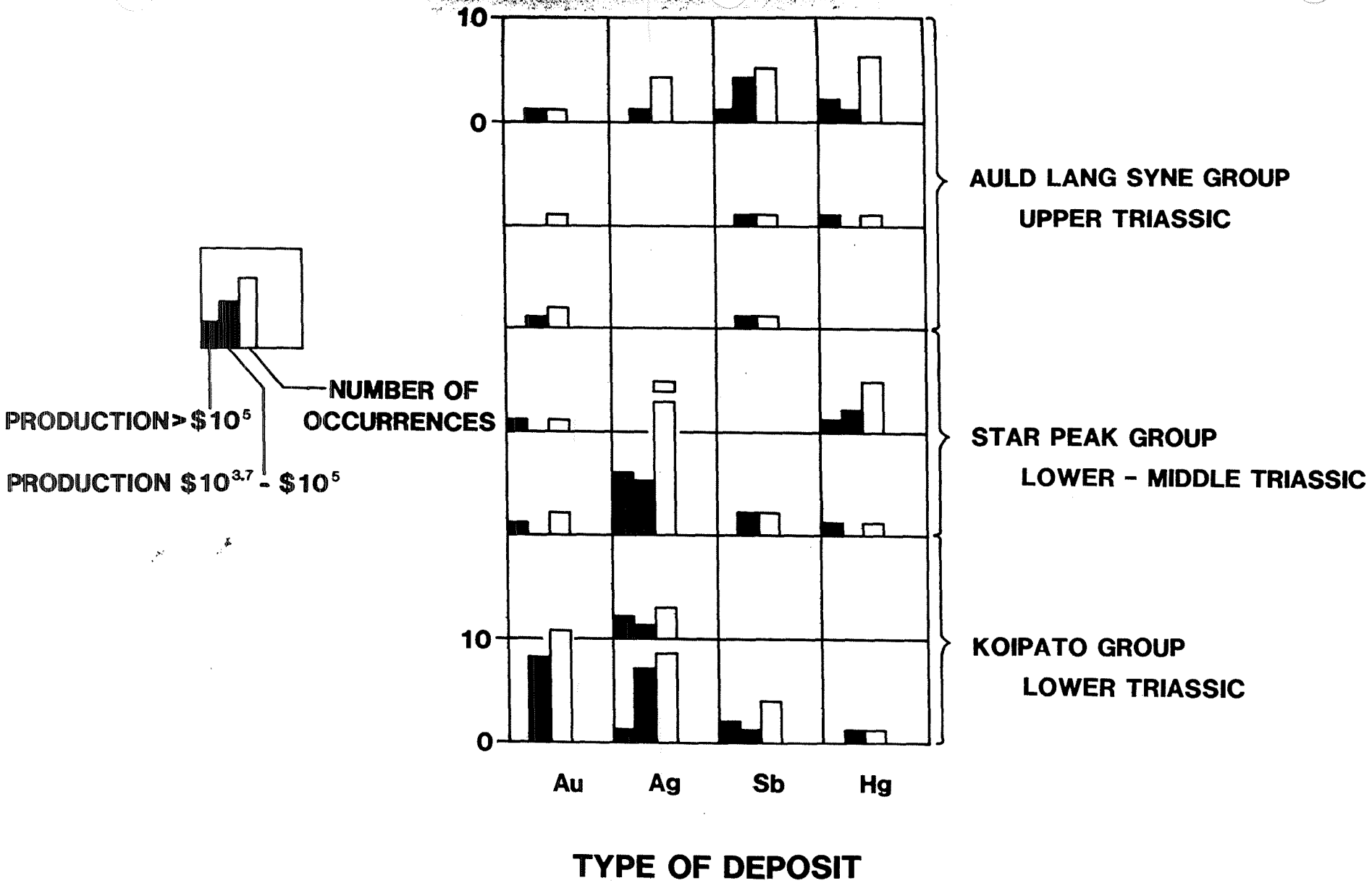

FIGURE 4. Production and frequency of metal deposits related to Mesozoic stratigraphy.

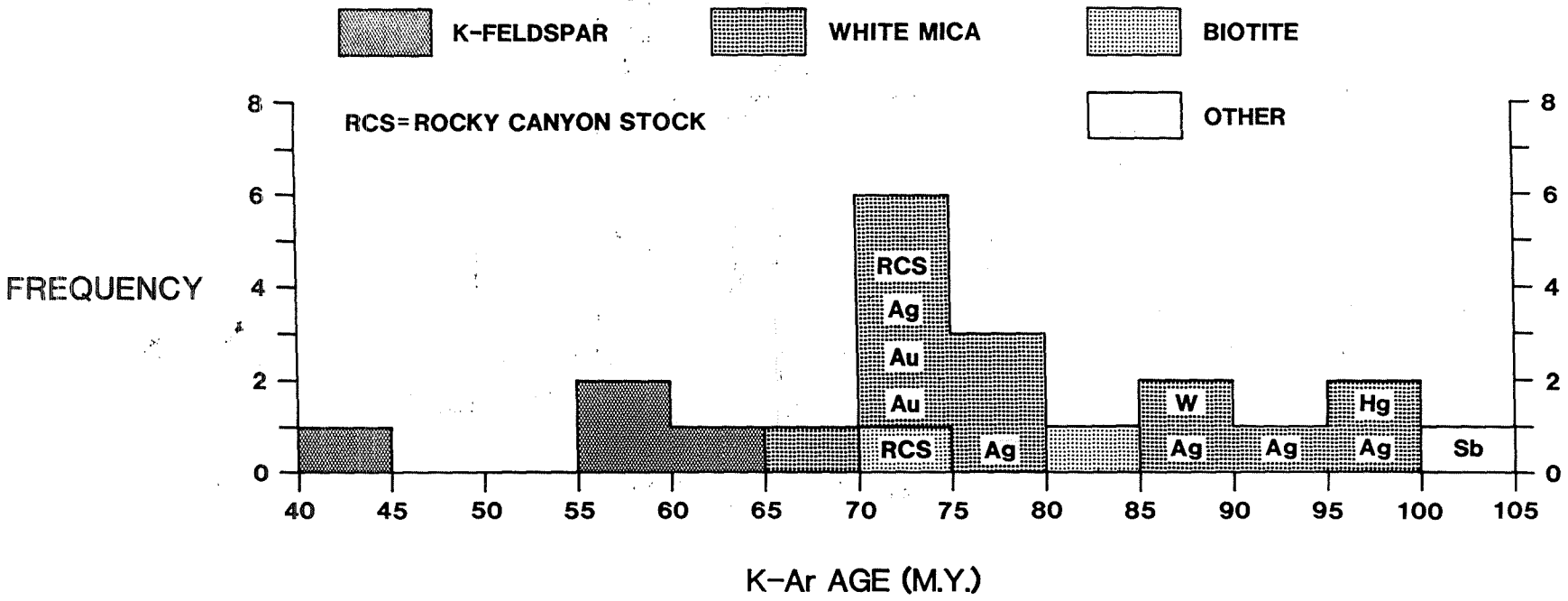

FIGURE 5. Age-frequency plots of K-Ar dates on rocks and hydrothermal minerals from the Humboldt Range.

SAMPLE DESCRIPTIONS

HR79-104 K-Ar
Quartz-sulfide–K-feldspar vein (NW/4 S5,T31N,R34E; Upper Imlay Canyon; Pershing Co., NV). *Analytical data:* K_2O = 14.6%; $^{40}Ar^*$ = 9.1286 × 10^{-10} mol/g; $^{40}Ar^*/\Sigma^{40}Ar$ = 0.872. *Comment:* Age considered anomalously young perhaps due to Ar loss or late-stage addition of K (note extremely high value of K_2O).
(K-feldspar) 42.9 ± 1.2 m.y.

HR81-1 K-Ar
Quartz-sulfide–K-feldspar vein (NW/4 S4,T28N,R34E; Hoover Mine, Limerick Canyon; Pershing Co., NV). *Analytical data:* K_2O = 15.4%; $^{40}Ar^*$ = 1.2550 × 10^{-9} mol/g; $^{40}Ar^*/\Sigma^{40}Ar$ = 0.539. *Comment:* Age considered anomalously young perhaps due to Ar loss or late-stage addition of K (note extremely high value of K_2O).
(K-feldspar) 55.7 ± 2.2 m.y.

F-22 K-Ar
Quartz-sulfide–K-feldspar vein (SE/4 S16,T28N,R34E; Friedman level, Nenzel Hill; Pershing Co., NV). *Reference:* Vikre, 1981, table 3A.
(K-feldspar) 57.9 ± 2.9 m.y.

HR80-10 K-Ar
Quartz-sulfide–K-feldspar vein (NE/4 S23,T29N,R33E; Pole Canyon Mine, Pole Canyon; Pershing Co., NV). *Analytical data:* K_2O = 12.03%; $^{40}Ar^*$ = 1.1174 × 10^{-9} mol/g; $^{40}Ar^*/\Sigma^{40}Ar$ = 0.642. *Comment:* Age considered anomalously young perhaps due to Ar loss.
(K-feldspar) 63.4 ± 2.3 m.y.

RD82-2 K-Ar
Quartz-sericite-dumortierite schist (NE/4 S1,T28N,R33E; Lone Mountain Ridge; Pershing Co., NV). *Analytical data:* K_2O = 5.04%; $^{40}Ar^*$ = 4.9623 × 10^{-10} mol/g; $^{40}Ar^*/\Sigma^{40}Ar$ = 0.907.
(white mica) 67.2 ± 2.1 m.y.

HR80-7 K-Ar
Quartz-sulfide-sericite vein (NE/4 S2,T30N,R33E; Rye Canyon Agnes Mine, Panther Canyon; Pershing Co., NV). *Analytical data:* K_2O = 6.56%; $^{40}Ar^*$ = 6.8236 × 10^{-10} mol/g; $^{40}Ar^*/\Sigma^{40}Ar$ = 0.766.
(white mica) 70.8 ± 2.1 m.y.

K-Ar
Quartz monzonite (NW/4 S2,T29N,R33E; Rocky Canyon; Pershing Co., NV). *Reference:* Silberman and others, 1973; Vikre, 1981, table 3A.
(biotite) 71.4 ± 3.0 m.y.

8. *HR81-2* K-Ar
Pegmatite in quartz monzonite (SE/4 S11,T29N,R33E; Wright Canyon; Pershing Co., NV). *Analytical data:* K_2O = 10.64%; $^{40}Ar^*$ = 1.1241 × 10^{-9} mol/g; $^{40}Ar^*/\Sigma^{40}Ar$ = 0.909.
(white mica) 71.9 ± 2.1 m.y.

9. *LO-1* K-Ar
Quartz-sulfide-gold vein (NW/4 S19,T19N,R34E; Looney Mine, Rochester Canyon; Pershing Co., NV). *Reference:* Vikre, 1981, table 3A.
(sericite) 72.5 ± 2.2 m.y.

10. *Black Canyon Mine* K-Ar
Quartz–K-feldspar vein (SE/4 S19,T31N,R34E; Black Canyon Mine, Black Canyon; Pershing Co., NV). *Reference:* Silberman and others, 1973; Vikre, 1981, table 3A.
(K-feldspar) 73.2 ± 2.0 m.y.

11. *CM-1* K-Ar
Quartz-sericite-dumortierite vein (SW/4 S36,T29E,R33E; Champion Mine, Rolands Canyon; Pershing Co., NV). *Reference:* Vikre, 1981, table 3A.
(sericite) 73.7 ± 2.2 m.y.

12. *OF-SD* K-Ar
Quartz-sericite-andalusite-dumortierite schist (SE/4 S12,T28N,R33E; Tate's prospect, High Grade Canyon; Pershing Co., NV). *Reference:* Vikre, 1981, table 3A.
(sericite) 77.6 ± 2.3 m.y.

13. *POI-127* K-Ar
Quartz-sericite schist (NE/4 S27,T28N,R34E; Black Ridge; Pershing Co., NV). *Analytical data:* K_2O = 4.89%; $^{40}Ar^*$ = 5.6369 × 10^{-10} mol/g; $^{40}Ar^*/\Sigma^{40}Ar$ = 0.500.
(white mica) 78.3 ± 2.4 m.y.

14. *NP-CA* K-Ar
Quartz-sulfide vein (SW/4 S28,T28N,R34E; Nevada Packard Mine; Pershing Co., NV). *Reference:* Vikre, 1981, table 3A.
(sericite) 78.8 ± 2.4 m.y.

15. *SP80-1* K-Ar
Quartz-biotite vein (SE/4 S6,T29N,R34E; Stalin's Present Mine, Rocky Canyon; Pershing Co., NV). *Analytical data:* K_2O = 8.04%; $^{40}Ar^*$ = 9.6710 × 10^{-10} mol/g; $^{40}Ar^*/\Sigma^{40}Ar$ = 0.740.
(biotite) 81.7 ± 2.4 m.y.

16. *HR79-56* K-Ar
Quartz-diopside-sericite skarn (NW/4 S7,T31N,R34E; Starlight Mine, Humboldt Canyon; Pershing Co., NV). *Analytical data:* K_2O = 10.59%; $^{40}Ar^*$ = 1.3312 × 10^{-9} mol/g; $^{40}Ar^*/\Sigma^{40}Ar$ = 0.932.
(white mica) 85.3 ± 2.5 m.y.

17. *BCV-1* K-Ar
Quartz-sulfide-sericite vein (SW/4 S15,T28N,R34E; Crown Point level, Nenzel Hill; Pershing Co., NV). *Reference:* Vikre, 1981, table 3A.
(sericite) 85.7 ± 4.3 m.y.

18. *RD82-1* K-Ar
Quartz-sericite-pyrite altered rhyolite (SW/4 S15,T28N,R34E; Pitt level, Nenzel Hill, 460 ft from E portal; Pershing Co., NV). *Analytical data:* K_2O = 10.25%; $^{40}Ar^*$ = 1.4339 × 10^{-9} mol/g; $^{40}Ar^*/\Sigma^{40}Ar$ = 0.934.
(white mica) 94.6 ± 2.8 m.y.

19. *RD304-275* K-Ar
Quartz-sulfide-sericite vein (SW/4 S15,T28N,R34E; DDH, Nenzel Hill; Pershing Co., NV). *Analytical data:* K_2O = 4.74%; $^{40}Ar^*$ = 6.8444 × 10^{-10} mol/g; $^{40}Ar^*/\Sigma^{40}Ar$ = 0.615.
(white mica) 97.6 ± 3.0 m.y.

20. *SAC85-1* K-Ar
Sericitized fault zone (SW/4 S11,T28N,R34E; mercury prospect; Pershing Co., NV). *Analytical data:* K_2O = 0.88%; $^{40}Ar^*$ = 1.27169 × 10^{-10} mol/g; $^{40}Ar^*/\Sigma^{40}Ar$ = 0.535. *Comment:* Pyrophyllite is a major component of the sample.
(pyrophyllite + quartz + white mica) 97.7 ± 2.9 m.y.

21. *HM85-1* K-Ar
Quartz-clinochlore-stibnite vein (SE/4 S2,T26N,R34E; Hollywood Mine; Pershing Co., NV). *Analytical data:* K_2O = 0.05%; $^{40}Ar^*$ = 7.66362 × 10^{-12} mol/g; $^{40}Ar^*/\Sigma^{40}Ar$ = 0.094. *Comment:* Potassium occurs either in clinochlore or in an undetected phase.
(clinochlore) 103.4 ± 10 m.y.

REFERENCES

Carlson, J. E., Laird, D. W., Peterson, J. A., Schilling, J. H., Silberman, M. L., and Stewart, J. H. (1975) Preliminary map showing distribution and isotopic ages of Mesozoic and Cenozoic intrusive rocks in Nevada: U.S. Geological Survey Open-File Report 75-499.

Dalrymple, G. B., and Lanphere, M. A. (1969) Potassium-argon dating—principles, techniques, and applications to geochronology: San Francisco, W. H. Freeman Co., 258 p.

Ingamells, C. O. (1970) Lithium metaborate flux in silicate analysis: Analytica Chimica Acta, v. 52, no. 2, p. 323–334.

Johnson, M. G. (1977) Geology and mineral deposits of Pershing County, Nevada: Nevada Bureau of Mines and Geology Bulletin 89, 115 p.

Silberling, N. J., and Wallace, R. E. (1967) Geologic map of th Imlay Quadrangle, Pershing County, Nevada: U.S. Geologic Survey Geologic Quadrangle Map GQ-666.

Silberman, M. L., Johnson, M. G., Koski, R. A., and Roberts, R. (1973) K-Ar ages of mineral deposits at Wonder, Seve Troughs, Imlay, Ten Mile, and Adelaide mining districts in ce tral Nevada: Isochron/West, no. 8, p. 31–35.

Silberman, M. L., and McKee, E. H. (1971) K-Ar ages of granit plutons in north-central Nevada: Isochron/West, no. 71-1 p. 15–20.

Smith, J. G., McKee, E. H., Tatlock, D. B., and Marvin, R. F (1971) Mesozoic granitic rocks in northwestern Nevada—link between the Sierra Nevada and Idaho batholiths: Geolog cal Society of America Bulletin, v. 82, p. 2933–2944.

Stacey, J. S., Sherrill, N. D., Dalrymple, G. B., Lanphere, M. A and Carpenter, N. V. (1981) A five-collector system for th simultaneous measurement of argon isotopic rations in a stati mass spectrometer: International Journal of Mass Spectrome try and Ion Physics, v. 39, p. 167–180.

Steiger, R. H., and Jager, E. (1977) Subcommission on geo chronology—convention on the use of decay constants in geo and cosmochronology: Earth and Planetary Science Letters v. 36, p. 359–362.

Vikre, P. G. (1981) Silver mineralization in the Rochester district Pershing County, Nevada: Economic Geology, v. 76, p. 580 609.

Wallace, R. E., Silberling, N. J., Irwin, W. P., and Tatlock, D. B (1969a) Geologic map of the Buffalo Mountain Quadrangle Pershing and Churchill Counties, Nevada: U.S. Geological Survey Geologic Quadrangle Map GQ-821.

Wallace, R. E., Tatlock, D. B., Silberling, N. J., and Irwin, W. P (1969b) Geologic map of the Unionville Quadrangle, Pershin County, Nevada: U.S. Geological Survey Geologic Quadrangle Map GQ-820.

Geothermal Resources Council, TRANSACTIONS, Vol. 11, October 1987

AN OVERVIEW OF THE GEOLOGY AND SECONDARY MINERALOGY OF THE HIGH TEMPERATURE GEOTHERMAL SYSTEM IN DIXIE VALLEY, NEVADA

A.F. Waibel

Columbia Geoscience
22495 NW Quatama Rd.
Hillsboro, Oregon 97124

ABSTRACT

Lithologic units encountered in the Dixie Valley geothermal field range from Triassic marine sediments to Recent basin-filling sediments. Structural features affecting the location of the geothermal activity include Mesozoic thrusting, late Tertiary normal faulting and Quaternary to Recent normal faulting. The hydrothermal mineral suite is variable, due in part to rock-gas reactions.

INTRODUCTION

The geology of the Dixie Valley Geothermal Field (fig. 1) is quite varied. The stratigraphic sequence, in the order encountered in the majority of the drill holes, includes basin-filling sediments, silicic tuff-rich sediments, Miocene basalt, Miocene sediments, Oligocene silicic volcanics, Jurassic oceanic crust, Jurassic marine sediments, Cretaceous granodiorite and Triassic marine sediments (fig. 2). The most recent published geological mapping for the general area includes Page (1965), Wilden and Speed (1974) and Speed (1976).

The structural history is as complex as the lithology is diverse. Carbonaceous marine sediments of Triassic age are underlying, in thrust-fault contact, Jurassic oceanic crustal rocks. North-striking normal faulting occurred in this area in the Miocene, followed by a superimposed NNE-striking set of normal faults. The Dixie Valley graben and the Stillwater Range are artifacts of the most recent episode of faulting. Highly fractured areas hosting geothermal production appear to be best developed in tensional zones resulting from strike-slip and normal faulting at the intersections of the two generations of normal faults in a manner similar to that described by Aydin and Nur (1982). Recharge for the northern portion of the system is most probably coming from the north.

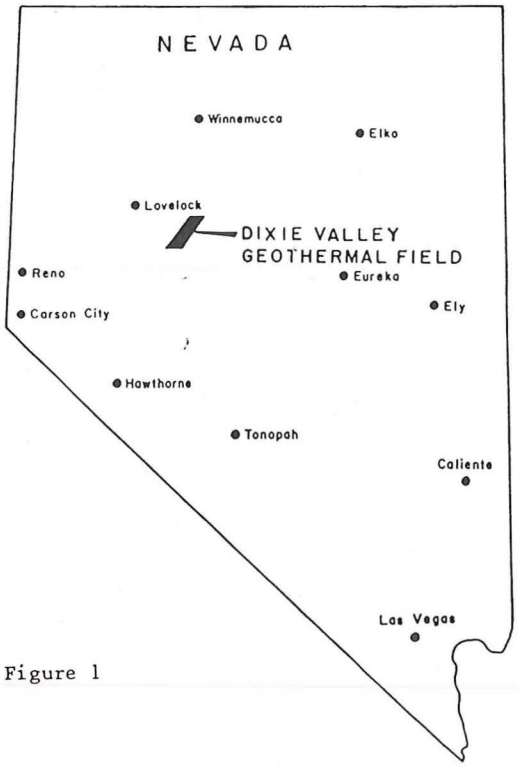

Figure 1

LOCATION OF DIXIE VALLEY GEOTHERMAL FIELD
CHURCHILL COUNTY, NEVADA

LITHOLOGY

Basin Filling Sediments

Horst and graben structure appears to have dominated the Dixie Valley area since the Miocene. The current Dixie Valley basin is asymmetrical with the deepest portions occurring to the west along the Stillwater Range. The basin-filling sediments are observed to be in excess of 7000 feet thick in some of the geothermal wells. Seismic data suggest that toward the center and along the eastern portion of Dixie Valley these sediments are usually no more than 2000 to 3000 feet thick.

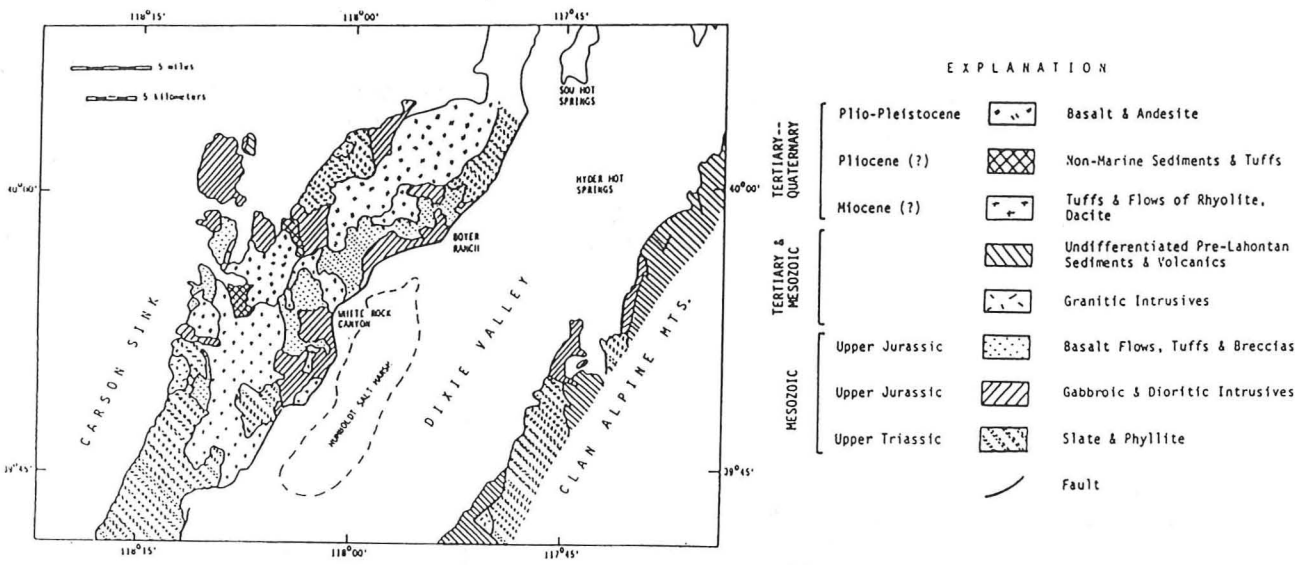

Figure 2 Generalized geology of the Dixie Valley, Nevada, area (from Denton, et al, 1980).

The composition of the fill which makes up the basin sediments is somewhat variable. Toward the center and along the eastern portions of the valley the section is predominantly reworked silicic tuffs, eroded from the Clan Alpine Range. Along the Stillwater Range the contributing rock types are more varied. Reworked silicic tuffs tend to be predominant among the deepest (earliest) sediments in the geothermal production area. With decreasing depth the sediments are usually variations of a pebble conglomerate with a clay matrix. Near the discharge of major Stillwater Range drainages (i.e. Cottonwood Canyon) conglomerates are most common and horizons of clay and silt are minor. Areas away from major drainages have basin-filling sediment sections dominated by clay, silt, and sand-size particles while conglomerate horizons are less common.

Cobble and sand-rich horizons within the basin-filling sediments are able to support pore space permeability and fluid movement. Fracture permeability occurs but is not common in this section. The abundance of clay, and the moderate to poor lithification in these sediments, are not conducive to the propogation of fault related fracturing. The total lithostatic pressure is low enough, however, to permit permeability of limited duration to occur along normal faults. The permeable zones hosting geothermal fluids are, in most cases, readily identifiable by the shift in stable mineral phases resulting from geothermal fluids with low oxygen activity interacting with oxidized basin-filling sediments.

Miocene Basalt

The Miocene basalts overly Miocene lacustrine sediments, and are overlain by as much as 6000 to 7000 feet of basin-filling sediments in the area of the geothermal field. These same basalts crop out as high as 8000 feet in elevation in the Stillwater Range. Page (1965) estimates the age of these basalts to be Pliocene or younger. A K-Ar date of a sample from the Stillwater Range, analyzed for Sunedco in 1981, shows an age of 8.5 $\pm$ .4 million years. Outcrops in the Stillwater Range show the basaltic volcanic sequence to be quite varied in form, ranging from flat-lying lava flows to agglutinates, scoria and palagonite tuffs characteristic of evolved maar complexes. In the area of Kitten Springs Pass, about five miles northwest of the Dixie Valley geothermal field, the palagonite tuff sequence is approximately 800 feet thick. The basalt section as observed in geothermal drill holes is often abbreviated due to normal faulting. Observed thicknesses in the drill holes range from less than 300 ft. to greater than 1900 ft.

In hand specimen the basalt flows range from aphanitic hypocrystalline to porphyritic. Thin-section specimens show the crystal compositions most commonly to include plagioclase (An_{50} or greater), clinopyroxene, olivine, and opaque iron-titanium oxide. Millimeter-size phenocrysts of olivine are present in many, though not all, of the specimens. The rock texture ranges from pilotaxitic to ophitic.

In outcrops the basalt alteration is characterized by oxidation of femic minerals, zeolite and calcite alteration of plagioclase, and devitrification of glassy matrix. This is a typical surface alteration suite resulting from downward percolation of oxygenated meteoric water. Two distinct alteration mineral suites are observed in the Miocene basalt section in drill holes. The effects of weathering are plainly visible in portions of the basalt chips recovered during drilling. Other portions of the basalt show a later overprinting of alteration resulting from interaction with geothermal fluid of low oxygen activity.

Miocene Sediments

The Miocene lacustrine sedimentary section is conformably overlain by Miocene basalt, and is conformably underlain by silicic volcanic tuffs of late Oligocene age. The sediments are composed of intercalated volcaniclastics, carbonaceous siltstone, and silicic volcaniclastic tuff. The section is observed in a truncated form in many of the drill holes in Dixie Valley due to normal faulting.

The upper portion of the section consists of intercalated volcaniclastic sediments and carbonaceous siltstone. The volcaniclastic sediments appear to be derived predominantly from silicic volcanics and tuffs. Authigenic chlorite and illite alteration predominate in the groundmass and detrital subhedral to euhedral quartz is usually present in minor amounts. The dark brown to black carbonaceous siltstone horizons are fissil and often pyritic. Attempts to separate and identify microfossils from the siltstone have been made to more precisely bracket the age of sedimentation. To date these attempts have been unsuccessful due to the poorly preserved state of the fossils.

The lower portion of the sedimentary section is composed of silicic tuffaceous sediments with only minor carbonaceous siltstone horizons. Authigenic illite and chlorite dominate the mineralogy of these reworked devitrified silicic volcanics. Detrital subhedral to euhedral quartz, originally a primary component of the silicic tuffs, is present in minor amounts. The basal boundary of this sedimentary unit is not distinct. A progression is observed from reworked silicic tuffs, to primary devitrified silicic tuff, to primary welded silicic tuff. The latter is part of the Oligocene silicic volcanics.

Clays represent the dominant mineralogy in this sedimentary section. As a result, tectonic strain tends to cause plastic deformation rather than brittle failure and rock breakage. It is unusual, therefore, to find significant fracture related permeability within this sedimentary section. Fault related permeability would likely be limited and transitory.

Rock-water-gas interaction between the sediments and the geothermal system is limited due to the low potential for porosity and permeability. The thermal effects of the geothermal system, however, can be observed. The formation clays are predominantly illite, non-expanding Fe-bearing clays, and fine crystalline authigenic chlorite. The present phyllosilicate suite is the result of very low-grade metamorphism of smectite clays. Organic matter in the carbonaceous siltstone is near thermal maturity. Gas chromatograph monitoring during drilling indicates that methane is the only hydrocarbon currently being generated from these sediments.

Oligocene Silicic Volcanics

Oligocene silicic volcanics dominate the Clan Alpine Range to the east of the Dixie Valley geothermal field, and are present in the Stillwater Range to the south and west of the geothermal field. These volcanics are only rarely encountered in the geothermal drill holes, however. In the Clan Alpine Range intercalated beds of cemented and welded tuffs are in excess of 4000 feet thick. Oligocene tuff cropping out in the Stillwater Range seldom exceeds a few hundred feet thick. These volcanics have only rarely been encountered in the geothermal drill holes, where the section appears to often be faulted out by basin-bounding normal faults. A single good, though incomplete, section of these silicic tuffs is observed in one well, where a 180 foot section of predominantly welded biotite-quartz-sanidine tuff is overlain by Miocene sediments. A normal fault contact truncates this section with the foot wall consisting of Jurassic oceanic igneous rock.

Welded portions of the Oligocene silicic tuffs are brittle and generally fracture when subjected to strain. Poorly welded and cemented aspects of the tuff sequence are generally soft and undergo plastic deformation rather than structural failure when subjected to strain. The potential for fracture permeability is good in the highly welded portions of the tuff and low in the poorly welded and cemented portions of the tuff.

Cretaceous Granodiorite

A silicic plutonic rock is observed in a number of the drill holes. The mineralogy of the rock is distinctly different from the igneous rocks of the Jurassic oceanic crust. Where least altered this rock consists of quartz, plagioclase, biotite, muscovite, hornblende, and minor K-feldspar, sphene, rutile, and Fe oxide. The mafic minerals usually are slightly chloritized. In a few areas where the rock has been strongly altered the mafic minerals have been almost completely replaced by chlorite, the plagioclase has been albitized, secondary K-feldspar has formed at the expense of muscovite, and secondary epidote and calcite are present in minor amounts. The less altered portions of this rock can best be described as quartz monzonite to granodiorite.

The genetic and structural relationship of this silicic intrusive to other igneous rocks in the area is not clear. It is typically observed as a foot wall in fault contact with Jurassic rock. The mineralogy and texture resemble intrusives cropping out along the west side of the Stillwater Range in the New York Canyon area that have been dated as late Cretaceous. This would place the intrusive event after the allochthonous thrust faulting and would explain thin fingers or layers of granodiorite observed within thrust fault zones as intrusive sills.

No commercial geothermal production has been developed from the granodiorite in the Dixie Valley geothermal field. The rock is mechanically competent and should fracture when under stress. Fracture permeability would tend to slowly be sealed in the unaltered granodiorite as calcic plagioclase is altered to albite, calcite and epidote.

Jurassic Spilite

The Jurassic section in the Stillwater Range is complex and diverse, and the term "spilite" is used in possibly a misleading way. The predominantly igneous suite ranges from spilitic basalts, keratophyres, and trondhjemites to albitites, plagiogranites, and gabbro. The minerals commonly present include plagioclase (generally An 5-15), hornblende, calcite, augite, biotite, Fe-Ti oxides, and minor epidote, pyrite, sphene, apatite, and rutile. Chlorite is observed as a very common alteration product of hornblende, augite, and biotite. Locally lenses of sedimentary rock, most commonly siltstone, are observed within the igneous series.

Published work on the area (Willden and Speed, 1974; Speed, 1976) describe the Jurassic igneous rock as a locally intruding lopolith. Autochthonous thrusting has been associated with the intrusion of the lopolith. Field and laboratory evidence suggests an alternative interpretation; that the entire Jurassic igneous section is an allochthonous fragment of oceanic crust, thrust over Triassic marine shelf and slope sediments. The most obvious points leading to this re-interpretation include extensive sodium metasomatization, pervasive secondary calcite, and abundant lamellar plates, lenses and nappes, markedly disrupting specific lithologic and stratigraphic continuity. The "lopolith" is remarkably similar to igneous portions of ophiolites observed in many places throughout the world.

The large blocks of spilite, keratophyre, and trondhjemite rock tend to be very brittle and are capable of maintaining good fracture permeability. The albitite and plagiogranite are somewhat less prone to host good fracture permeability. The prevailing mineral assemblage (albite, calcite, chloritized hornblende, chloritized biotite, and chloritized augite) tend to be stable in the chemical and thermal environment of the currently active geothermal system.

The mineral suite is not mechanically stable in the cataclastic environment of thrust faulting, shear planes, and nappes. The mafic minerals are usually altered to serpentine and chlorite; the albite tends to be broken up into small angular fragments; and the calcite tends to recrystallize as a matrix mineral. The result is lenses of mechanically unstable rock within the more competent formation. While these lenses have the potential of hosting permeability, the permeability does not always have good communication with major geothermal production, and the formation tends to slough during well flowing.

Jurassic Marine Sediments

Jurassic shallow marine sediments are observed in the Stillwater Range to the west of the Geothermal field. Compositionally these sediments consist of carbonate, quartzite, and minor conglomerate. Willden and Speed (1974) refer to these sediments as the Boyer Ranch Formation, and describe the carbonate and conglomerate as basal and the quartzite or quartz arenite as the upper unit. The continuity of this section is not obvious in the Stillwater Range. Thrusting of the Jurassic oceanic crust clearly involved the Boyer Ranch Formation. Portions of the sediments can be observed overlying, overridden by, and mechanically incorporated into, the allochthonous oceanic crust. The Boyer Ranch Formation may represent shallow marine sedimentation in a closing basin, bounded in part by the encroaching oceanic crustal block.

The quartz arenite portion of the Boyer Ranch Formation is lithified and tends to host open permeability along fault planes. Outcrop evidence suggests, however, that it is not prone to extensive fracture propogation. The rock is composed largely of lithified quartz grains and should be chemically and mineralogically stable in the geothermal system.

The basal carbonate and conglomerate portion of the Boyer Ranch would likely fracture under stress, though the fractures would tend to reseal with recrystallization. Dolomitic portions of the carbonate show the development of serpentine along fault and shear planes. Both fracture permeability and mechanical stability would likely be quite variable in the basal carbonate portion of the Boyer Ranch Formation.

Triassic Marine Sediments

Calcareous carbonaceous shale, siltstone, and silty carbonates crop out in the Stillwater Range underlying the allochthonous Jurassic oceanic crustal rock. Fragments and lenses also occur incorporated into the lamellar shear zones within and near the base of the Jurassic oceanic block. These carbonaceous marine sediments are correlative to the Favret Formation, a lower member of the Star Peak Group.

In fresh hand-specimen the marine sediments are commonly black to gray, variably carbonaceous, variably pyritic siltstone to dark gray carbonaceous limestone. A few of the outcrop exposures show siltstone which has been oxidized to light gray, light green-gray, and purple. Within the drill holes of the geothermal field the Triassic sediments are observed as cataclastized lensed in lamellar shear zones within the Jurassic rocks.

Mechanically the Triassic sediments will deform rather than fracture and fail when subjected to strain. Dolomite-bearing horizons form secondary serpentine during deformation. These characteristics make this formation a poor host for geothermal production.

The presence of these sediments at depth, below the thrust fault, plays an important role in the character of the geothermal system. The Favret

formation is rich in hydrocarbons and is sub-mature in exposures to the northeast of Dixie Valley. The maturation level is much higher in the hottest portion of the geothermal system. Much of the gas associated with the geothermal fluid likely originates in the metamorphosing Triassic sediments in the deep portions of the geothermal system. CH_4, H_2S, N_2, NH_3 and CO_2 are likely derived from late stage thermal degradation of organic matter and sulfur compounds in the carbonaceous sediments.

STRUCTURAL HISTORY

Geothermal production in Dixie Valley is related to an extended, complex network of fault and fracture permeability. The combined tectonic history is, therefore, an important component in interpreting the production potential of any given location within the geothermal field. Three major faulting patterns are recognized in the vicinity of the Dixie Valley Geothermal Field. The first of these is thrust faulting; the second and third are both normal faulting.

Thrust faulting of Jurassic oceanic crustal rocks over Triassic shelf-related marine sediments is observed in the Stillwater Range. This thrust faulting event is part of the last in a series of crustal shortening events that involved allochthonous thrusting of deep marine strata over older rocks (Antler Orogeny, Devonian-Mississippian; Sonoma Orogeny, Triassic; and Nevadan Orogeny, Jurassic-Cretaceous).

The Jurassic oceanic rock has undergone differential movement along horizonal planes within the overthrusting block resulting in horizonal cataclastic zones. Inclusions of marine sediments, including argillite, sandstone, and locally, limestone, into the thrusting Jurassic plate, are observed in outcrops along the Stillwater Range. Turbulence in zones along the leading edge of the thrust block, and locally within the block, has resulted in the development of small scale melange-like features. These features usually include cataclastized fragments from both the underlying Triassic strata and the overlying Jurassic strata. Serpentinization of portions of the Jurassic mafic igneous rocks and of Triassic dolomitic sediments is common within these melange-like features.

The Stillwater Range-Dixie Valley area of Nevada appears to have been structurally quiet from the Cretaceous through the Oligocene. Subsequent to the eruption of silicic volcanism in the late Oligocene a series of north-striking normal faults developed. The best surface expressions of these faults can be observed along the western edge of the Clan Alpine Range and in the White Rock Canyon area in the Stillwater Range. Seismic data show similar north-striking patterns to continue into Dixie Valley, now buried by basin filling sediments (fig. 3). The surface expressions of this episode of normal faulting show evidence of rotation, suggesting that these were listric faults. The relationship between the timing of the late Miocene basalt eruptions and the north-striking normal faulting is unclear. Field evidence shows quite clearly that both Jurassic and Oligocene rocks were affected by this fault movement. No outcrops show a similar rotational relationship involving the Miocene basalt.

The development of the current high-angle NNE-striking normal faulting that defines the Stillwater Range and Dixie Valley physiographic features is relatively young, and is superimposed over the earlier two tectonic features. The uplift of the Stillwater Range occurred after the late Miocene basalt eruptions, as is evidenced by the flat-lying basalt flows and palagonite tuffs which occupy some of the highest elevations within the range. The onset of this last episode of faulting, therefore, could be no older than late Miocene to early Pliocene. Historic earthquakes along the basin-range boundaries attest to the continuing activity.

The NNE pattern of extensional faulting, superimposed on earlier N-striking normal faulting, has resulted in differential movement of the blocks which make up the Stillwater Range. The older N-striking faults exhibit subsequent strike-slip movement, a reaction to current WNW extension. The combination of dip-slip movement on the NNE-striking faults and strike-slip movement on the N-striking faults has resulted in localized zones of tension and compression along the western portion of Dixie Valley similar to the basin structures described by Aydin and Nur (1982). The tensional features form asymetrical rhombograben-

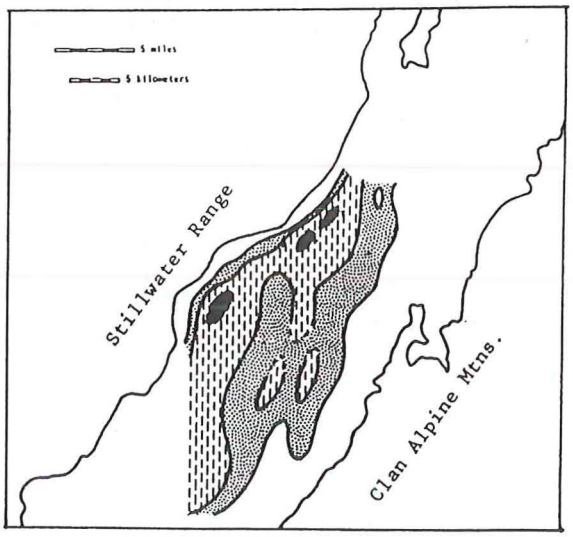

Figure 3 Estimated thickness of the Tertiary to Recent section in Dixie Valley, Nevada, based on seismic data from Sunedco, Southland Royalty and Amoco.

3000 to 6000 feet thick
6000 to 7500 feet thick
greater than 7500 feet thick

like structures bound by steeply dipping normal faulting toward the Stillwater Range and by shallow dipping normal faulting toward the vally. These features are identifiable on many of the seismic lines which cover much of the northern portion of Dixie Valley (Waibel, 1985). Figure 3 shows locallized deep basins associated with the north-trending normal faulting in the central to eastern portion of the valley and with the more recent combined normal and strike-slip faulting along the western edge of the valley. Increased fault and fracture permeability associated with the localized rhombograbens plays a major role in hosting geothermal fluid. The degree to which pereability develops in these structures is modified, however, by the physical characteristics of the rock involved at any givel location.

The occurrance of faults or fractures within a brittle rock in itself does not guarentee production. Fault planes are not always "planer". Normal faults associated with extentional tectonics in Dixie Valley tend to undulate somewhat. This unevenness results in portions of fault planes being under high compression and impermeable, regardless of the rock type involved. Conversely other portions will be under tension and support open spaces possibly tens of centimeters wide.

HYDROTHERMAL MINERALOGY

Multiple thermal and metasomatic events have affected the rock that now makes up the areas of Dixie Valley and the Stillwater Range. Each of these events have left a mineralogical signature in the host rock. The temperatures of most of these metasomatic events appears to have ranged from 50 to 250^{o}C, similar to the range of temperatures in currently active Dixie Valley geothermal systems. As a result, many of the secondary minerals are stable in, and characteristic of, more than one thermal event. The mineralogical effects of fossil thermal events must be distinguished from those of the currently active system before any interpretations pertaining to this current system can be made. Detailed mineral associations and morphologies are employed to assist in separating the effects of individual thermal events. It is possible in many cases, through careful observation, to identify which mineral occurrances are associated with the current geothermal activity.

The earliest thermal and metasomatic event recognized in the rocks of the Stillwater Range involves the Jurassic oceanic crustal rocks which Speed (1976) refers to as the Humboldt Lopolith. The pre-alteration rocks of this group were predominantly basalt, diabase, gabbro, and locally more leucocratic fractionations of this suite. The major primary mafic minerals are clinopyroxene and hornblende with local occurrences of biotite. Extensive sodium metasomatization is manifested in very extensive albitization and local scapolitization of plagioclase. Secondary calcite occurs both disseminated within the rock and in veins. Chloritization of mafic minerals is ubiquitous, and varies in degree from minor to near complete replacement of the mafics. Additional secondary minerals, including epidote, pyrite and chrysotile, are irregularly distributed throughout portions of the Jurassic igneous suite. The postalteration rock suite includes spilite, keratophyre, trondhjemite, albitite, and plagiogranite.

The spilitic rock suite of the Jurassic section in the Stillwater Range is typical of the igneous rock suites observed in many ophiolite complexes. The sodium metasomatization may likely have occurred while this section was still in a marine environment. A reasonable sodium reservoir to support this type of extensive alteration would be sea water.

A second metasomatic event, confined to the Jurassic oceanic rocks, involves silica and iron oxides. Along the eastern edge of the Stillwater Range this event is represented by quartz filled veins in association with specular hematite replacement of Jurassic spilitic rock. Fragments up to 15 cm across within the fault zone are observed to be completely replaced by hematite. Thin-sections of rock samples from the host rock in the vicinity of these quartz-filled faults show specular hematite replacement of the rock outward from the veins. Along the western margin of the Stillwater Range, in the Buena Vista Hills, specular hematite and magnetite replacement of Jurassic spilitic rock has been locally intense enough tc allow for commercial mining of iron ore.

Neither the sodium metasomatization nor the quartz-hematite mineralization has been fully investigated. The timing and possible relationship between the two events has not been determined. Convection of water in the Jurassic rock was clearly involved in thermal energy and chemical changes associated with both the sodium metasomatization and the hematite-quartz mineralization. It is possible that both of these secondary features developed at or near the same time, while these rocks were still part of an ocean environment.

Additional thermal and metasomatic events in the Dixie Valley-Stillwater Range area include contact metamorphism associated with Cretaceous plutonic intrusives as well as Oligocene silicic volcanism. Evidence of the former is observed in the Stillwater Range to the south of the current geothermal activity. The older secondary mineral suites are characterized by skarns and quartz-calcite veins. These alteration zones are observed to contain predominantly sub-economic sphalerite, chalcopyrite and galena in a gangue of epidote, garnet, pyrite, quartz, calcite and magnetite. The Chalk Mountain, La Plata and I.X.L. Mining Districts are in these contact metamorphic areas.

Toward the southern end of Dixie Valley, contact metamorphism and hydrothermal activity are associated with Oligocene and early Miocene silicic volcanism. Hydrothermal activity resulted in precious metals, quartz, adularia, and local minor fluorite being deposited in breccia, fault, and contact shear zones. The Wonder and Fairview Mining Districts are examples of this activity.

The most recent volcanism in the Dixie Valley area is the late Miocene eruption of basalt. Subvolcanic dikes are observed in the Stillwater Range to the west of the geothermal field. Contact metamorphic effects are usually limited to a few tens of centimeters away from the edge of the intrusives and consist mainly of chloritization. No hydrothermal activity has been observed to be associated with this event.

Hydrothermal mineralization associated with the currently active geothermal system varies with temperature and type of host rock. The fluid has low oxygen activity, low total dissolved solids, limited sulfur activity (Benoit, 1987), and is likely saturated in methane. The character of the fluid appears to be influenced by low-grade metamorphism of carbonaceous marine sediments. Precipitation mineralization in the deeper production from Jurassic igneous rock is usually limited to quartz. Host rock alteration by the hot fluid is limited to pyrite, forming at the expense of Fe-Ti oxide. The host rock is already at a chlorite-albite grade of greenschist metamorphism and is chemically stable in the presence of the hot fluid. Calcite veining, as observed in cuttings from production zones within the Jurassic section does, not appear to be co-genetic with the druse quartz which is currently forming. Both the calcite veining observed in the well cuttings and the abundant calcite veining observed in the Jurassic section in the Stillwater Range are probably artifacts of much earlier sodium metasomatization.

Hydrothermal mineral reactions within the Miocene basalt are substantially different from the reactions observed in formations underlying the basalt. Major chemical reactions between the basalt and the geothermal system involve oxidation of hydrogen sulfide and methane, reduction of the iron in hematite and albitization of relict plagioclase. The resulting alteration minerals include chlorite, pyrite, albite, calcite and localized epidote. Precipitation minerals include quartz, chlorite, and epidote or Ca-zeolites. The occurrences of epidote and laumontite tend not to overlap except in those areas where a retrograde shift in mineral stability from epidote to laumontite has occurred. No mineral-chemical evidence for mixing of geothermal and non-geothermal water in the basalt has been identified.

The marked difference between the hydrothermal mineral assembleges in the two mafic igneous units is the combined result of the presence of different secondary mineral phases prior to the introduction of the geothermal fluids and the composition of the geothermal fluid. Buried Miocene basalt remains oxidized where unaffected by geothermal fluids, with reddish hematite as a major Fe mineral. The Jurassic spilitic series has been albitized and partially chloritized prior to the current geothermal activity. The significant change within the geothermal fluid as it passes through the Jurassic section is a limited conductive heat loss. This results in slight but steady silica oversaturation, manifested by the precipitation of druse quartz along fracture surfaces. The reduced geothermal fluid, and associated H_2S and CH_4 gases, react with the weathered Miocene basalt. The major reactions involve oxidation of gases by hematite and sodium replacement of calcium in plagioclase. From these chemical reactions iron, sulfur, carbonate and calcium are available to form the hydrothermal minerals observed in the cuttings.

Geothermal fluids discharging into the basin filling sediments react with the rock in a manner similar to the fluids in the Miocene basalt. In the sediments, however, the temperature of the fluids has decreased to below the epidote and wairakite stability range for a near-neutral pH. Lower temperature mineral reactions in the sediments involve smectite altering to illite, hematite altering to chlorite, and precipitation of quartz, chlorite, and laumontite or heulandite.

Age estimates have been made on two hydrothermal silica specimens from the geothermal system using the ionium/thorium method (Struchio, personal communication). The facilities at the Argonne National Laboratories in Argonne, Illinois were used. The first sample is of dense clear cryptocrystalline silica from a silicious sinter hot spring deposit in section 15, T24N, R36E. The hot spring is no longer active, and the area has been uplifted by ongoing normal faulting along the Stillwater Range front. Total uplift since the hot springs deposits formed may be as much as 200 feet. The estimated age of this deposit is determined to be 9,000 $\pm$ 2,000 years.

A second sample was collected for dating from hydrothermally precipitated cryptocrystalline silica near the Senator Fumaroles in section 32, T25N, R37E. This sample formed near the boiling plane below the topographic surface. Subsequent uplift by normal faulting along the Stillwater Range front now positions this rock 250 feet above the Dixie Valley floor. The age of this sample is much less difinitive, with a maximum possible age of 300,000 years and a minimum possible age of 150,000 years.

CONCLUSIONS

Geothermal production in the Dixie Valley field is defined by fault and fracture permeability. Rather than being strata bound, permeability is defined by, and varies with, the physical characteristics of each rock type. The production potential of a rock is best defined by its mechanical and mineral-chemical stability. The existence of open fractures is dependent on the presence brittle rock; rock that will fail rather than deform under tectonic strain. In the Dixie Valley, field producing fractures are, therefore, most likely to occur in brittle igneous rock, and least likely to occur in soft clay-rich sedimentary rock with secondary hydrous Mg minerals. Subsequent to fracturing, the longevity of permeability is dependent upon the mineral and chemical stability of the rock in the presence of geothermal fluid and gas.

The secondary hydrothermal minerals associated with the high temperature geothermal system in Dixie Valley do not lend themselves to the rote or blind "mineral=temperature" interpretation presented for many other geothermal fields. The Dixie Valley field is likely not unique in this feature, as secondary minerals are an artifact of multiple populations of chemical components reacting with each other in variably changing conditions. Secondary minerals can be used as useful tools in reducing exploration and production drilling costs only after site-specific constraints on rock-water-gas reactions are developed.

ACKNOWLEDGMENTS

The author would like to thank the Hughes group from Tyler, Texas and Oxbow Geothermal from Reno, Nevada for permission to publish the Dixie Valley data.

REFERENCES CITED

Aydin, Atilla and Nur, Amos, 1982, Evolution of pull-apart basins and their scale independence: Tectonics, Vol. 1, No.1, pp. 91-106.

Benoit, W.R., 1987, Early stage carbonate sealing characteristics in Dixie Valley well bores: Geoth. Res. Council Trans., Vol. 11, in press.

Denton, J.M., Bell, E.J. and Jodry, R.L., 1980, Geothermal reservoir assessment case study--northern Dixie Valley, Nevada: Final Report: for U.S. Dept. of Energy, DOE/ET/27006-1, NTIS.

Johnson, Maureen G., 1977, Geology and mineral deposits of Pershing County, Nevada: Nevada Bur. Mines and Geol. Bull. 89.

Page, B.M., 1965, Preliminary geologic map of a part of the Stillwater Range, Churchill County, Nevada: Nevada Bur. Mines Map 28.

Speed, R.C., 1976, Geologic map of the Humboldt Lopolith: Geol. Soc. Amer. Map Series MC-14.

Struchio, Niel, 1986, Age dating of thermal springs deposits: Argonne Nat. Lab., unpublished data.

Waibel, A. F., 1985, Dixie Valley, Nevada: A summary of the Hughes et al geothermal lease block: Columbia Geoscience Report, unpublished.

Willden, R. and Speed, R.C., 1974, Geology and mineral deposits of Churchill County, Nevada: Nevada Bur. Mines Bull. 83.

PROCEEDINGS, Twenty-Second Workshop on Geothermal Reservoir Engineering
Stanford University, Stanford, California, January 27-29, 1997
SGP-TR-155

THERMAL SIGNATURE OF SUBSURFACE FLUID FLOW NEAR THE DIXIE VALLEY GEOTHERMAL FIELD, NEVADA

Colin F. Williams
U.S. Geological Survey
Menlo Park, CA 94025

John H. Sass
and
Frederick V. Grubb
U.S. Geological Survey
Flagstaff, AZ 86001

ABSTRACT

Most of the geothermal development in the United States during the past decade has occurred within the Great Basin. One of the largest developments to date has been the Dixie Valley Geothermal Field (DVGF), one of a number of geothermal fields located along the southern margin of the "Battle Mountain High," a region of high heat flow (> 100 mW/m^2) extending over much of the northern Great Basin. The DVGF lies east of the Stillwater Range and is centered on a southwest-northeast trending thermal anomaly generated by hot water moving up the Stillwater fault, a basin-bounding normal fault characterized by pervasive fracturing and hydrothermal alteration. As part of a multidisciplinary investigation of fracture permeability, in-situ stress, and fluid flow within the Dixie Valley hydrothermal system, we measured subsurface temperatures in four deep wells bordering the DVGF. Precision temperature logs from two flowing wells (45-14 and 66-21) provide detailed information on the location and in-flow rates of permeable fractures intersecting the well bores. Temperature logs from two shut-in wells (76-28 and 62-21) provide information on conductive heat flow near the DVGF. Analysis of the combined dataset yields estimates of the rate and resulting thermal effects of fluid flow along the Stillwater fault. In well 66-21, located 6 km southwest of the current producing limits of the DVGF, and in well 45-14, located 17 km southwest of the DVGF, water flowing up the Stillwater fault may increase the measured heat flow by 20 to 40% over the regional value. In wells 62-21 (4 km southeast of the DVGF) and 76-28 (2 km northeast of the DVGF), heat flow above the fault is close to the regional value, despite the presence of permeable fractures at depth. The limited spatial extent of anomalous heat and fluid flow associated with the DVGF is consistent with deep crustal thermal conditions indicated by the maximum hypocentral depths of nearby earthquakes and suggests that permeability enhancement along the Stillwater fault is highly localized to regions a few kilometers in extent.

INTRODUCTION

Over the past decade, geothermal power developments in the Basin and Range Province of the western United States have reached an installed capacity of approximately 510 MW (Benoit, 1994). Of the fourteen producing geothermal reservoirs located in the Basin and Range, ten are associated with a regional thermal feature known as the "Battle Mountain High" (Sass et al., 1971; Sass et al., 1981), which covers much of the northern Basin and Range (hereafter referred to as the Great Basin) and is characterized by conductive heat flow exceeding 100 mW/m^2. The "typical" geothermal reservoir in the Great Basin lies within basin-bounding normal faults produced as a consequence of Cenozoic extension throughout the region (e.g. Blackwell, 1983). These extensional processes are directly responsible for both the permeable fault zones and the high heat flow necessary for the circulation of thermal waters.

One of the largest developments in the Great Basin is the Dixie Valley geothermal field (DVGF), operated by Oxbow Geothermal Corporation. Dixie Valley is located in west-central Nevada between the Stillwater Range to the northwest and the Clan Alpine Mountains to the southeast (Figure 1). In addition to the high heat flow typical of the northern Great Basin, Dixie Valley lies within an area of active seismicity and late Cenozoic volcanic activity (Thompson and Burke, 1973; Wallace, 1984). The DVGF produces approximately 62 MW of electric power from a series of wells drilled along the Stillwater fault zone (SFZ), an active basin-bounding

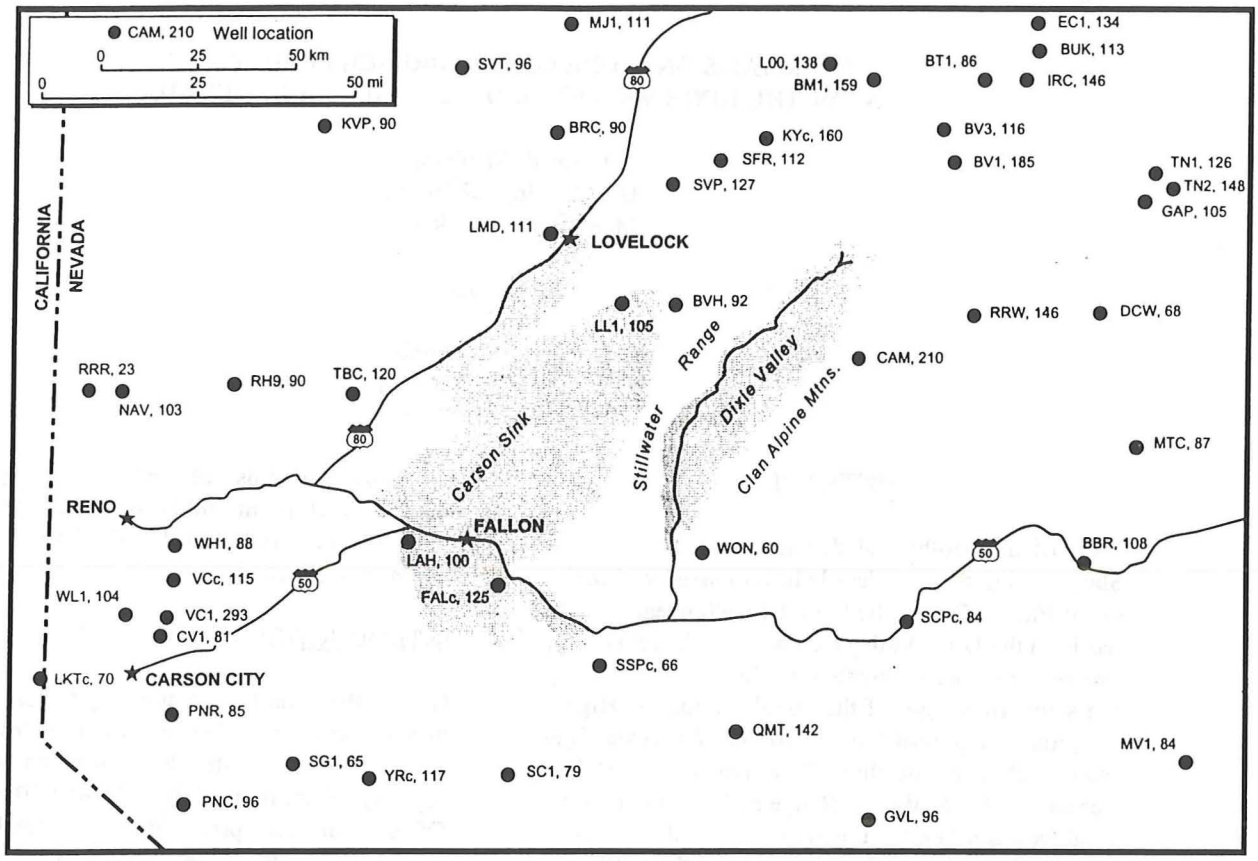

Fig. 1. Map showing heat flow measurements (mW/m^2) in the vicinity of Dixie Valley, Nevada.

normal fault which has displaced the floor of the basin relative to the adjacent Stillwater Range by approximately 3 km over the past 10 Ma (Figure 2; Okaya and Thompson, 1985). The fault cuts and deforms a Jurassic multiphase intrusive body (the Humboldt Lopolith; Speed, 1976), and the subsurface intersection of the SFZ with the lopolith serves as the primary producing zone for the DVGF (Benoit, in press, 1997).

Hot water moving up the SFZ and other subsidiary faults and fractures introduces abnormally high temperatures in a narrow zone along the front of the Stillwater Range. Temperature gradients along this zone have been mapped in the range from 100 to greater than 200°C/km, with the corresponding heat flows exceeding 300 mW/m^2 in places.

This paper reports on thermal aspects of an ongoing, multidisciplinary study of the factors controlling spatial and temporal variations in fracture permeability within and around the DVGF (Hickman and Zoback, this volume and Barton et al., this volume). We examine thermal data from wells bordering the DVGF and analyze evidence for the magnitude and extent of fluid flow up the SFZ at these locations. Comparison of these results with information from the DVGF proper should help provide quantitative constraints on the factors controlling the development of permeability on the SFZ.

DATA

The primary thermal data used in this study come from four observation wells (45-14, 66-21, 62-21 and 76-28) located southwest, southeast and northeast of the DVGF (Figure 2). Wells 45-14 and 66-21 were drilled in 1979 and have been left open at the surface, allowing continuing flow up the wellbore from permeable fractures at depth. Well 62-21 was drilled in 1980 and also intersects significant permeability at depth, although the well has been kept shut-in at the surface. Well 76-28 was drilled in 1984 and differs from the other three in that it is not artesian. The fluid level in this well is encountered at a depth of 550 meters (1800 feet). These and most

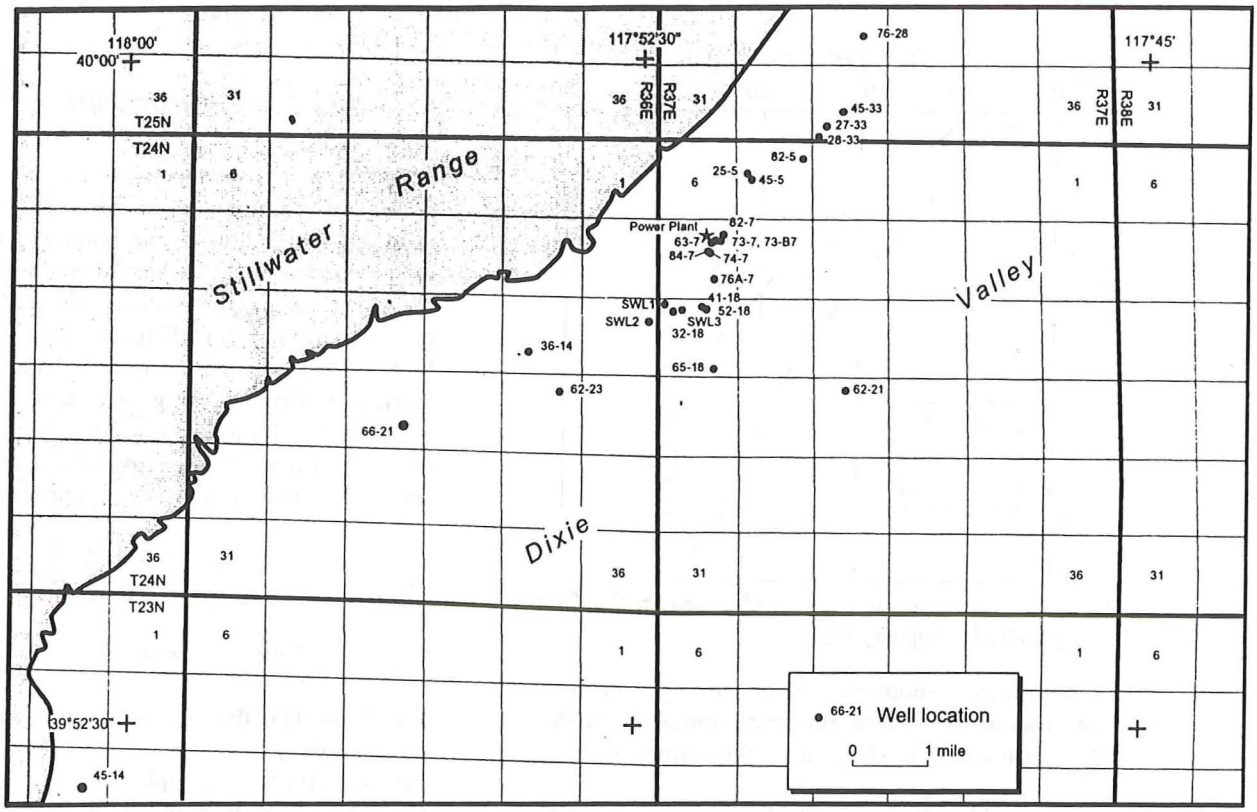

Fig. 2. Map showing locations of geothermal wells (producing, non-producing, and injecting) in Dixie Valley.

other wells in Dixie Valley pass through more than 1000 meters of basin-filling sediments and volcanics before entering the Mesozoic igneous and metamorphic rocks comprising the basement (e.g. Waibel, 1987). The four study wells are cased through the younger units and into the Mesozoic basement, with the length of the open hole sections in the basement ranging from 780 to 880 meters.

Temperature data acquired from all four wells in August, 1996, are shown in Figure 3. The primary factor controlling the differences among the four temperature profiles is the presence or absence of fluid flow within the wellbore. In well 76-28, temperatures follow a gradient varying between 35 and 70°C/km from the water level at 550 meters to the bottom of the log at 2350 meters. The measured gradient variations correspond well with changes in lithology from alternating sand- and clay-rich valley fill to volcanic tuffs to metasediments, with the highest gradients corresponding to the high porosity alluvium and the lowest to the low porosity metasediments. There is no thermal evidence for substantial fluid movement within well 76-28.

In well 62-21 temperatures follow the same general pattern as those within 76-28 with some notable exceptions. Temperature gradients reach or exceed 50°C/km in the sediments and volcanics of the upper 1800 meters and then decline to between 25 and 45°C/km in the mafic igneous and metamorphic rocks of the Humboldt lopolith and the underlying Triassic metasedimentary unit. Curvature in the temperature profile from 2200 to 3000 meters is consistent with entry of fluid into the wellbore (or behind the casing) at 2200 meters (near the top of the lopolith section) and consequent downflow with an exit at about 3000 meters (just below the base of the casing in the Triassic metasediments). Differences between the temperature gradient above 2200 meters and below 3000 meters reflect contrasting thermal conductivities.

The temperature profile in well 66-21 is dominated by the thermal signature of persistent flow up the wellbore to the surface, with abrupt offsets in the temperature profile opposite fluid entries from fractures within the lopolith. This upward flow results in the relatively high surface temperature (~42°C). The other prominent feature of the 66-21 temperature profile, a reversal with a temperature minimum at 2740 meters, appears to be a transient of unknown origin. This feature may reflect entry of gaseous fluid into the wellbore or transient convective instabilities. Subsequent temperature logs showed a

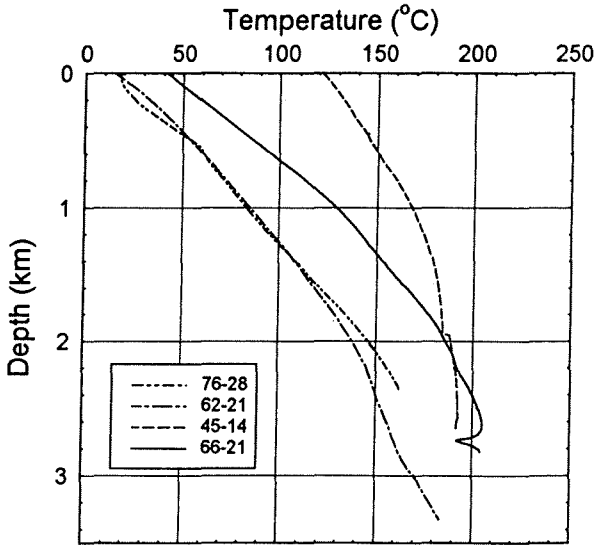

Fig. 3. Temperature profiles obtained in the four study wells in August, 1996.

diminishing anomaly, with nearly complete restoration of equilibrium temperatures in 24 days (C. Barton and R. Norman, written comm.).

More rapid upflow leads to higher temperatures in 45-14, with water entering from fractures within the phyllite basement (the lopolith is not present within this well) and exiting at the surface at a temperature of 122°C. As with well 66-21, the main fluid entries are easily located from offsets in the temperature profile.

THERMAL EFFECTS OF WELLBORE WATER FLOW

In order to determine the thermal effects of naturally occurring fluid flow along the SFZ and related faults and fractures, the anomalous effects of fluid flow within the wellbore first have to be removed from the measured profiles. An analytical model for the long-term thermal effects of vertical fluid flow in a well was presented by Ramey (1962). The equation for temperature above the entry point takes the form of

$$T(z) = T(0) + \Gamma \cdot (z - z_f) - (\exp((z - z_f)/A) - 1) \cdot \Gamma A \quad (1)$$

in which T is temperature, z is depth, z_f is the depth of fluid entry, Γ is the undisturbed geothermal gradient, and A is a measure of the rate of heat transfer. This time dependent factor is given by

$$A = v\rho_f C_f r^2 f(t)/2\lambda \quad (2)$$

in which v is the velocity of the fluid, ρ_f is the density of the fluid, C_f is the specific heat of the fluid, r is the radius of the borehole, f(t) is a time function describing the thermal response of the rock formation to the fluid flow, and λ is the thermal conductivity of the rock formation. This model is best applied when the ratio $\alpha t/r^2$ (where α is the thermal diffusivity) is greater than 1000 (Drury, 1984), which for a normal range of borehole radii is reached on the order of weeks to months. At these times, the function f(t) can be approximated by

$$f(t) = -\ln\left(\frac{r}{2\sqrt{\alpha t}}\right) - \frac{\Gamma}{2} \quad (3)$$

where Γ is Euler's constant (0.5772...).

Equations (1) through (3) were applied to the temperature profiles from wells 45-14 and 66-21. Figure 4 illustrates sample curve-fits of equation (1) to temperatures in well 45-14 resulting from fluid entries at depths of 1940 and 2510 meters. The temperature profile is well-matched with A=1400 and 1500 meters, although variations of A by 10% in either direction are also close to the observed profile. With the assumption that well 45-14 has been flowing at the same rate for approximately 15 years, the estimated rate of flow is 1.1 l/s or 14 gpm.

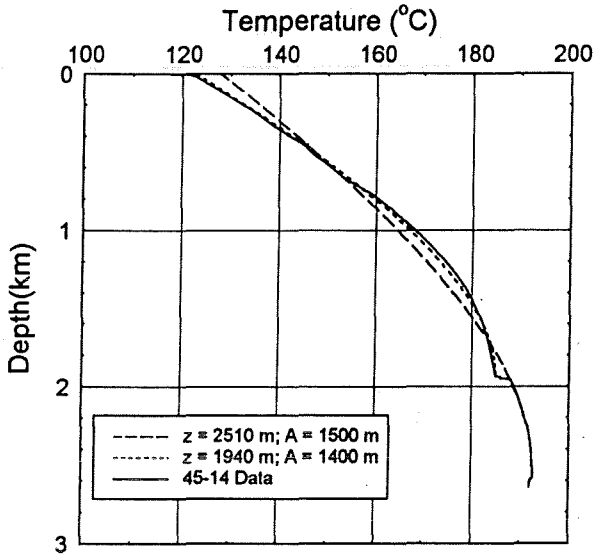

Fig. 4. Temperature profile from well 45-14 along with modeled temperatures for fluid entries at depths of 1940 and 2510 m.

Application of the same analysis to a fluid entry at a depth of 2260 meters in well 66-21 gives A=250 meters (Figure 5) and a flow rate of 0.17 l/s or 2.5 gpm. This is close to the measured flow from 66-21 of 0.12 l/s or 1.8 gpm (S. Hickman, pers. comm.)

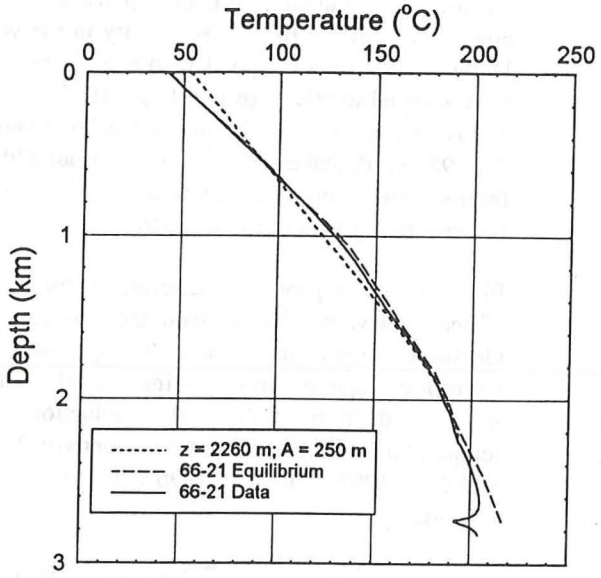

Fig. 5. Temperature profile from well 66-21 along with modeled temperatures for fluid entry at depth of 2260 m. Equilibrium curve reflect temperatures after dissipation of the transient centered at 2800 m.

The flow rates estimated from the Ramey (1962) model are likely to deviate from the true value by 10 to 20% due to the effects of vertical conduction in the rock adjacent to the well (Beck and Shen, 1987) and to the vertical variation in the undisturbed geothermal gradient due to variations in formation thermal conductivity. This is particularly noticeable in the results from well 45-14. The additional fluid entering at 1940 meters should increase the value of A above this point, but the model yields a slightly lower value. However, the primary value of this analysis lies in providing an estimate of the depth section disturbed by the wellbore flow. For distances more than 3A from the fluid entry point, the measured gradient varies by less than 5% from the true gradient (Drury, 1984). Consequently, in well 66-21 temperature gradients from the upper portion of the well and the temperature of the lowest fluid entry can be used in estimating undisturbed thermal conditions. In well 45-14 the high rate of flow as indicated by the large value of A leads to depressed gradients through the entire depth of the well. Only the temperature of the lowest fluid entry can be equated with the undisturbed formation temperature and used to estimate the overall geothermal gradient.

THERMAL EFFECTS OF FLUID FLOW ON THE STILLWATER FAULT

Removal of the effects of wellbore flow in wells 45-14 and 66-21 provides information on undisturbed deep thermal conditions in all four wells. Available thermal conductivity data are limited, but some simple assumptions regarding the similarity of lithologies encountered in each of the four wells provides useful information on relative differences in conductive heat flow.

In well 76-28, application of alluvium thermal conductivity values from nearby exploratory heat-flow holes (M. Walters, written comm.) give an estimated heat flow of 110 mW/m^2, a typical background value for this part of Nevada. This in turn yields an approximate average thermal conductivity for the metasedimentary section of 2.5 W/m·K, assuming constant heat flow with depth. Applying these values to the calculated temperature gradient in well 45-14 (which penetrates a similar section of alluvium, volcanics and metasediments) yields an estimated heat flow of 140 mW/m^2. Application of the same thermal conductivity data to well 62-21 yields a heat flow 90 mW/m^2, which equates to a lopolith thermal conductivity of 2.6 W/m·K. Data from the equivalent section in 66-21 yields a value of 130 mW/m^2.

If the relative differences in apparent heat flow among the four wells are significant, then it is possible to estimate the thermal effect of flow up the SFZ at the locations where it is penetrated by wells 45-14 and 66-21. A simple 2-D model for the change in heat flow across an inclined fracture with water moving along the fracture was derived by Lewis and Beck (1977). If the flow along the inclined fracture has persisted for enough time to develop thermal equilibrium above and below the fracture, the difference in conductive heat flow across the fracture can be determined as

$$\Delta q = WC_f \Gamma \sin(\theta) \qquad (4)$$

where W is the mass rate of flow per unit length of the fracture, C is the heat capacity of the fluid, Γ is the undisturbed geothermal gradient, and θ is the dip of the fracture plane. For the SFZ, θ is approximately 52°, and the difference in heat flow between wells with heat flow elevated by flow up the SFZ (66-21, 45-14) and wells with relatively undisturbed heat flow (62-21, 76-28) provides a Δq = 20-40 mW/m^2. With these values we find W =

1.4-2.8 x 10^{-4} kg/m.s. This works out to 4.4 to 8.8 m^3/yr for each meter of fault length southwest of the DVGF, compared to estimated flow rates of 23 to 46 m^3/yr for each meter of fault within the DVGF itself (Benoit, this vol.).

The validity of this model is limited by two primary factors. First is the assumption that increased heat flow in wells 45-14 and 66-21 is due to flow along the SFZ alone and does not reflect spatial variations in thermal properties, thermal refraction adjacent to the range front, or other unknown advective or conductive processes. Second is the 2-dimensional nature of the model. Near well 45-14 in particular, there is evidence from shallow temperature-gradient holes for 3-dimensional focusing of the thermal anomaly associated with the SFZ (Koenig et al., 1976). Given these limitations, the analysis may not provide precise quantitative information on the magnitude of flow up the SFZ but does indicate the spatial extent of flow outside of the DVGF.

In summary, subsurface temperatures and resulting heat flow values in wells 76-28 and 62-21 are consistent with regional averages. Subsurface temperatures and heat flow values in wells 45-14 and 66-21 are higher, perhaps by as much as 40%. These higher values of heat flow are consistent with local fluid flow up the SFZ southwest of the DVGF. The SFZ should lie at a depth of approximately 6 km below the site of well 62-21, yet the thermal data suggest the heat flow is consistent with the regional average. An implication of this observation is that thermally significant fluid flow up the SFZ is not a factor at depths greater than 3 to 4 km in the vicinity of well 62-21. The validity of these results can be tested by considering other available information on deep crustal thermal conditions: well-established relationships between the maximum depth of seismic faulting and crustal thermal conditions provide one such approach.

SEISMIC EVIDENCE OF DEEP CRUSTAL THERMAL CONDITIONS

As noted above, Dixie Valley lies in a region of active seismicity. Most notably, in the 1954 Rainbow Mountain-Fairview Peak-Dixie Valley sequence, five earthquakes of moment magnitude (M) ranging from 5.9 to 7.2 ruptured the faults in and south of Dixie Valley (Doser, 1986). The M=6.7 Dixie Valley earthquake was located approximately 30 km south of the DVGF and was responsible for up to 2 m of vertical offset along the SFZ to the southwest of the DVGF (Slemmons, 1957). Relocation of the hypocenter for the Dixie Valley earthquake places it at a depth of 12 ± 3 km (Doser, 1986), with similar results for the other, more distant, earthquakes in the sequence. Numerous studies of thermal constraints on brittle faulting and the nature of the seismogenic crust constrain the base of seismicity in the western United States to correspond with a temperature less than or equal to 400°C (e.g. Sibson, 1982; Williams, 1995). Consequently, the maximum focal depths of the 1954 earthquake sequence provides an additional thermal constraint on temperatures at depth and the corresponding value of heat flow.

Figure 6 shows geotherms determined for the range of heat flow values derived from the four study wells. Geotherms were determined through use of the appropriate equations for one-dimensional steady-state heat conduction with heat production and a temperature-dependent thermal conductivity (Williams and Sass, 1995; Williams, 1996). The basic equation is given by

$$T = \frac{1}{b}\cdot\left[\exp\left(\frac{bq_s}{\lambda_0}z - \frac{bA_s}{2\lambda_0}z^2 + \ln(1-bT_s)\right) - 1\right] \quad (5)$$

where T_s is the surface temperature (15°C), q_s is the surface heat flow (varied), λ_0 is the thermal conductivity at 0°C (3.0 W/m • K), A_s is the surface radiogenic heat production (2.0 μW/m^3) and b is the temperature coefficient of thermal conductivity (0.0024 - 0.0052/λ_0).

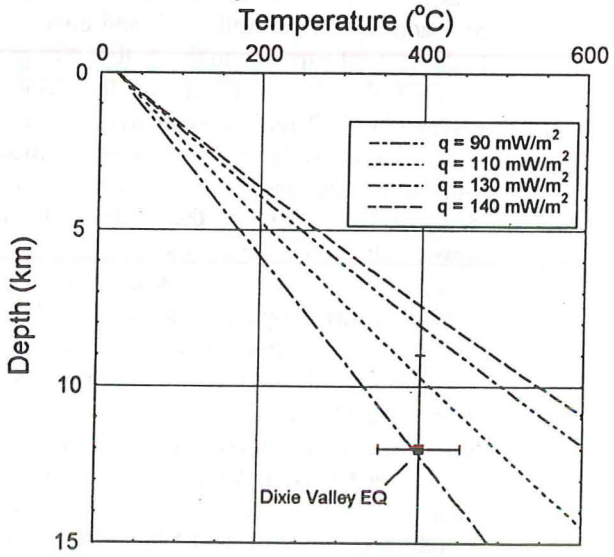

Fig. 6. Crustal temperature profiles determined for the range of estimated heat flow from the four study wells. Note the discrepancy between the temperature inferred for the hypocenter of 1954 Dixie Valley earthquake and temperatures from heat flow values above 110 mW/m^2.

The primary result of interest is the consistency of the hypocentral depth of the Dixie Valley earthquake with temperatures near 400°C for heat flow values of 90 mW/m^2 (well 62-21) and 110 mW/m^2 (well 76-28). Temperatures at this depth for heat flow values of 130 mW/m^2 (well 66-21) and 140 mW/m^2 (well 45-14) are far too high to represent in situ conditions at the hypocenter of the Dixie Valley earthquake. The consistency of the apparent heat flow in wells 76-28 and 62-21 with the regional average for the northern Great Basin and the focal depths of nearby earthquakes strongly suggests that these sites are not affected by fluid flow along the SFZ. Conversely, the apparent heat flow in wells 45-14 and 66-21 is inconsistent with either the regional average or the earthquake focal depths. Consequently, permeability along the SFZ must be highly localized and flow along the SFZ in the vicinity of the DVGF may be restricted to depths less than 6 km.

CONCLUSIONS

Analysis of the temperature profiles from the four study wells provides valuable information on coupled heat and fluid flow within Dixie Valley. In particular, in the two wells (66-21 and 45-14) located southwest of the DVGF heat flow is elevated by 20 to 40% above the regional background value. Fluid flow up the SFZ may be responsible for this. By contrast, heat flow southeast (62-21) and northeast (76-28) of the DVGF is indistinguishable from the regional value. The limited magnitude and spatial extent of anomalous heat and fluid flow is confirmed by comparison with thermal conditions likely to exist at maximum hypocentral depths of nearby earthquakes. Future research to test these preliminary results should involve thermal properties measurements, detailed mapping of subsurface temperature and permeability, and numerical modeling.

ACKNOWLEDGEMENTS

We thank Dick Benoit of Oxbow Geothermal for his enthusiastic support of the USGS research team. This project was funded by the Dept. of Energy Reservoir Technology Program through the assistance of Marshall Reed and Joel Renner and by the EQ Hazards Reduction Program of the USGS. Steve Hickman and Art Lachenbruch provided thoughtful reviews.

REFERENCES

Beck, A.E., and P.Y. Shen, 1985, Temperature distribution in flowing liquid wells, *Geophysics*, v. 50, no. 7, p. 1113-1118.

Benoit, W.R., 1997, Injection of geothermal fluid in Nevada as typified by the Dixie Valley project, in *Deep Injection Disposal of Hazardous and Industrial Wastes*, Academic Press, in press.

Benoit, W.R., 1994, A review of geothermal resources in the western Basin and Range, 1994, *Geothermal Resources Council Bull.*, v. 24, n. 5, p. 153-156..

Blackwell, D.D., Heat flow in the Northern Basin and Range, 1983, in *The Role of Heat in the Development of Energy and Mineral Resources in the Northern Basin and Range Province, Geothermal Resources Council Spec. Paper 13*, p. 81-92.

Doser, D.I., 1986, Earthquake processes in the Rainbow Mountain-Fairview Peak-Dixie Valley, Nevada region 1954-1959, *J. Geophys. Res.*, v. 91, no. 12, p. 12,572-12,586.

Drury, M.J., 1984, Perturbations to temperature gradients by water flow in crystalline rock formations, *Tectonophysics*, 102, p. 19-32.

Koenig, J.B., R.W. Greensfelder, and C.W. Klein, 1976, Geothermal potential of the Quest leasehold Dixie Valley, Nevada, unpublished technical report, GeothermEx, Inc.

Lewis, T.J., and A.E. Beck, 1977, Analysis of heat flow data - detailed observations in many holes in a small area, *Tectonophysics*, 41, p. 41-59.

Okaya, D.A. and Thompson, G.A., 1985, Geometry of Cenozoic extensional faulting: Dixie Valley, Nevada, *Tectonics*, v. 4, p. 107-125.

Ramey, H.J., Jr., 1962, Wellbore heat transmission, *J. Petrol. Tech.*, 14, 427-435.

Sass, J. H., A. H. Lachenbruch, R. J. Munroe, G.W. Greene, T. H. Moses, 1971, Heat flow in the Western United States, *J. Geophys. Res.*, 76, p. 6376-6413.

Sass, J.H., D.D. Blackwell, D.S. Chapman, J.K.

Costain, E.R. Decker, L.A. Lawver, and C.A. Swanberg, 1981, Heat flow from the crust of the United States, in Y.S. Touloukian, W.R. Judd, and R.F. Roy, eds., *Physical Properties of Rocks and Minerals*, McGraw-Hill Book Company, p. 503-548.

Sass, J.H., S.S. Priest, T.A. Ehlers, P. Morgan, D.S. Chapman, A.H. Lachenbruch, and C.F. Williams, 1996, Thermal regime of the Great Basin, *EOS*, v. 77, no. 46, F665.

Sibson, R.H., 1982, Fault zone models, heat flow, and the depth distribution of earthquakes in the continental crust of the United States, *Bull. Seismol. Soc. Am.*, 72, p. 151-163.

Slemmons, D.B., 1957, Geological effects of the Dixie Valley-Fairview Peak, Nevada earthquakes of December 16, 1954, *Bull. Seismol. Soc. Am.*, 47, p. 353-375.

Speed, R.C., 1976, Geologic map of the Humboldt lopolith and surrounding terrane, Nevada, *Geol. Soc. Amer. Map and Chart Series*, n. 14.

Thompson, G. A., and D. B. Burke, 1973, Rate and direction of spreading in Dixie Valley, Basin and Range province, Nevada, *Geol. Soc. Am. Bull.*, 84, 627-632.

Waibel, A.F., 1987, An overview of the geology and secondary mineralogy of the high temperature geothermal system in Dixie Valley, Nevada, *Trans. Geothermal Resources Council*, v. 11, p. 479-486.

Wallace, R.E., 1984, Patterns and timing of late Quaternary faulting in the Great Basin province and relation to some regional tectonic features, *J. Geophys. Res.*, v. 89, p. 5763-5769.

Williams, C.F., 1995, Temperature and the seismic/aseismic transition: a new look, *EOS*, 76, p. 410.

Williams, C.F., and J.H. Sass, 1996, The thermal conductivity of rock under hydrothermal conditions: measurements and applications, *Proc. 21st Stanford Geothermal Workshop*, p. 335-341.

Williams, C.F., 1996, Temperature and the seismic/aseismic transition: observations from the 1992 Landers earthquake, *Geophys. Res. Lett.*, v. 23, no. 16, p. 2029-2032.